UNIVERSITY OF CALIFORNIA

Los Angeles

Novel Climbing Robot with an Extendable and Bendable Tape Spring Limb

A dissertation submitted in partial satisfaction

of the requirements for the degree of

Doctor of Philosophy in Mechanical Engineering

by

Justin Rei Quan

2024

ABSTRACT OF THE DISSERTATION

Novel Climbing Robot with an Extendable and Bendable Tape Spring Limb

by

Justin Rei Quan
Doctor of Philosophy in Mechanical Engineering
University of California, Los Angeles, 2024
Professor Dennis W. Hong, Chair

Climbing robots are a growing area of interest for tasks that involve vertical mobility in locations that are difficult or dangerous to access for humans. These robots are often designed for inspection, surveillance, or maintenance tasks, but have not been widely deployed due to key limitations with existing designs. Wheeled climbers have little to no adaptability to surface variations, and can generally only climb a single flat, featureless surface with no obstacles. Legged climbers possess better adaptability with their additional degrees of freedom, but can only step over small obstacles and are also heavy, slow, and expensive.

This dissertation details the development of a novel climbing robot that overcomes these problems with an innovative limb that utilizes tape springs. Like the common tape measure, tape springs can be used for a lightweight, long-reach, low-cost structure that spools into a compact package. This research resulted in two major innovations: the robotic limb EEMMMa (Elastic Extending Mechanism for Mobility and Manipulation) and the climbing robot EEWOC (Extended-reach Enhanced Wheeled Orb for Climbing).

The EEMMMa extendable limb can exhibit controlled bending using only a single primary motor through mechanical multiplexing. With this additional degree of freedom, it can bend its end effector to reach over ledges and around corners or obstacles. EEWOC combines this novel limb with additional magnetic grippers, actuators, and wheels to allow it to freely

traverse 3D surfaces. EEWOC weighs 2.1 kg and is only 26 cm tall, and its limb can extend up to 1.2 m.

To better understand the impact of EEWOC's novel design, several performance tests were carried out in controlled lab and outdoor settings. Compared to existing robots, EEWOC's climbing performance was found to be equal or superior, with a climbing speed of 4.4 m/min and payload capacity of 3.4 kg. Simplified kinematic models were developed for the limb's bending mode and for swinging across gaps, which were verified using visual tracking markers and video capture of real bending and swinging maneuvers while climbing.

The dissertation of Justin Rei Quan is approved.

Jonathan Hopkins

Xiaochun Li

Veronica Santos

Dennis W. Hong, Committee Chair

University of California, Los Angeles

2024

Contents

List of Figures

List of Tables

Page

ACKNOWLEDGMENTS

I am so incredibly grateful for all of the many, many people who have supported me as an engineer and have helped shape me into the person I am today.

To Dr. Dennis Hong, my advisor, mentor, and friend, I am so lucky to have had your guidance on my academic journey, serving as a shining example of what an engineer can be: optimistic, energizing, purposeful, and excited to take ideas into the future. Thank you for your endless support and enthusiasm, and helping me be less afraid of my own ideas and encouraging me to try new things, both in engineering and in life.

To my committee members, Dr. Jonathan Hopkins, Dr. Xiaochun Li, and Dr. Veronica Santos, I am so honored to have received your guidance and encouragement during my time at UCLA. I have had the opportunity to see the limits of engineering being pushed in wildly different ways in each of your labs, and your clear love of your respective research fields is inspiring. You have also been my favorite instructors, and your classes and design approaches have helped grant me the creative and practical tools to make this project even possible.

To my fellow RoMeLa members, thank you for making every day in lab exciting and full of joy. You are some of the most incredibly talented, hardworking, witty, and kind people that I've ever met. You've given me countless memories of comradery and comedy during the late nights in lab and trips around the world, and it's been so much fun forging the future with you all. Working with robots has been cool, but working with the humans has been even cooler. You'll continue to inspire me long after we all graduate.

Finally, to my family and friends, thank you so, so much for your unwavering love, support, and guidance over these many years. You are the reason that I'm here, and why I've gotten so far. There is still a long journey ahead of me, and I'm proud to have you along with me. You keep the fire in me burning every day, and we all shine brighter together.

CURRICULUM VITAE

B.S. in Mechanical Engineering, *University of California, Irvine* 2011 - 2015

M.S. in Mechanical Engineering, *University of California, Irvine* 2015 - 2016

PUBLICATIONS

Justin Quan, Mingzhang Zhu and Dennis Hong, "Re-Examining Climbing Robots: Design and Performance of a Lightweight, Low-Cost Robot with a Highly Extendable Limb," 2024 6th IEEE International Conference on Reconfigurable Mechanisms and Robots (ReMAR), Chicago, IL, USA, 2024, pp. 409-416

Justin Quan, Mingzhang Zhu, Dennis Hong, "EEWOC: Extended-Reach Enhanced Wheeled Orb for Climbing," presented at the 2024 IEEE International Conference on Robotics and Automation (ICRA), Yokohama, Japan, May 13-18, 2024.

Justin Quan, Mingzhang Zhu, and Dennis Hong, "Swinging To Traverse Gaps For A Lightweight Mobile Robot With Highly Extendable Limb," presented at the 2023 Southern California Robotics Symposium (SCR), Irvine, CA, USA, September 14-15, 2023.

Justin Quan, Mingzhang Zhu, and Dennis Hong, "A Lightweight Mobile Robot for Climbing Steel Structures With An Extending and Bending Tape Spring Limb," 2023 ASME International Design Engineering Technical Conferences and Computers and Information in Engineering Conference (IDETC-CIE), American Society of Mechanical Engineers, 2023

Justin Quan and Dennis Hong, "Flexible Long-Reach Robotic Limbs Using Tape Springs for Mobility and Manipulation," ASME Journal of Mechanisms and Robotics, vol. 15, no. 3, p. 031009, 2023.

Justin Quan and Dennis Hong, "Extending and Bending Robotic Limbs Using Tape Springs for Mobility and Manipulation: Preliminary Investigations," 2022 ASME International Design Engineering Technical Conferences and Computers and Information in Engineering Conference (IDETC-CIE), vol. 86281. American Society of Mechanical Engineers, 2022, p. V007T07A044.

Gabriel Ikaika Fernandez, Samuel Gessow, Justin Quan, and Dennis W. Hong, "Self-Aligning Rotational Latching Mechanisms: Optimal Geometry for Mechanical Robustness," ASME Journal of Mechanisms and Robotics, vol. 16, no. 1, p. 011007, 2024.

Gabriel Ikaika Fernandez, Samuel Gessow, Justin Quan, and Dennis W. Hong, "Self-Aligning Rotational Latching Mechanisms," 2022 ASME International Design Engineering Technical Conferences and Computers and Information in Engineering Conference (IDETC-CIE), vol. 86281. American Society of Mechanical Engineers, 2022, p. V007T07A024.

Spencer Backus, Jacob Izraelevitz, Justin Quan, Rianna Jitosho, Eitan Slavick, and Arash Kalantari, "Design and Testing of an Ultra-light Weight Perching System for Sloped or Vertical Rough Surfaces On Mars," 2020 IEEE Aerospace Conference, 2020, pp. 1–12.

Chapter 1

Introduction

1.1 Motivation

Climbing robots present a growing area of interest for tasks that involve safety risks to humans in environments high off the ground. This commonly includes inspection, surveillance, or maintenance tasks, where vertical mobility is useful for accessing locations that are difficult or dangerous to reach for humans. For example, urban and industrial environments are filled with hard-to-reach structures such as power lines, antennas, pipes, poles, towers, and bridge trusses. These vital pieces of infrastructure require regular inspections and maintenance to ensure safety. For these dangerous environments, deploying a robot instead of a human inspector can be greatly preferred. Using remotely controlled robots can prevent human exposure to electrical, chemical, and fall hazards. Robots can also greatly reduce the burden of inspecting a very large structure such as a bridge or a ship hull, since they can autonomously perform a usually tedious and labor-intensive process. They can also be used to explore large, remote environments such as caves or forests to collect scientific data without risking human safety.

While flying robots can also access hard-to-reach areas with ease, the ability to climb on a surface is often required to do meaningful work in these dangerous environments. Many inspection and maintenance tasks require close contact with surfaces or carrying heavy task-specific equipment, both of which are difficult for aerial systems. As such, flying robots in this field are generally only used for cursory visual inspection of large areas. In comparison, climbing robots can carry much greater payloads and can apply forces to surfaces more easily for common tasks like scraping, painting, structural testing, and sample collecting.

Despite this clear need, climbing robots are not yet widely used due to shortcomings in speed, strength, adaptability, and cost. A key issue that limits the performance of existing climbing robots is their overreliance on conventional ground-based mechanical designs. Many typical robot morphologies with wheels or legs are not well suited for climbing, with inadequate surface adaptability or excess mass that is poorly distributed.

This dissertation details the development of a novel climbing robot that is better suited for climbing. By re-examining the requirements for climbing, this new system utilizes unconventional mechanisms and structures to achieve climbing that is faster, stronger, and more versatile compared to most existing robots, with simple control and low cost.

1.2 Existing Climbing Robots

There are a wide variety of existing climbing robots developed by labs around the world, but most can be sorted into general categories based on adhesion and locomotion methods. For each robot, adhesion and locomotion are highly dependent on the intended task and climbing environment.

Adhesion Type	Pros	Cons	Example Environments
Magnetic (Permanent)	• Simple • Pull-in assistance, no contact • Passive adhesion	• Heavy • Removal can be difficult/complex	• Metal surfaces • Bridges • Ships • Factories • Transmission towers
Magnetic (Electromagnet)	• Simple • Pull-in assistance, no contact	• Heavy • Active power draw, inefficient	
Pneumatic (Passive)	• Simple • Lightweight • Passive adhesion	• Sensitive to surface conditions • Low payload capacity	• Flat, smooth surfaces • Glass, plastic, metal
Pneumatic (Active)	• High environment versatility • Pull-in assistance, no contact	• Requires air pumps or propellers • Active power draw, inefficient • Low payload capacity	• Many surface types and topologies
Microspine / Hook Array	• Lightweight • Passive adhesion • High strength-to-weight ratio • High payload capacity	• Sensitive to engagement direction • Lower reliability, stochastic • Complex manufacture/assembly • Wears out over time	• Rough surfaces • Brick, concrete, caves • Tree bark or branches • Asteroids
Dry Adhesive	• Lightweight • Passive adhesion • High strength-to-weight ratio • Fast attach/detach	• Sensitive to surface conditions • Lower reliability, stochastic • Complex manufacture/assembly	• Flat, smooth surfaces • Glass, plastic, metal
Clamping	• Simple • High reliability	• Little to no adaptability	• Wires and cables • Pipes and poles

Table 1.1: Summary of pros and cons of climbing adhesion types.

1.2.1 Adhesion

Existing climbing robots use many different approaches to attach onto surfaces, with some common types including magnetic attraction, mechanical attachment using hooks or microspine arrays, pneumatic suction, and dry adhesives (or "gecko" adhesives that use van der Walls forces). Others operate by simple clamping friction by wrapping around structures, a common method for robots that climb cables, pipes, or poles [1, 2]. A few examples can be seen in Fig. 1.1, and a summary table of the adhesion types and their pros and cons can be found in Table 1.1, as well as a list of environments in which they can be used. While not the focus of this study, rurther explanations of the different types of adhesion can be found in the Appendix.

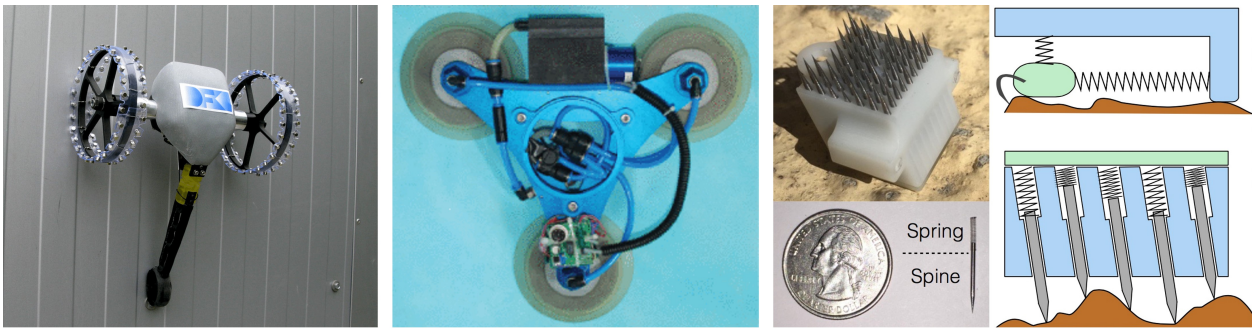

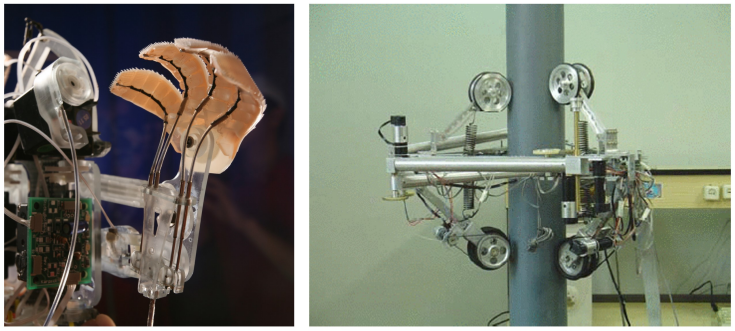

Figure 1.1: Examples of climbing robot adhesion. a) MINOAS, which uses an array of permanent magnets on its wheels to climb steel surfaces [3]. b) Pneumatic triple suction cup pad used for W-Climbot for flat, smooth surfaces [4]. c) Microspine array used for climbing rough surfaces with RoboSimian, with a summary diagram of microspine operation [5]. d) Dry adhesive "gecko" pads on Stickybot for flat, smooth surfaces surfaces [6]. e) Clamp-type adhesion with pole climbing robot UT-PCR [7].

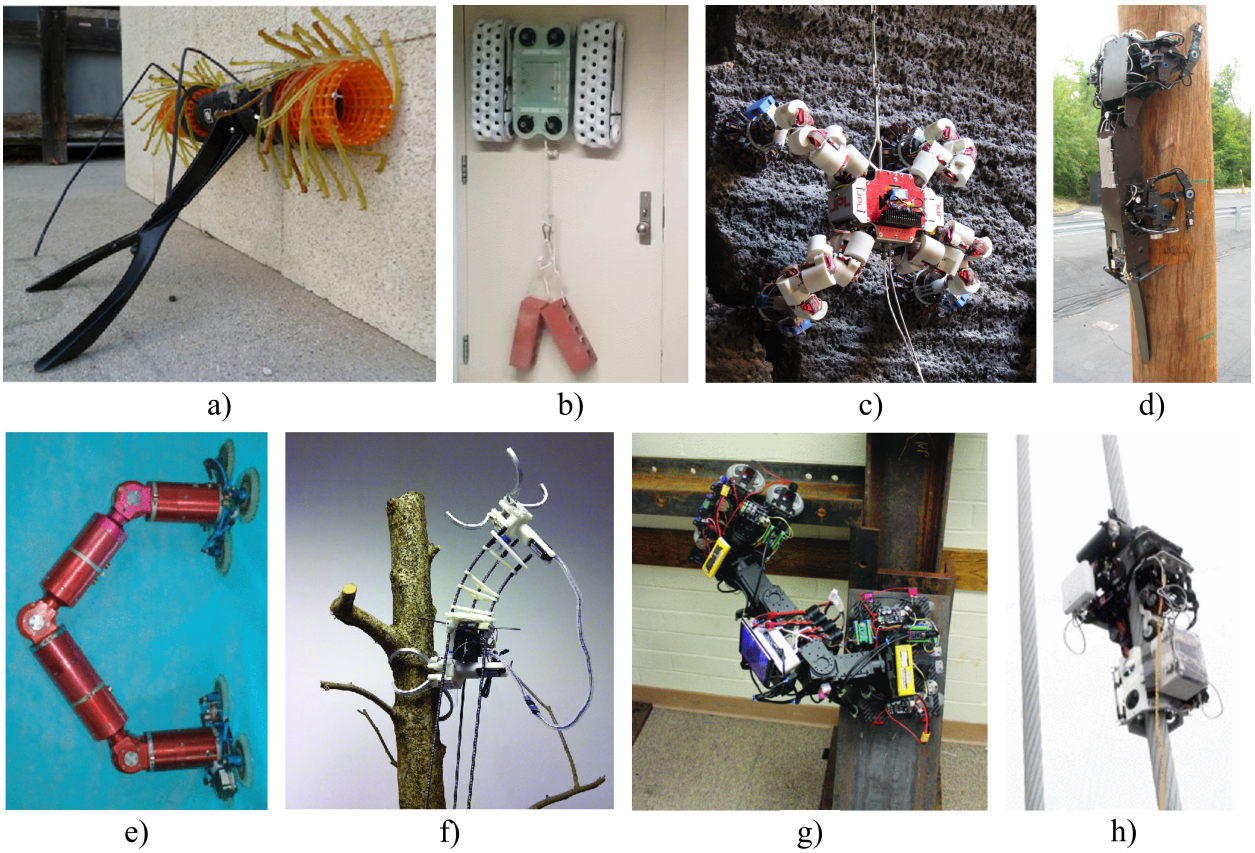

Figure 1.2: a) DROP, a wheeled robot that uses rotary microspine arrays to climb rough surfaces [8]. b) RISE-ROVER, which uses pneumatic suction treads. c) LEMUR-3, which uses radial microspine grippers to climb cave walls [9]. d) RiSE V3, which uses a microspine array to climb telephone poles [10]. e) W-Climbot, an inchworm-type robot that uses a 5-DOF manipulator arm and suction cup pads [4]. f) Treebot, an inchworm-type soft robot that uses a 4-finger microspine gripper to climb trees [11]. g) A hybrid inchworm + wheels magnetic robot by ARA labs for bridge inspection [12]. h) MRC^{2}IN, a clamp-type robot designed to climb wires by compressing them with treads. [13].

1.2.2 Locomotion

Climbing robots have a wide variety of locomotion methods and gait types. A few examples of modern experimental climbing robots can be seen in Fig. 1.2. Conventional climbing robots often use either wheels or legs with some form of adhesion to climb, with some examples shown in Fig. 1.2.

Robots that climb with wheels or treads tend to be very fast and lightweight due to their

simple design [3, 8, 14, 15, 16]. However, wheels offer little to no adaptability to surface variations due to their need for continuous contact. These robots can generally only climb flat, featureless surfaces and cannot overcome a wide variety of external features such as bolts, seams, cracks, pipes, and ledges, making them impractical in complex 3D real-world environments. Some wheeled robots attempt to address the lack of adaptability with additional wheels and an extra degree of freedom (DOF) [15, 17]. Other hybrid robots combine wheels and a multi-DOF arm to transition between surfaces and over small obstacles [12, 14, 18]. There are also clamp-type robots that are very fast and reliable, but have even lower adaptability and are generally confined to 1D motion along a single pipe or cable [7, 13, 19].

Limbed robots that climb with arms or legs possess much greater adaptability and can easily step over obstacles or rough terrain using limbs with additional DOFs. Adhesion occurs at the end effectors, which can be moved to distant anchor points in the limb's reachable workspace. This allows them to step over obstacles as large as 10-20 cm, depending on their limb length. Multi-limbed robots generally feature multi-DOF arms that mimic animal limbs to conform to surface variations, with extra limbs for redundancy and safety [10, 20, 21, 22, 23, 24, 25]. Inchworm robots have also been developed that consist of a single limb that moves between consecutive points [4, 11]. This reduced morphology eliminates weight from redundant limbs and simplifies motion planning.

The adaptability of limbed robots makes them much more practical for deployment in unstructured real-world environments. However, this comes at the cost of complexity, as these robots are often heavy, slow, and expensive, especially for multi-limbed systems.

The shortcomings with current climbing robots are likely due to their reliance on conventional, ground-based mechanical designs that do not take into account certain fundamental differences between climbing and walking. Many ground-based robots utilize excessive actuators and structures, but are mostly unaffected by this extra weight since they are directly supported by the ground. In contrast, climbing requires this weight to be accelerated by the

Locomotion Type	Pros	Cons	Common Types
Wheeled	• Fast • Lightweight • Simple motion planning	• Little to no adaptability • Lower payload capacity	• Wheeled • Treads • Clamp-type
Multi-limbed	• Adaptable • High potential payload capacity • Safety from redundant limbs	• Heavy • Slow • Complex motion planning • Bilateral gap, out-of-plane forces	• Quadruped • Hexapod • Hybrid w/ wheels
Inchworm	• Adaptable • High potential payload capacity • Simpler motion planning	• Heavy • Slow • No redundant limbs for safety	• Conventional arm • Soft arm • Hybrid w/ wheels

Table 1.2: Summary of pros and cons of climbing locomotion types.

robot against gravity, increasing the energetic cost of climbing.

Ground-based robots can easily step and move in the 2D ground plane since gravity conveniently forces them against the floor. Meanwhile, climbing robots must employ an additional adhesion mechanism to overcome gravity that must be turned on and off between each step, making motion planning for climbing vertical or 3D surfaces much more complex.

1.3 Proposed Solution

This dissertation details the development of a novel form of climbing robot that addresses the aforementioned problems for existing systems. The design process focuses on two main goals: 1) create a new robotic limb better suited for climbing, and 2) simplify the overall robot morphology as much as possible while still allowing robust, free movement on a 3D structure.

The first major innovation is the introduction of a tape spring structure for robotic limbs, implemented in the new prototype limb module EEMMMa (Elastic Extending Mechanism for Mobility and Manipulation). Tape springs are thin curved strips of material similar to a

common carpenter's tape that exhibit natural directional stiffness. This allows them to serve as lightweight structural members, making them useful for large scale deployable structures. Their ability to elastically fold allows them to be spooled into a tight package for excellent compactness.

EEMMMa utilizes a unique U-shaped tape spring structure to place its end effector hooks at distant points for climbing shelves and ladders. The tape offers a greatly enhanced reachable workspace and can handle very high loads in tension while climbing. Its U-shape also allows it to handle loads in compression, and it can easily support the weight of its end effector while ascending. The overall limb design is much better suited for climbing, with a long reach and no extra weight from unnecessary structures.

The limb can also exhibit controlled bending, using mechanical multiplexing with only a single primary motor to achieve a functionally 2-DOF system. By toggling between two kinematic modes with a small microservo, EMMMa's design saves weight on heavy actuators while still having controllable DOFs for manipulation tasks. It saves more weight by using simple passive compliant grippers and hooks on the end effector and main body. The compliance at these locations, combined with the compliance of the limb itself, allows for very robust climbing and passive alignment without the need for extra actuators and controllable DOFs.

The second major innovation is the development of a novel mobile robot named EEWOC (Extended-reach Enhanced Wheeled Orb for Climbing) with a simplified morphology that is optimized for climbing steel structures, shown in Fig. 1.3. EEWOC utilizes a hybrid locomotion scheme that combines the extendable EEMMMa limb with additional DOFs and wheels to allow it to aim and meaningfully interact with surfaces in 3D space. It is equipped with two magnetic grippers, with one at the end effector and the other attached directly to the main body. A pair of wheels replaces the lower limbs for bracing while climbing, eliminating the weight from an additional limb. The wheels also allow EEWOC to drive efficiently on

Figure 1.3: EEWOC's ability to extend and bend to place its magnetic grippers on complex features grants it a wide variety of mobility options on steel structures. Here, it is shown extending over a small gap on HVAC machinery, bending to reach the top of a ledge, and climbing up a tall support truss.

horizontal surfaces. Several compliant mechanisms throughout its design grant passive DOFs when necessary to avoid heavy actuators. With only a single limb and a minimum set of controllable DOFs, EEWOC is lightweight, compact, fast, strong, and simple to control.

These two innovations form the base of a new type of mobile robot with features optimized for climbing. In the following sections, this dissertation will discuss: 1) a re-examination of the requirements for effective climbing, 2) the mechanical design and manufacture of EEMMMa, 3) demonstrations of climbing and bending with EEMMMa, 4) analysis of EEMMMa's bending behavior and kinematics, 5) the mechanical design and manufacture of EEWOC, 6) demonstrations of EEWOC climbing and movement in a real-world environment, 7) analysis of these experiments, and finally 8) conclusion and future goals of this work.

Chapter 2

Analysis of Climbing Requirements

2.1 Climbing Forces and Torques

To better understand the differences between climbing and ground-based movement, let's consider the 2D case in Fig. 2.1a, depicting a robot climbing a vertical surface. Past research on the biomechanics of climbing vertical structures divide the problem into three bodies: 1) the *main body* of the animal that contains most of the mass, 2) the *substrate*, which is the underlying surface or structure that the animal is ascending, and 3) the *limbs*, which transfer forces between the main body and the substrate [26]. To simplify this model further, we will assume the limbs are massless and that our robot has only two limbs, an upper limb and a lower limb that contact the substrate at some *anchor points*. This general case is applicable to all forms of climbing, as these fundamental bodies, forces, and actions remain consistent regardless of robot morphology.

The largest difference between ground-based movement and climbing is the need to support the system's weight directly against gravity. Climbing robots require an additional gripper on each limb to generate an *adhesion force* F_a. (with claws, clamps, etc.) to attach to the

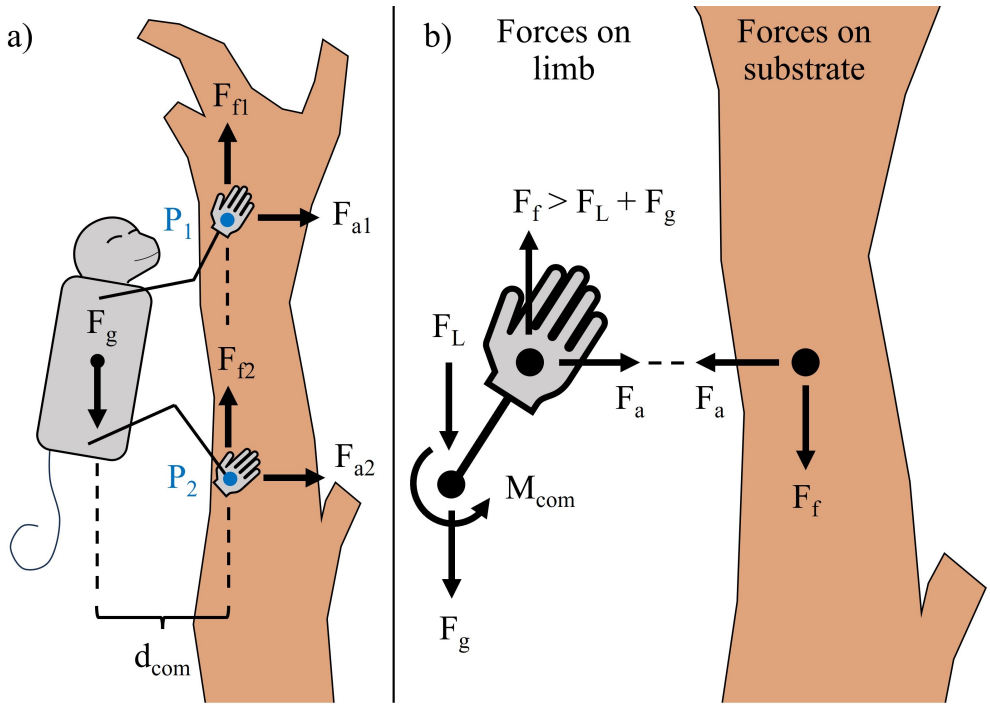

Figure 2.1: a) 2D Free-body diagram of forces while climbing, showing the main body, limbs (upper and lower), and substrate. b) Simplified view for climbing with a single limb, showing the anchor point and forces exerted between the limb and the substrate while ascending.

surface and generate the *friction* F_f necessary to support the *weight* F_g from the main body. The adhesion forces must also compensate for the *pitch-back moment* M_{COM} that results from the center of mass (COM) being located some distance d_{COM} away from the substrate. These are not issues for ground-based systems, since the robot's weight conveniently provides the adhesion force that the robot needs to generate the friction required for horizontal movement using wheels or legs. Their direct contact with the ground also makes supporting extra weight trivial, whereas extra weight is undesirable for climbing robots since it increases the energetic cost of climbing.

Once static equilibrium is achieved, the action of climbing requires exerting a force to ascend. Generally, the main body mass accelerates upwards as the limb(s) exert a downward *lifting force* F_L on the substrate, shown in Fig. 2.1b for climbing with a single limb.

Two additional non-slipping conditions are required for climbing safely. First, as seen in Fig.

2.1b, the friction forces F_f at the anchor points must be greater than the total combined weight force F_g and lifting forces F_L, or else the robot will slip. Second, the substrate must be strong enough to support the combined forces, and not break from the weight of the robot as it forces its mass up, which will result in slipping. This is a key consideration when climbing weaker surfaces like tree bark, rusted metal, or sandstone. These factors can significantly affect how gait planning is performed.

2.2 Climbing Gaits

Climbing gaits require several extra steps compared to ground-based gaits that increases the complexity of path planning. For climbing, the first step before moving is 1) *identification*, where the robot must first identify a desired anchor point located some distance away. Viable points are limited, as they must be within the robot's reachable workspace, and have suitable surface topology and condition to maximize the chance of successful adhesion, as shown in Fig. 2.2. The robot must then 2) *detach* its limb(s) from the substrate, 3) *move* its limb(s) in the stance phase to reach the desired anchor point at a specific position and orientation, 4) *re-attach* its limb(s) to the substrate. 5) *move* its main body in the swing phase to transport its mass upwards, and 6) *repeat* steps 1-4 for each limb until its new position is reached.

It should be noted that this sequence is a general case, and many animals apply loads to their limbs in different ways. There are many gait types in nature, including tripod gaits with six legs, bounding with leg pairs, trotting between two pairs, inchworm gaits, moving the main body while all limbs are still attached, with many other minor differences. For wheels and other non-biological climbing methods that utilize true continuous contact with the surface, no phase change is usually needed unless it is transitioning between two surfaces (e.g. from a horizontal to vertical surface). Regardless, while this analysis is inspired by biology and limbed animals, these fundamental bodies, forces, and actions remain generally

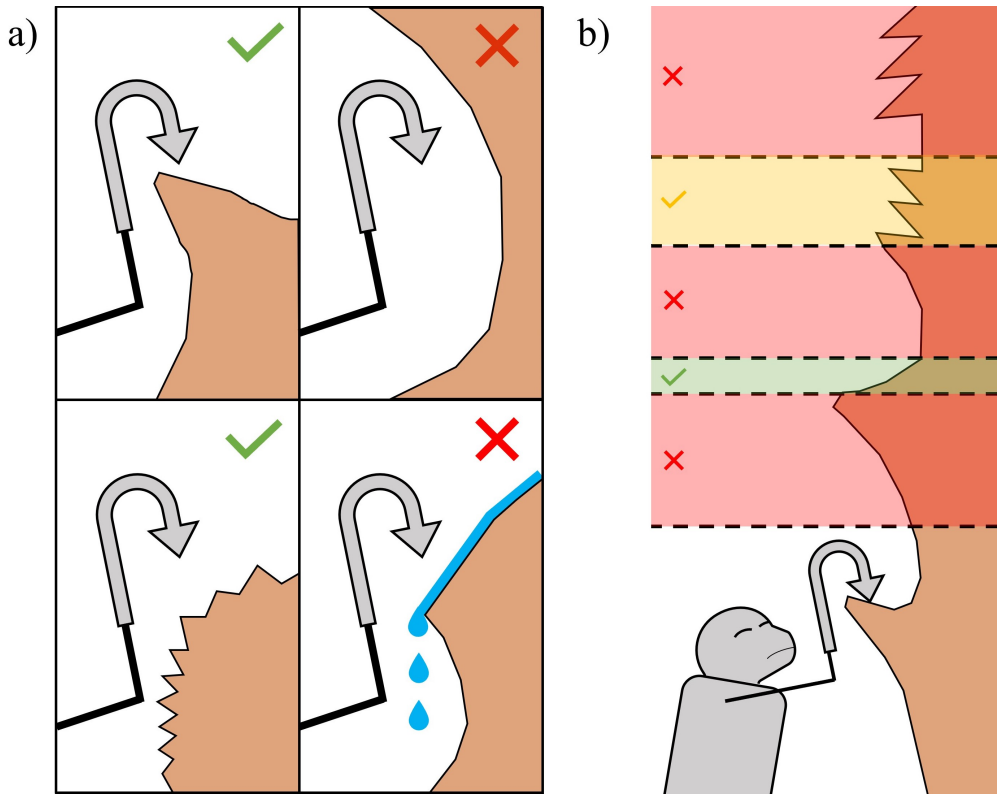

Figure 2.2: a) Example surface topologies and surface conditions for a hook-based gripper. Surfaces with convex topology are viable, but concave topologies are not. Surface roughness can make a point more favorable, while a wet surface may disqualify an otherwise viable point. b) Example of anchor point identification process. Red regions are not viable for anchoring due to surface topology. The yellow region has suitable surface topology, but is not within the reachable workspace. Only the green region has both viable surface topology and is within the reachable workspace.

consistent regardless of morphology.

2.3 Preferred Attributes For Climbing

With the fundamental requirements for climbing clearly outlined, we can identify some key performance metrics and physical attributes that are preferable for climbing robots:

A) High Climbing Speed

A higher raw *climbing speed* allows for more tasks to be completed in a shorter mission time. Normalized climbing speed is also commonly measured to analyze scaling effects, described in bodylengths per second. Since a dog-sized robot will generally walk faster than an insect-sized one, the normalized speed tells us how comparatively fast a robot is for its size. An important part of this is how quickly the robot can identify suitable anchor points and attach/detach from the surface, since this cycle occurs for every single step.

B) High Payload Capacity

Payload capacity is the amount of additional weight the robot can climb with, not including its own weight. A higher payload is beneficial since the robot can carry more task-specific equipment such as measurement instruments, manipulators, or drills, which can weigh several kg each. To convey how comparatively strong the robot is for its size, we use normalized payload capacity, or payload-to-weight ratio, which is also a common metric for studying climbing robots. This is especially important for space missions that have very strict weight and size budgets.

C) Large Reachable Workspace

Since performing useful work in a complex 3D real-world environment can require traversing obstacles or gaps at various scales, it is highly preferred for climbing robots to have a *large reachable workspace*, especially in environments where viable anchor points are spread out or limited. This can allow the robot to reach past larger obstacles, slippery regions, holes, or patches of weak substrate. To simplify this concept, we can look at a robot's *step length*. Also known as *stride* or *stroke length*, this is the maximum distance traveled between each attaching/detaching instance, and indicates the robot's ability to overcome surface obstacles.

Large step length has many other benefits, as it reduces the number of steps needed to travel a given distance. This improves climbing speed, since it reduces the time spent between steps for motion planning and identifying suitable anchor points. This also improves safety by minimizing the number of chances that adhesion can fail between steps.

Small step length is a major limitation for existing climbing robots that restricts their practical use. Wheeled climbing robots are severely limited since their need for continuous contact only allows access to points directly next to them. This gives them a reachable workspace of essentially zero and makes them unable to overcome small obstacles. Legged robots do have the adaptability to overcome larger obstacles, but are currently limited by their dependence on ground-based designs that are poorly suited for climbing. These typically use rigid links that mimic animal limbs for ground-based movement, with solid metal inner structures and outer shells to support loads in arbitrary directions. Most multi-legged robots have relatively small step lengths, preventing them from stepping over obstacles larger than 10-20 cm [10, 20, 21]. Inchworm robots have a larger reachable workspace since their main body and limb are essentially the same structure, with step lengths of 30-75 cm [4, 11].

D) Lightweight

Climbing robots are preferred to be *lightweight* for power, scaling, and safety reasons. Since the robot must constantly be able to support its own weight against gravity, lower mass is ideal to reduce the energetic cost of climbing. Lower mass also helps prevent the substrate from breaking, especially when climbing brittle surfaces like tree bark, since it affects both F_g and F_L. It also makes the robot more likely to survive a fall due to the lower impact forces from less mass.

Most existing legged robots have a significant amount of excess weight stemming from two main issues: 1) excessive weight from limb structures, and 2) excessive actuators from overly complex robot morphology. As previously mentioned, excess weight from limb structures is due to their reliance on bulky and rigid ground-based designs, which can contribute 20% to 40% of the total weight depending on the robot's morphology.

Actuators account for an even higher proportion of excessive weight, especially for robots that mimic multi-limbed animals with quadrupedal or hexapedal forms [20, 21, 22]. For common legged robots such as Boston Dynamics' Spot, actuators can constitute 30% to 60% of their total weight, which they have to carry constantly even if the extra adaptability is only needed for infrequent motions like climbing stairs. This weight problem is further exacerbated with multiple limbs, as Spot's quadrupedal form and 3-DOF limbs result in 12 actuators total being added to its weight.

E) Strong, Fast, and Reliable Adhesion

Climbing robots require a strong, fast, and reliable adhesion method for safety and utility reasons, since adhesion F_a and friction F_f are vital to support the robot against gravity. There are a few main attributes for adhesion that are desirable.

First, the ability to generate a high adhesion force is beneficial, since it gives a more sturdy attachment and allows a higher payload to be carried and thus, more useful task-specific equipment. While adhesion strength is valued, it is important to note that the adhesion force must also be easy to both engage and disengage while climbing.

Second, the time spent to attach or detach is preferably minimized, as several robots have their maximum climbing speed limited by the time spent attaching and detaching.

Third, it's important to have a high reliability and probability of success, since each method having a different mode of failure in certain situations. For example, an attachment attempt may be unsuccessful when a pneumatic suction robot gets an imperfect seal on the surface, or when a microspine array does not encounter enough suitable rock micropores to grip on.

Finally, it's important to consider whether the adhesion method is active or passive. Active adhesion methods require a constant power supply to stay attached, like vacuum suction with a fan, while passive adhesion methods do not require power to stay attached, like a suction cup that remains stuck to a surface once it's placed. In general, passive adhesion is preferred since it reduces overall power consumption and allows the system to "perch" on a surface for an extended duration. It also ensures the robot will not fall in the event of a power loss.

F) Compact Body

Climbing robots should preferably have a *compact body design* with their COM close to the surface, since this decreases the pitch-back moment arm d_{COM} and M_{COM}, reducing the likelihood of adhesion failure. Compact size also allows the robot to access a greater range of spaces, such as the corners of trusses or small cracks in caves.

Most legged climbing robots have animal-based legs that extend away from the main body,

which increases M_{COM} as the COM is further from the wall. This poor mass placement causes these systems to require much stronger adhesion mechanisms to compensate for M_{COM}.

G) Redundancy

Since transitioning between each step can result in slippage, climbing robots value *redundancy* in the form of multiple limbs or wider gripper contact areas. This increases safety and reliability, since overall adhesion to the surface can still be maintained in the event of a localized failure.

However, systems with redundant limbs have significant problems with excess weight and other major issues. Controlling and planning for multiple limbs greatly increases system complexity and has a negative effect on motion planning and gait, resulting in slow climbing speeds. This is especially pronounced when free climbing in unstructured environments, since multiple limbs must be coordinated and each step requires the full identification, attachment, and detachment cycle. For example, LEMUR-3 climbs very slowly due to its requiring 3 minutes to attach and detach between each step [20]. Multi-limbed robots can also have undesirable dynamic effects due to their bilateral symmetry, with off-center legs that cause twisting moments while climbing at higher speeds [23].

H) Low Cost

Climbing robots are preferably low-cost for several reasons. Since they are usually deployed in dangerous environments, lower cost allows a robot to be more easily replaced if the unit is damaged from a fall or from chemical or electrical hazards. Lower cost of production also means that units can be deployed in more missions, since more units can be made for a given budget. If multiple units are deployed at once, large-scale inspection tasks can be completed even faster.

Most legged climbing robots are very expensive to produce. As previously mentioned, this is primarily due to their large number of excess actuators from their ground-based designs, since actuators are often the most expensive parts of a robot.

2.4 EEMMMa and EEWOC Design Focus

With the fundamental requirements of climbing now clearly understood, we can now discuss how EEWOC's novel design focuses on enhancing these desirable attributes:

A) High climbing speed: EEWOC's single limb design, inchworm-type gait, and very long step length greatly simplifies system complexity and motion planning, reducing the total time spent for attach/detach cycles.

B) High payload capacity: For a given motor size, the power required to lift EEWOC's own weight is greatly reduced due to its lightweight design. As a result, more motor power is available for carrying a useful payload, giving EEWOC an excellent strength-to-weight ratio compared to other systems.

C) Large reachable workspace: EEWOC's tape spring limb can extend up to 1.2 m, much further than a conventional limb's reach of 0.1-0.2 m. EEWOC's workspace is further enhanced by its ability to actively bend its limb, allowing it to reach around corners and obstacles.

D) Lightweight: Similar to climbing with a grappling hook and cable, EEWOC's tape spring provides a long-reach structure that is very strong when loaded in tension. When climbing as shown in Fig. 2.1, the upper limb almost always experiences only tensile loads from the F_g and F_L, since the main body's COM is at a lower height. This asymmetric loading condition allows the limb structure to be reduced to a thin extendable tape. While conventional limbs can weigh 20-40% of the system's weight, EEWOC's limb only weighs 155 g thanks to its very thin structure. At only 8.6% of

the total mass, the limb is extremely light for its large size.

EEWOC saves even more weight by minimizing the number of actuators through two methods: 1) a highly simplified morphology, and 2) by replacing actuated DOFs with various passive, compliant, and switchable mechanisms. EEWOC uses a minimum set of powered DOFs necessary for climbing, and further simplifies the two-link inchworm form by replacing the lower link with two wheels for bracing against the surface while climbing. The wrist and wheel drives utilize switchable mechanisms to repurpose existing motors for additional controllable DOFs.

E) Strong, fast, reliable adhesion: EEWOC uses magnetic adhesion for its simplicity and reliability. Magnets have higher reliability than other adhesion types due to their ability to apply adhesive forces to the surface from a distance, which naturally assists with pulling the gripper into contact.

F) Compact body: EEWOC's design concentrates its mass into a point that remains very close to the wall. Since the limb tape can be spooled and deploys prismatically, its mass stays as close to the wall as possible. Its main base concentrates additional electronics and drive components into a thin space below the limb module, which can be rotated to move the COM even closer to the wall, minimizing the pitch-back moment M_{COM}.

G) Redundancy: Despite only having one limb, EEWOC still possesses some redundancy thanks the positioning of its belly gripper. Unlike other inchworm robots which must move their grippers away from the wall during each swing phase, EEWOC's belly gripper remains positioned directly against the wall while climbing. If the top gripper fails, EEWOC's belly gripper can be quickly reactivated to adhere to the wall, assisted by the magnetic force pulling it into contact.

H) Low cost: EEWOC's simple, lightweight construction, plastic frame, and use of passive, compliant, and switchable mechanisms make EEWOC relatively inexpensive to produce, with a single prototype costing around $1250 USD.

Chapter 3

EEMMMa: Elastic Extending Mechanism for Mobility and Manipulation

3.1 Mechanical Design of EEMMMa

As described in the previous section, the EEMMMa limb module was developed as a first step towards a robotic system that is better suited towards climbing.

Figure 3.1a shows the EEMMMa prototype, a lightweight 1-DOF robotic limb that uses an extendable tape spring mechanism to demonstrate promising mobility and manipulation abilities. EEMMMa can climb shelves and ladders using compliant hooks, and can ascend rough vertical walls when equipped with microspines. The extendable limb can also morph its shape with a form of mechanical multiplexing. As seen in Fig. 3.1b, the limb can bend using a simple braking function to change the limb's kinematics. This allows a second rotational DOF to be effectively controlled using only a single primary motor. As a result,

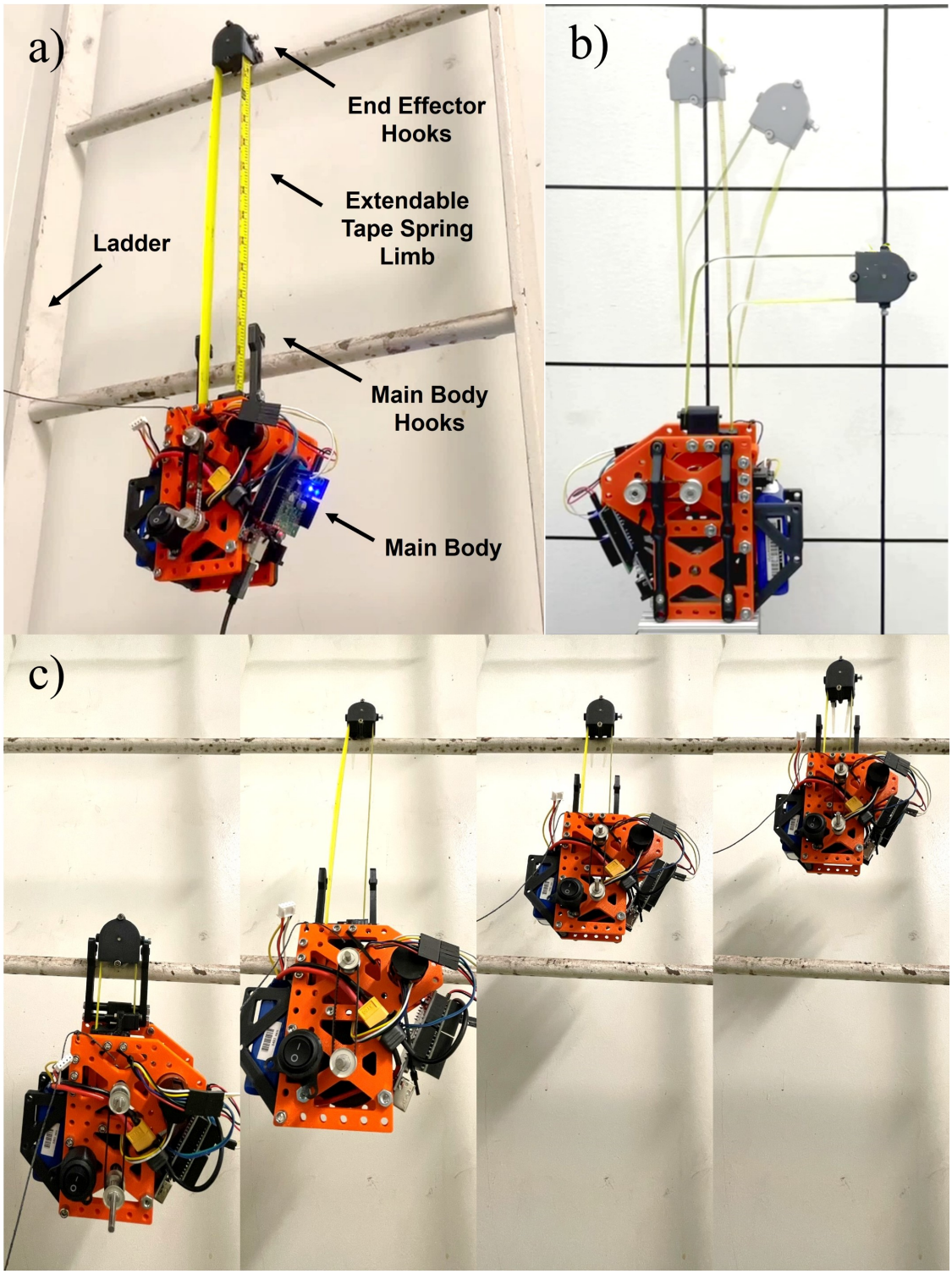

Figure 3.1: a) EEMMMa overview, with main body and tape spring limb. The limb can extend to place hooks on the next ladder rung, allowing it to climb vertically. b) The limb can both extend and bend using a single motor, achieving 2-DOF with a form of mechanical multiplexing. c) Snapshots of the climbing sequence, which can be repeated to scale the entire ladder.

the system is very lightweight, since it can achieve more complex motions without needing additional large actuators at the distal regions. A summary video of its capabilities is in Appendix A.

EEMMMa's ability to both extend and bend grants it great potential as a manipulator, as it can bend around or over obstacles and extend to reach into tight spaces. This could allow it to retrieve distant or submerged objects, position cameras around corners, or place grappling anchors above overhangs such as cliffs. Additionally, the tape's elastic properties enable it to self-correct from perturbations for tasks that require alignment. The limb is also relatively safe to use for manipulation tasks since it simply elastically deforms during a collision or if a target is missed.

EEMMMa's design will be broken down into five main parts: 1) background information on extendable limbs and tape springs, 2) description of EEMMMa's tape spring limb optimized for climbing, 3) an overview of operations, 4) design of the main body containing the motorized spool, tension management subsystems, and electronics, and 5) design of the end effector that serves as the end of the limb, and has a braking function to initiate bending.

3.1.1 Background

Existing Extendable Robotic Limbs

EEMMMa's tape spring based design offers several advantages over existing extendable or bendable robotic limb designs. Conventional extendable limbs that utilize telescoping [29] or collapsible scissor structures [30, 31] exhibit good loading capabilities and rigidity. However, they have high mechanical complexity, relatively poor compactness, and only expand the available robot's available workspace by a few times its body span. Additionally, many bending robotic limbs have recently been developed, with a variety of soft robots and con-

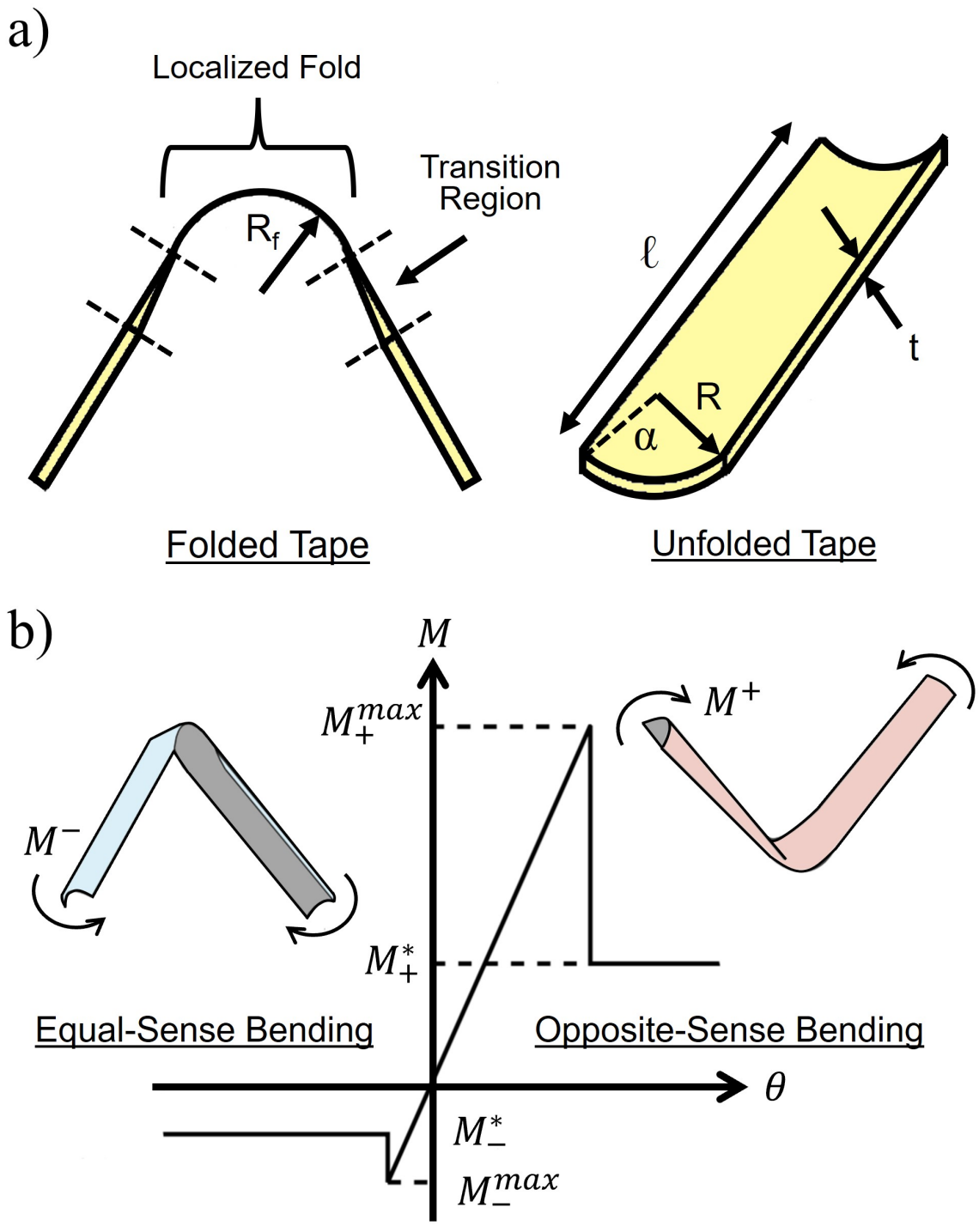

Figure 3.2: a) Geometric parameters that define tape springs. A locally folded segment is shown on the left, with an unfolded tape segment on the right. [27] b) Moment-rotation characteristics of 2D folding. [28]

tinuum arms that offer excellent adaptability to arbitrary geometries that could be useful for manipulation tasks [32, 33, 34, 35]. However, these also suffer from high complexity, requiring complex cable-driven drives with multiple actuators, or accompanying air/liquid systems for pressure-based actuation schemes. This often results in manipulators that are bulky or heavy for their size and poorly suited for use on a lightweight mobile robot. These issues can be remedied with tape springs, which offer far better deployable length with low weight and excellent compactness thanks to their ability to be tightly spooled.

Tape Springs

Tape springs are curved thin shells of material that have the ability to elastically deform and transition between a straight configuration and a folded configuration as depicted in Fig. 3.2a. In this way, localized "folds" generally serve as revolute joints, while unfolded straight segments can serve as links that can withstand significant forces in tension, as well as limited compression forces and bending moments. The rigidity exhibited by unfolded segments can be attributed to their transverse curvature, which increases the energetic cost of bending longitudinally [36, 37].

When folded, tapes exhibit a characteristic longitudinal curvature or bending radius R_f that is unique for each tape depending on its material and geometric properties, including thickness t, swept angle α, and radius of curvature R. Localized folds will naturally form with this radius, although they can be stressed to conform to larger or smaller radii as well. Similarly, the transition regions also have some characteristic length that depends on the tape's material and geometric properties.

Tape springs exhibit several useful features for serving as flexible or structural members. When a moment is applied, tape spring segments will not fold until a peak moment M^{max} is reached. As depicted in Fig. 3.2a, this localized fold exhibits zero transverse curvature and a

uniform longitudinal curvature. If the peak moment is exceeded, the tape spring will exhibit a snap-through buckling behavior with a sudden change in stiffness properties at the fold as it is formed. Tape springs can also unfold passively, exhibiting a level of self-actuation as the tape elastically returns to its unfolded neutral state when bent or twisted [38].

Because of the directionality of the tape's curvature, the value of the peak moment M^{max} changes depending on the direction of the applied moment. As depicted in Fig. 3.2b, tapes subjected to "equal-sense" bending will fold much more easily than for "opposite-sensed" bending [39], which requires a significantly higher applied moment to form a coherent fold. It should also be noted that folds can move, split, and join along the tape's continuous surface, depending on loading conditions. The development and propagation of folds is highly dependent on the loading and boundary conditions present at the end sections of the tape spring [40]. Since the tape is a continuous material,

The benefits of tape spring mechanisms have been previously explored in a variety of fields, but there has been little prior work on utilizing the long range of such mechanisms for mobility or manipulation. Tape springs are used in deployable space structures, including extendable booms [41], automatically deploying solar reflectors [42, 43], and large closed-loop structures [44], which take advantage of tape spring's compactness and ability to self-deploy from a folded position to achieve large structures with little to no active actuation.

One notable example is a planar 3-DOF manipulator for UAVs, which utilizes the long reach of the tape to deploy an end effector below a UAV. This design utilizes a mechanical node that travels along the tape's length to "pinch" and induce a fold to control the bend location and angle up to 55°, and can extend up to 2 m [28]. This system depends on a bulky traveling node that increases system weight and limits its ability to be deployed in directions not aligned with gravity.

Another example is ReachBot [45], which utilizes a mobility scheme similar to our proposed

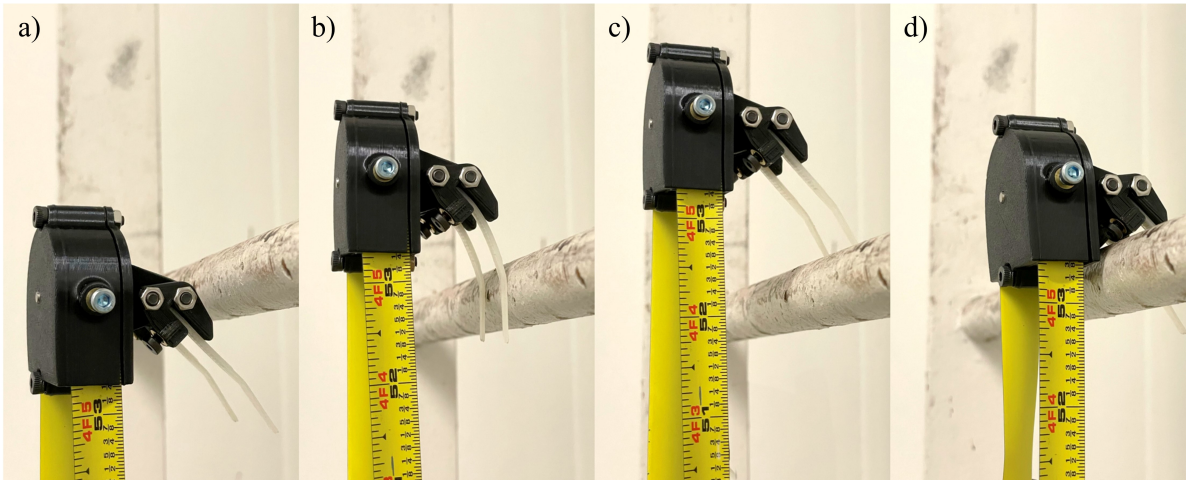

Figure 3.3: Sequence of operations for the compliant hooks. a) The hooks approach the underside of the rung. b) The hooks contact the rung and begin deforming as they continue to rise. c) The hooks pass the rung, and the compliant tips spring to their original shapes. d) The hooks are lowered onto the rung. The reaction force from the angled surface pulls the assembly towards the rung until it settles at the root of the hook, creating a sturdy anchor point.

concept. ReachBot uses single tapes for its limbs that extend prismatically and are designed to be loaded in tension for suspending the main body. Reachbot is intended for use in space or other low-gravity environments, which greatly reduces the performance requirements and weight restrictions of the system as it climbs.

3.1.2 EEMMMa Overview of Operations

Designed primarily to demonstrate climbing on shelves and ladders, EEMMMa is equipped with two sets of compliant hooks to climb successive levels as seen in Fig. 3.1c. The first set of hooks is attached to the end effector. The second set of hooks is located on the main body and serve to anchor the body at the current shelf or ladder rung.

The hook engaging sequence can be seen in Fig. 3.3. As the tape extends vertically, the end effector hooks gently deform to allow them to pass above the next level. The hooks then spring back to their original positions after they clear the level, resulting in a one-way

locking effect. The main body then retracts the spool to reel itself upwards. When the body approaches the next level, the second set of sloped hooks on the body passively guide the shelf or ladder rung onto the load-bearing back portion of the hook, establishing a new anchor point. Once the body hooks pass the next level and establish stable contact, this grappling and anchoring sequence can be repeated.

The overall weight of the system is 685 grams, consisting of a 640 g main body, 35 g end effector assembly equipped with hooks, and 10 g of steel tape.

3.1.3 Tape Spring Limb Design

Tape Structure

EEMMMa's limb is designed to take advantage of tape spring's natural elasticity and ability to be spooled to create a highly versatile and lightweight robotic limb well suited for climbing.

The tape provides the main structure for the limb, and is stored in a spool in the main body. It is folded into a continuous U-shape as seen in Fig. 3.5b. The U-shaped tape has one end connected to the spool and the other end fixed to the main body. This layout essentially creates three tape regions: two unfolded segments placed back-to-back, and a folded segment connecting them that makes up the bend of the U. In the U-shaped bend, an idler pulley passively follows the traveling fold at the "end" of the limb, allowing the end effector to move up and down. The idler and the U-shaped tape form a pulley system that provides mechanical advantage that halves the torque required to lift the main body while climbing. The tape can easily handle loads experienced while climbing, since it is loaded almost entirely in tension.

When tape springs are placed back-to-back, the overall structure exhibits significantly improved stiffness, since one of the tapes is subjected to opposite-sense bending regardless of

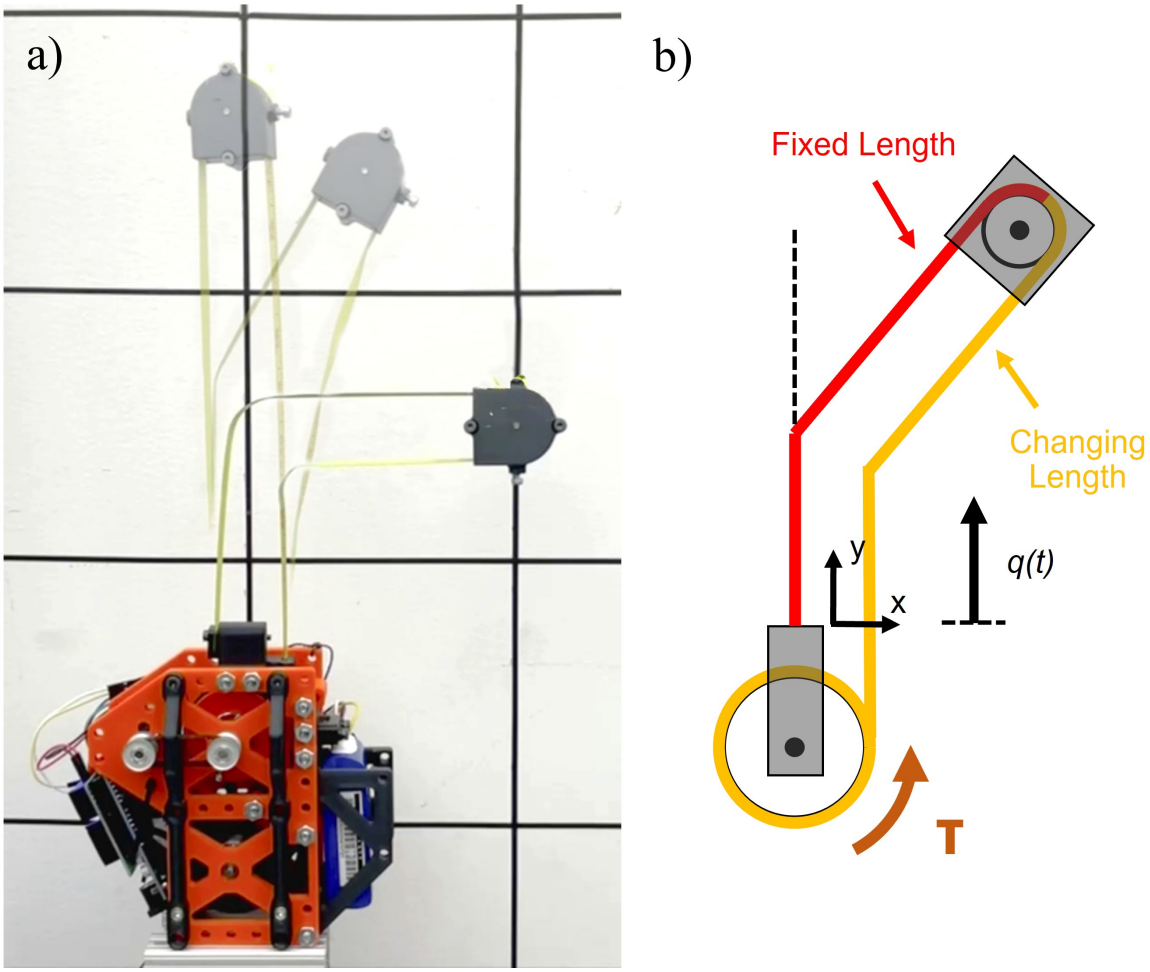

Figure 3.4: a) Overlaid snapshots of the bending sequence, deployed vertically and bending in the Z-axis. b) Diagram of the internal tape path in "brake" mode. The input $q(t)$ now controls only one side of the tape, and the resulting difference in segment lengths causes the limb to rotate until a fold is generated.

bend direction [46, 47, 48]. EEMMMa utilizes this advantageous property with its U-shape while only requiring actuation of a single continuous tape, unlike past examples that utilize two actuated tapes. This back-to-back support also allows the limb to handle some loads in compression, primarily for supporting the weight of the end effector.

Bending

EEMMMa can initiate shape morphing using a form of mechanical multiplexing to bend the limb, depicted in Fig. 3.4a. This effectively grants the arm 2-DOF capabilities with only a single main motor, minimizing weight.

Inducing a bend is simple and only involves two steps. First, the system's kinematic mode is switched by manually activating a braking function at the end effector. The brake is activated by rotating a small screw, which presses a rubber pad against the tape's surface and idler pulley. This locks the end effector relative to the tape's surface, creating a local "fixed" boundary condition. The "fixed" boundary condition causes the tape to have two distinct segments as seen in Fig. 3.4b, with the left segment stuck at a "fixed" length, and the other segment able to change length when the spool is actuated.

When the tape is retracted, the disparity in lengths causes the end effector assembly to rotate until folds are generated, which functionally serve as revolute joints as seen in Fig. 3.4b. The fold can easily be undone by extending the tape, which allows the folded tape to elastically return to its straightened unstressed state. In this way, the tape's natural elasticity serves as repeatable self-actuation similar to other lightweight spring and motor agonist-antagonist actuation schemes, except that the spring is the structure itself [38]. This simple on-off braking function allows EEMMMa to bend with minimal added weight, effectively granting the arm 2-DOF capabilities with only a single main motor, although it cannot actuate both DOF simultaneously. While the braking function requires manual activation for this proof-of-concept prototype, future versions have this feature fully automated.

It should be noted that EEMMMa is only intend to bend in a single "forward" direction, since bending was found to be much easier to initiate when the spool was retracted rather than extended. This is because retracting pulls the tape in tension, allowing it to transmit loads much better than for compressive loads. Additionally, when the limb is bent, one

tape segment experiences equal-sense bending and folds more easily, while the other tape segment experiences opposite-sense bending and serves as the main structure for supporting loads due to its greater rigidity. The tape's U-shape was chosen to be oriented with transverse curvatures facing outward so the fixed length is loaded in opposite-sense while bending. This allows it to serve as a better structure for reliably producing a coherent L-shaped limb.

The material used is a uniform segment of pre-stressed steel tape cut from a Pittsburgh brand 12 ft. x $\frac{1}{2}$ in. tape measure, with a 0.006 in. thickness. This tape width of $\frac{1}{2}$ in. is relatively small when compared to 1-$\frac{1}{4}$ in. used in other projects [28, 49]. This results in reduced bending stiffness and limb rigidity, but also easier shape morphing since the peak moment required to induce folds is lower. Since this prototype was designed for climbing, the reduced bending stiffness is inconsequential since the tape is almost always loaded in tension. The tape's total length is 1 m, allowing the limb to extend 50 cm away from the main body. This distance was chosen specifically for climbing ladders, which commonly have rungs with 4 cm diameter, spaced 30 cm apart. Both ends of the tape have 3 mm holes drilled in their centers to rigidly connect to the spool or frame.

3.1.4 Main Body Design

The main body forms the primary structure that houses the motorized spool, tension management subsystem, and electronics. These components are placed in specific locations to make the center of mass close to vertically aligned with the tape axis. This is to reduce pitching moments that can disrupt hook alignment while climbing or cause the system to fall [50]. The frame is primarily composed of 3D printed PLA and steel fasteners, and measures 130 x 140 x 95 mm. One end of the tape is attached to a 40 mm diameter spool with a bolt. The 3D printed spool is mounted to a 4 mm steel shaft with an aluminum hub. The spool then connects to the motor using an MXL timing belt and aluminum pulleys. A

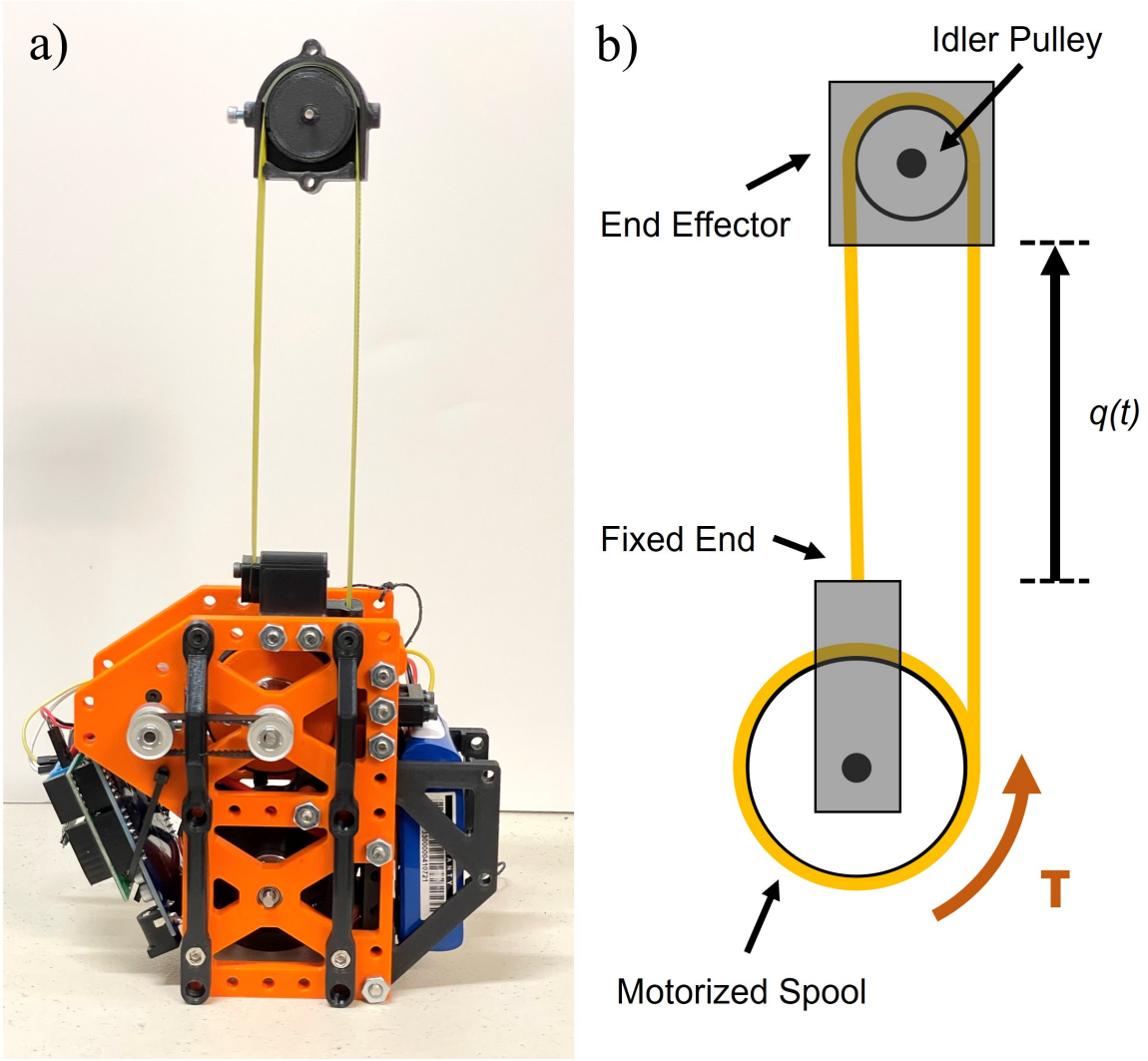

Figure 3.5: Overview of EEMMMa's tape mechanism. a) The prototype in basic prismatic configuration, with end effector casing removed to show the continuous U-shaped tape path. b) Diagram of the tape path, with the extended length $q(t)$ as the input variable.

belt drive system was chosen due to its small size and light weight, with the MXL being the most easy to source despite their lower performance compared to other belts. The motor chosen was the Pololu 25D HP 12V 47:1 DC motor with encoder. This motor was chosen to give EEMMMa a good balance of lifting torque and speed, able to deploy the arm to its full length in two seconds. It also has a high enough gear ratio to make it non-backdrivable, allowing the spool to maintain its current position while climbing without supplying power.

The spool's radius has design limitations, mainly that it must be larger than the tape's characteristic bend radius which is 14.5 mm for EEMMMa's tape. While this means the spool can be designed with a diameter as small as 29 mm, a diameter of 40 mm was chosen instead to reduce internal spool tension from coiling too many layers tightly. This also increases the speed that the tape deploys at for better climbing performance.

A CAD model of the main body drive system can be seen in Fig.

Tension Management

To maintain tension inside the spool, the spool is surrounded by an outer casing with a small exit hole to confine the coiled tape loops. Without a radial inward force to keep the spool tight, the coiled segments will unwind themselves or push out of plane due to instabilities while coiled [51]. The inside of the spool casing is lined with a strip of slippery PTFE film to reduce friction when the spool rotates. This spool casing is a much simpler alternative to other tension management systems. In industrial manufacturing settings for spooled materials like plastic or cloth, tension is usually maintained using a series of passive wheels and springs that press against the outside of the spool as it rotates to keep it tight. Early prototypes of EEMMMa used this wheel system, which proved to be unsuitably bulky and heavy from all the rotary components. With the PTFE film on the inner casing, the spool is kept confined with fewer moving parts, although the film does wear out and needs

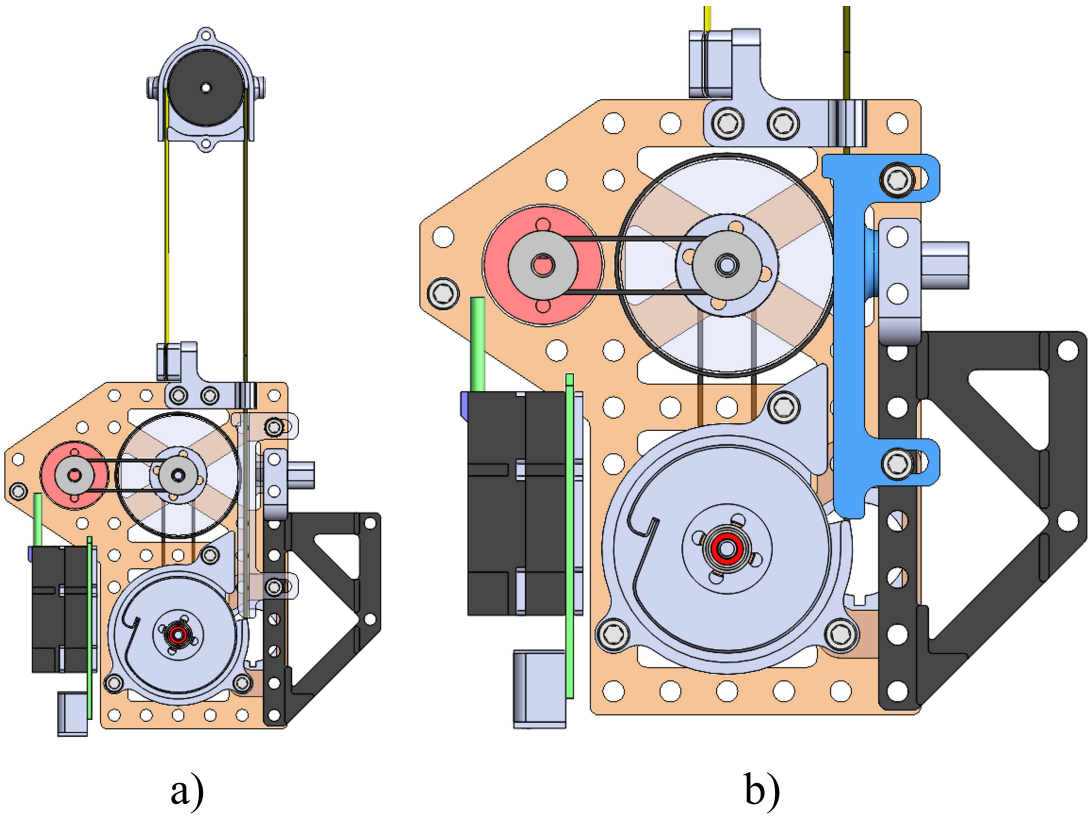

Figure 3.6: a) CAD of EEMMMa limb internal layout, showing the overall U-shaped tape and drive pulleys. b) Close-up view of the main body. The top output roller is transparent to show the drive pulleys behind it. The tension management backing channel is highlighted in blue, which presses against the tape and the output roller to maintain tension.

to be replaced after several hundred retractions.

After leaving the spool, the tape is then fed into an output roller, which is mounted on a second steel shaft. This can be seen in Fig. 3.6a, where it is transparent to show the drive belt behind it. The roller is covered with a non-slip rubberized surface (nitrile or Buna-N rubber tape) to grip against the tape, maintaining a tension force inside of the tape that keeps it properly coiled inside the spool. The spool and roller have the same diameter and are geared 1:1 using MXL timing belts to ensure the tape deploys smoothly. It is important to note that the spool diameter changes slightly as the tape is deployed, reducing slightly with each centimeter. This can cause the output roller and spool to not feed at a 1:1 rate, which can cause tensioning problems inside the spool. While this is a common problem for longer spooled materials that get deployed for hundreds of meters, EEMMMa's thin tape and relatively short deployment length means that this diameter only changes from 40 mm to 44 mm when fully spooled, so this does not have a significant effect on the current system.

Positioned opposite the roller is a thin channel lined with PTFE film that keeps the tape pressed against the roller, and a small screw can be turned to adjust the distance between the roller and the backing channel to ensure the appropriate amount of friction is applied for gripping the tape. This backing channel can be seen highlighted in blue in Fig. 3.6b. Early prototypes of this system instead used a passive wheel to apply the opposing force, but this was more complex, consumed more space, and was not adjustable like the final version.

Finally, the tape exits the main body at the output hole, which is spaced some distance away from the output roller to allow the tape to transition from its stressed flattened state to its natural unfolded state. This is to ensure the tape deploys in an unfolded state for maximum rigidity. The output hole has a curved shape that follows the tape's transverse curvature to further increase rigidity. When there are disturbances from forces at the end effector, the output hole's curved surfaces force the tape to retain its more rigid unfolded shape and reduces the likelihood of a stress concentration which may result in an unwanted fold.

Body Hook Grippers

The main body also features the first set of compliant hooks for climbing, which operate in the sequence depicted in Fig. 3.3. The ends of the hooks are made of angled zip-ties that gently deform as they pass a shelf or ladder rung. The hooks then spring back to their original states after they clear the next level, resulting in a one-way locking effect. The zip-ties then serve as slopes to passively guide the shelf or ladder rung into the load-bearing back portion of the hook, which is made of PLA. Once loaded, the hooks serve as a sturdy anchor. The hooks are spaced laterally to minimize unwanted twisting moments on the body. They also provide an anchor point that is close to vertically aligned with the main body's center of mass, to minimize unwanted peeling-back moments while climbing.

Electronics and Computer

EEMMMa's subsystems are powered by a Turnigy 1300 mAh 3S 30C Lipo pack, weighing 107 g. The 11.1v output is supplied to the microcontroller and motor driver, with an on/off rocker switch between for disconnecting the battery. For the microcontroller, an Arduino Uno was chosen for its simplicity and availability. The Pololu Dual TB9051FTG Motor Driver Shield was chosen to interface with the Uno and the spool's DC motor. This was chosen for its ability to supply the motor's 5 A peak current at stall, which may be necessary while lifting heavy loads.

EEMMMa's software is programmed in C++ and uses tethered serial communication from a laptop to send commands to the motor. The tether wire was chosen to be as long, compliant, and thin as possible to minimize the effect of any forces or torques being transmitted to the main body. The program uses basic PWM to control the motor's velocity.

A variety of commands are mapped to keys for easy user control. Simple commands use

open-loop control, sending a desired PWM value to make quick adjustments to the motor's position. More complex commands involved programming a sequence of movements for tasks like climbing consecutive levels on a ladder or shelf. These commands use closed-loop position control with feedback from the motor encoder to ensure that the end effector was deployed to the appropriate height before retracting. Assuming no slippage, the motor encoder data and and spool radius can be used to calculate the current extended height of the limb. No other sensors are needed since ladder rungs and shelves are evenly spaced, although the height between levels has to be manually measured and entered into the program before deployment.

3.1.5 End Effector Design

The end effector assembly provides a structure at the end of the limb for mounting additional mechanisms that interact with the environment, and can be equipped with hooks or microspines. A detailed view of the end effector can be seen in Fig. 3.7. Inside the end effector is the idler pulley, which is wrapped in rubberized tape and is 29 mm in diameter, the smallest allowable based on the tape's previously mentioned characteristic curvature.

This is also the mounting distance between the fixed end of the tape and the spool output, which was chosen to be 29 mm for simplicity to make the tape segments parallel while extending vertically. Changing this mounting distance in future studies may result in different, desirable limb properties. The slight angle between the segments should allow the limb to handle horizontal loads better and can increase the effects of the applied bending torque from the motor, allowing folds to be generated more easily.

An outer casing surrounds the idler and tape. The inside of the casing contains a small PTFE pad at the tip of the tape fold, which allows the end effector casing to transfer loads to the tape in both tension and compression with minimal friction. The casing also prevents

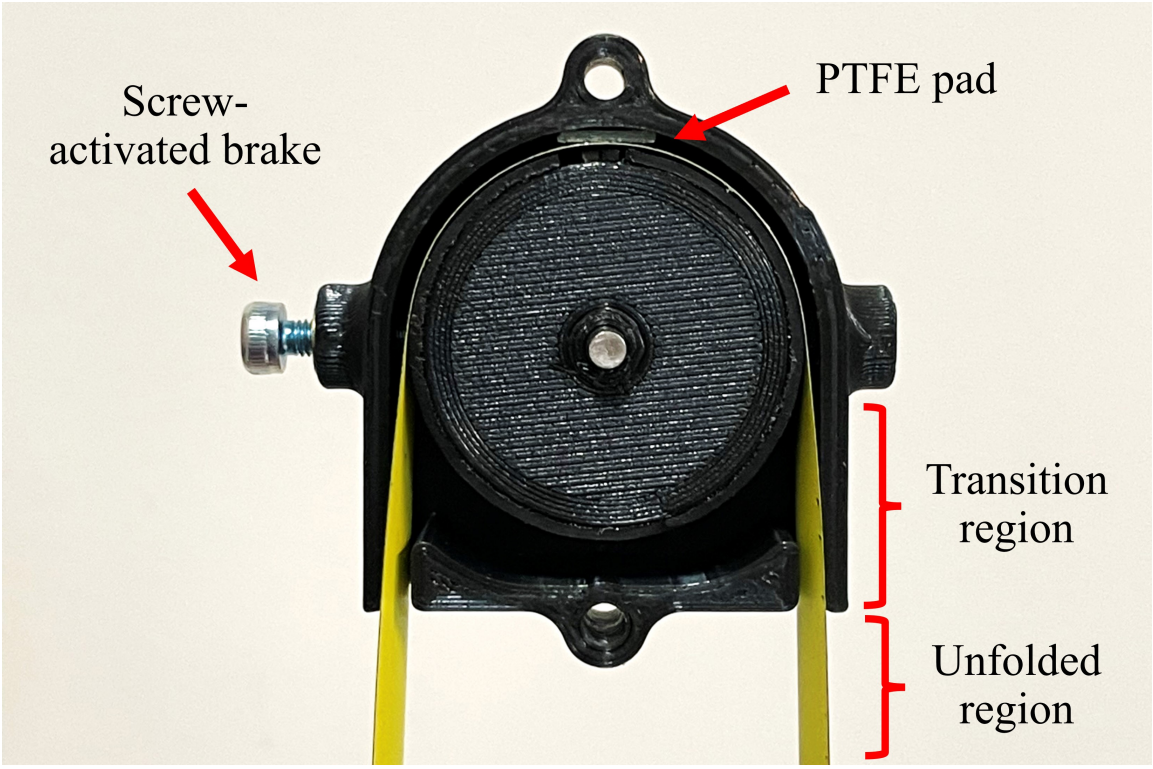

Figure 3.7: a) Close-up view of the end effector with the front plate detached. The screw-activated brake and PTFE pad can be seen. The casing extends beyond the idler pulley to allow the tape to transition into its unfolded state for better rigidity.

the traveling fold from splitting into two separate folds when loads are applied.Much like the tape output hole at the main body, the casing has exit holes located some small distance below the idler pulley's diameter to allow the tape to transition from its flattened stressed state to its more rigid unfolded state. The casing exit holes are also curved to keep the tape in its strong unfolded state when deployed.

The end effector's brake function to initiate bending is very simple and requires manual activation. The brake is activated with a small screw that protrudes from the end effector that can be tightened by hand. The end of the screw enters a hole in the casing and presses a small rubberized pad onto the surface of the tape. This prevents the tape from moving with respect to the casing and the idler pulley, which changes the limb's behavior from extending to bending as previously described. While this feature is not automated on EEMMMa, it serves as a simple proof-of-concept feature to test bending with a lightweight mechanism.

End Effector Hook Gripper

The end effector's compliant hooks operate similarly to the hooks located on the main body. For this 1-DOF design, the hooks are located off-center with respect to the tape. This is because the tape must be located off to the side of the shelf or ladder rung in order to extend past them as depicted in Fig. 3.3. This results in an unwanted pitching moment since the anchor point is not aligned vertically with the main body's center of mass. To compensate for this, both sets of hooks feature small stops to prevent this unwanted pitching moment. Additionally, the hooks are oriented to load the tape in the direction that best resists pitching. Future designs with additional degrees of freedom should be able to avoid this issue entirely by angling the tape as it extends, allowing the center of mass to be located almost directly beneath the anchor point for most of the climbing sequence.

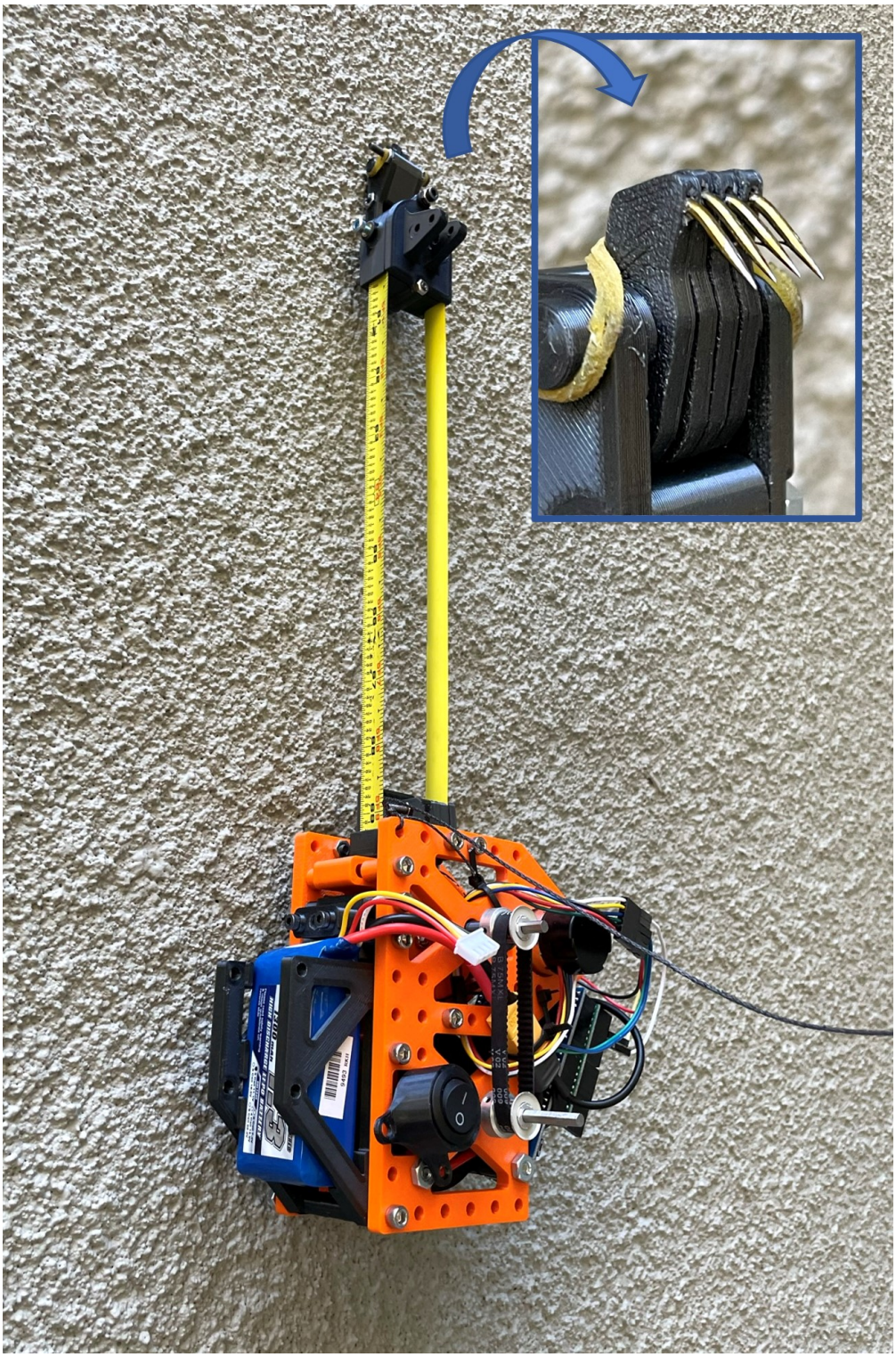

Figure 3.8: Snapshot of EEMMMa climbing a rough vertical wall. The end effector's small microspine array grips into asperities in the rocky surface.

Microspine Grippers

To test climbing on rough surfaces, a small microspine gripper was developed, as depicted in Fig. 3.8. The microspine array is composed of several small steel hooks made from fishhooks, with sharp points that engage in asperities on the rough surface. Each fishhook was cut to reduce its length and placed into a PLA 3D printed outer housing containing a small curved channel that closely matches the hook's curvature. The microspines were then glued into the channels.

Initial tests showed that four spines would be sufficient to carry the weight of EEMMMa thanks to its low weight. The microspine units were placed into an array on a dowel pin that allows them to share loads. The dowel pin goes through a slot in each microspine housing that allows them a small amount of translational and rotational compliance that allows them to share loads properly between each other during engagement. A rubber band is routed around the array to provide a force to bias the spine tips towards the surface for engagement. The microspine array connects to the end effector or main body with a single bolt, allowing for some limited compliance.

3.2 EEMMMa Demonstrations

In the following demonstrations, EEMMMa shows its effectiveness as a multimodal platform for both mobility and manipulation in a lightweight, compact package. Videos of all of these demonstrations can be found in the Appendix.

By leveraging the tape spring's unique properties, EEMMMa can demonstrate climbing, bending, pushing, and pulling. These tasks require only two parameters to be controlled: the length change of the tape, and the on/off of the end effector brake. All demonstrations were performed with simple open-loop control and manual input.

3.2.1 Climbing

To verify the limb's ability to handle loads in tension, EEMMMa was subjected to climbing trials in three scenarios: climbing a shelf, a ladder, and a rough vertical wall.

Shelves and ladders

Trials were first conducted on wire-frame shelves made of 5 mm diameter wire, seen in Fig. 3.9. The shelves had a thickness of 22 mm and were spaced 254 mm apart for a total of 276 mm to ascend per level. EEMMMa can ascend at 19 cm/s, traversing a level at top speed in about 2 seconds. This is about 1.5 body lengths per second (BL/s), which matches that of the fastest wall climbing robots [23]. For ladder climbing trials, straight vertical ladders were used, which are commonly seen in industrial or mechanical environments such as factories, buildings, and ships. The ladder chosen had cylindrical rungs with 2 cm diameter, spaced 28 cm apart for a total of 30 cm to ascend per level. The larger diameter of the ladder rungs caused more significant perturbations from the compliant hooks. When climbing at top speed, these perturbations caused hook alignment issues during multiple climbs in succession, although trials at slower speeds were successful.

3.2.2 Rough Vertical Walls

For the wall scaling trials, the end effector and body compliant hooks were swapped with small microspine arrays, seen in Fig. 3.8. EEMMMa could successfully cling to the wall and ascend small distances. However, this prototype was unable to perform multiple grappling and anchoring sequences in succession due to two main effects. First, the main body's center of mass being slightly off center caused the body to pitch and the limb to extend at an angle. At large extensions, this caused the end effector microspines to be too far away from the

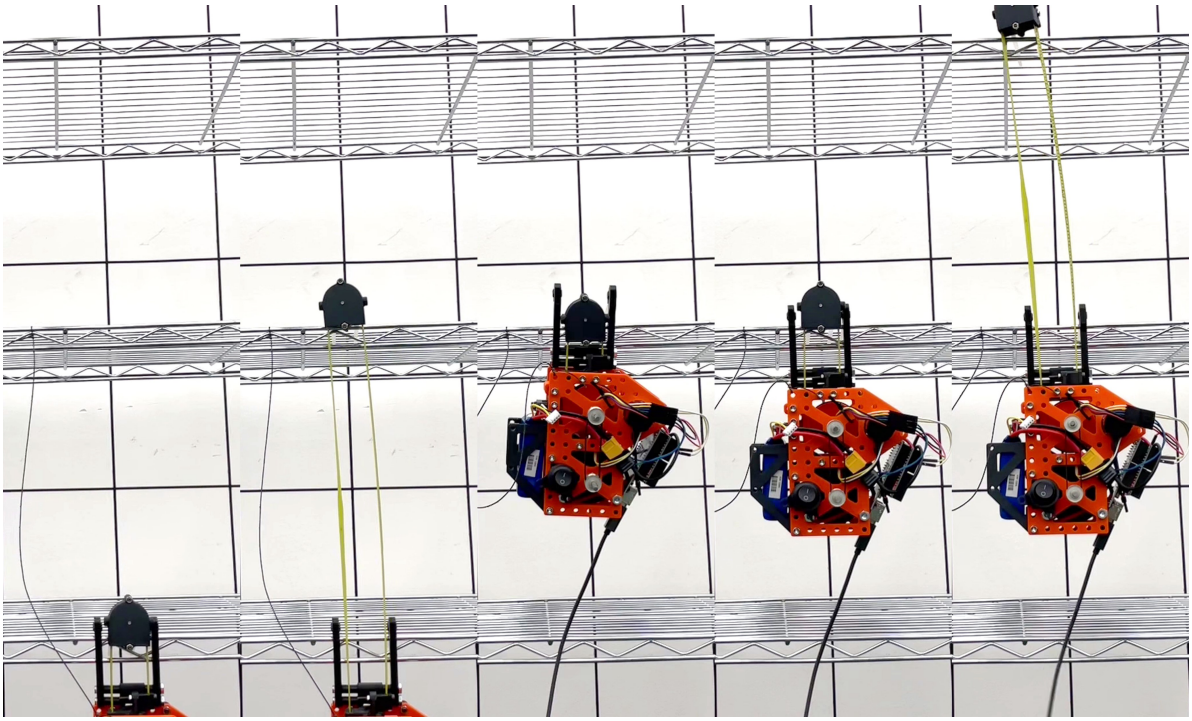

Figure 3.9: Snapshots of shelf climbing demonstration.

wall to engage the surface properly. Additionally, the microspine array footprint was small enough to be approximated as a point contact, which sometimes caused the anchor to twist off the surface during perturbations.

For all climbing trials, the elastic spring properties of the tape proved to be beneficial for resisting unwanted forces or moments at the end effector. Hooks require directional engagement, and they must approach the grappling features at a specific orientation to be effective. This is especially important for microspines, which can peel away or fail to engage if they are not properly aligned with the gripping surface. Because correctional forces are passively supplied by the tape's spring properties, the climbing sequence is robust and simple to control. However, future designs with larger extension lengths and heavier end effectors may experience additional difficulties since the end effector may oscillate over long periods without added damping. These trials demonstrate EEMMMA's ability to pull loads against gravity, which is vital for suspending the main body in midair from above, or for retrieving samples from below.

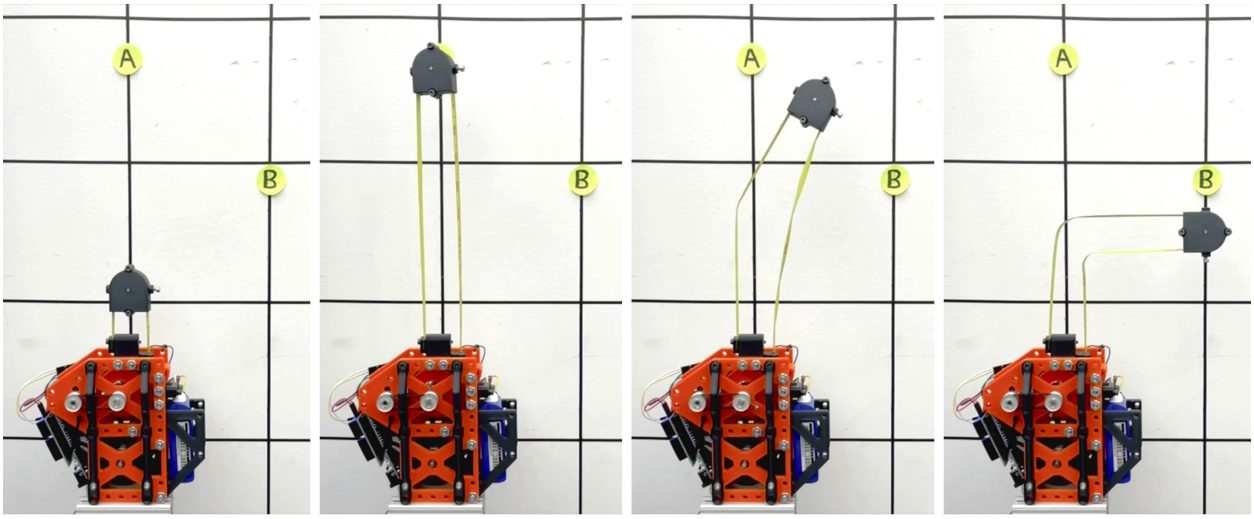

Figure 3.10: Snapshots of EEMMMa bending between two target points, point A (0, 20) cm and point B (10, 10) cm.

3.2.3 Bending

Robotic manipulation tasks commonly require reaching a target in space, so the next set of tests were devised to demonstrate EEMMMa's ability to reach a desired location on a plane using controlled bending.

In-lab Tests

Since it is trivial to reach any single point along the 1-DOF linear path, bending demonstrations involved 2-DOF reaching to two points on the plane, seen in Fig. 3.10. For the first set of trials, the limb was pointed vertically, extending in the direction opposite gravity. This was selected as the most relevant scenario for this system, since climbing actions generally involve vertical movement, and bending would be advantageous for reaching above tables or steps. For the first test, the limb was first extended to point A located 20 cm above the main body at coordinates (0, 20) cm. Next, the end effector braking system was engaged, allowing the motor to initiate limb bending. Actuation was applied slowly until a fold was created in both tape segments, essentially serving as a new revolute joint. After rotating

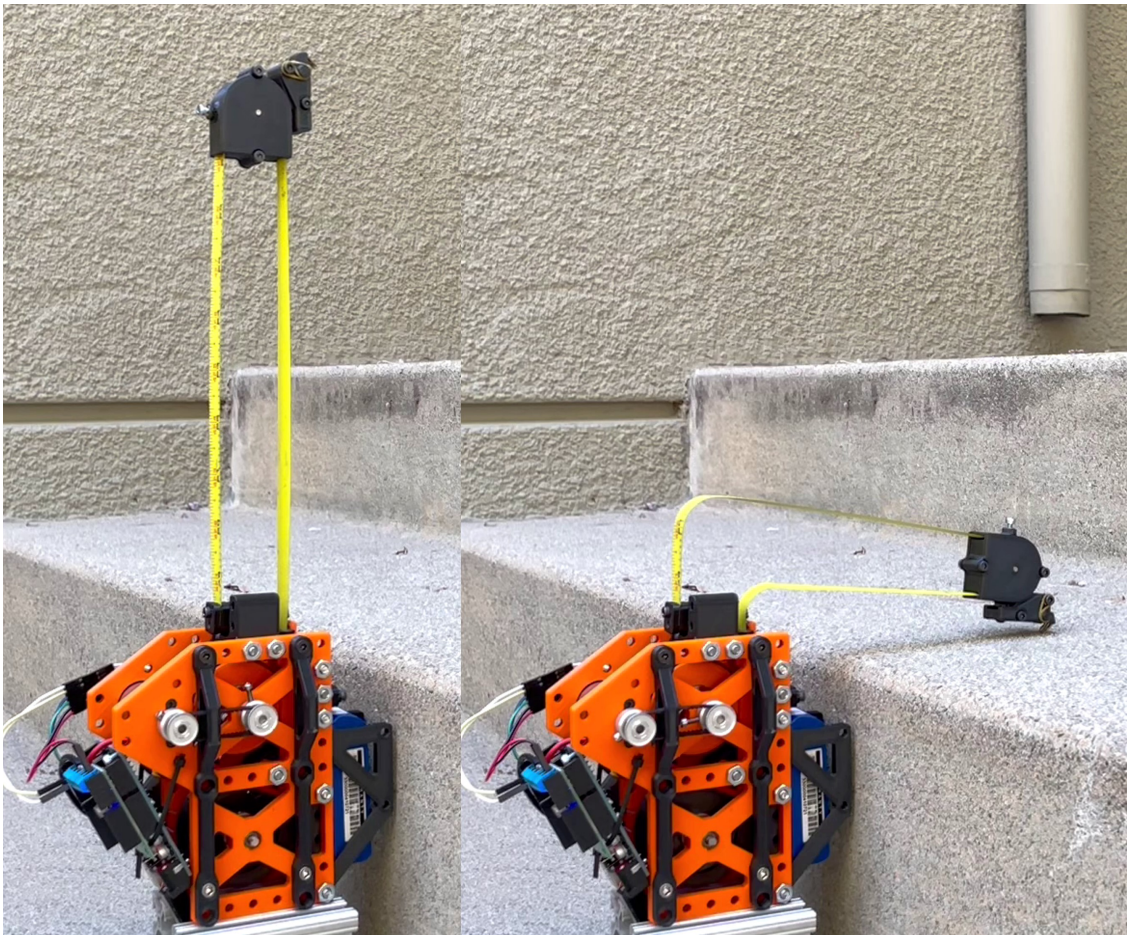

Figure 3.11: Snapshots of EEMMMa bending to place a microspine anchor on the top surface of a step, which is otherwise unreachable by simple prismatic extension.

90°, the end effector successfully reached point B located at (10, 10) cm. Video footage was taken on a gridded background to verify repeatability.

Subsequent bending trials to other positions revealed additional phenomena. Angling the revolute joint more than 100 degrees resulted in the folds suddenly migrating towards the main body, causing the limb to "collapse". Limb collapse also occurred when extending the spool to reach most points in the -X direction (see Fig. 3.4b for axes). This is due to the fixed segment being loaded in equal-sense bending rather than opposite-sense bending, which will cause buckling under a much lower peak moment.

Bending on Stairs

As a test application for bending, EEMMMa was placed on a stone staircase to demonstrate anchoring to the top surface of steps with microspines, shown in Fig. 3.11. Although EEMMMa was not designed to fully climb stairs, these trials still showcase the limb's mechanical multiplexing abilities to reach a target position and orientation that is otherwise inaccessible with a simple prismatic joint. The limb was first extended vertically above the next step, and a fold was induced to angle the end effector downwards.The limb was intentionally actuated to generate the fold close to the base instead of the midpoint to allow the hooks to contact the ground. The tape was then retracted slowly, allowing the spines to fully engage and pull the body in. Test footage showed that the tape's natural spring properties assist with maintaining proper spine orientation during approach, engagement, and retraction.

These preliminary tests demonstrate the potential for EEMMMa to serve as a flexible, long-reach manipulator arm. Future versions of EEMMMa will use these abilities to bend around or over obstacles to position grippers, cameras, or other tools in hard to reach places.

3.2.4 Standing

A simple "standing" test was performed as a demonstration of the limb's ability to handle loads in compression by serving as an extendable prismatic leg, as seen in Fig. 3.12. First, the end effector was placed in a vice with the main body carefully positioned directly above. The limb was extended and the main body was released, with its weight creating a compressive load on the limb. These static loading tests were successful up to 20 cm of limb extension. Beyond this point, the limb's rigidity was insufficient to prevent small perturbations from causing the body's center of mass to shift, which resulted in a collapse. Dynamically extending the limb also caused collapses since reaction moments at the main body resulted in the center of mass shifting and would cause the system to topple over.

Figure 3.12: EEMMMa standing demonstration. The limb is deployed downward, with the end effector secured in a vice. The weight of the main body loads the limb in compression, similar to a weight-bearing leg.

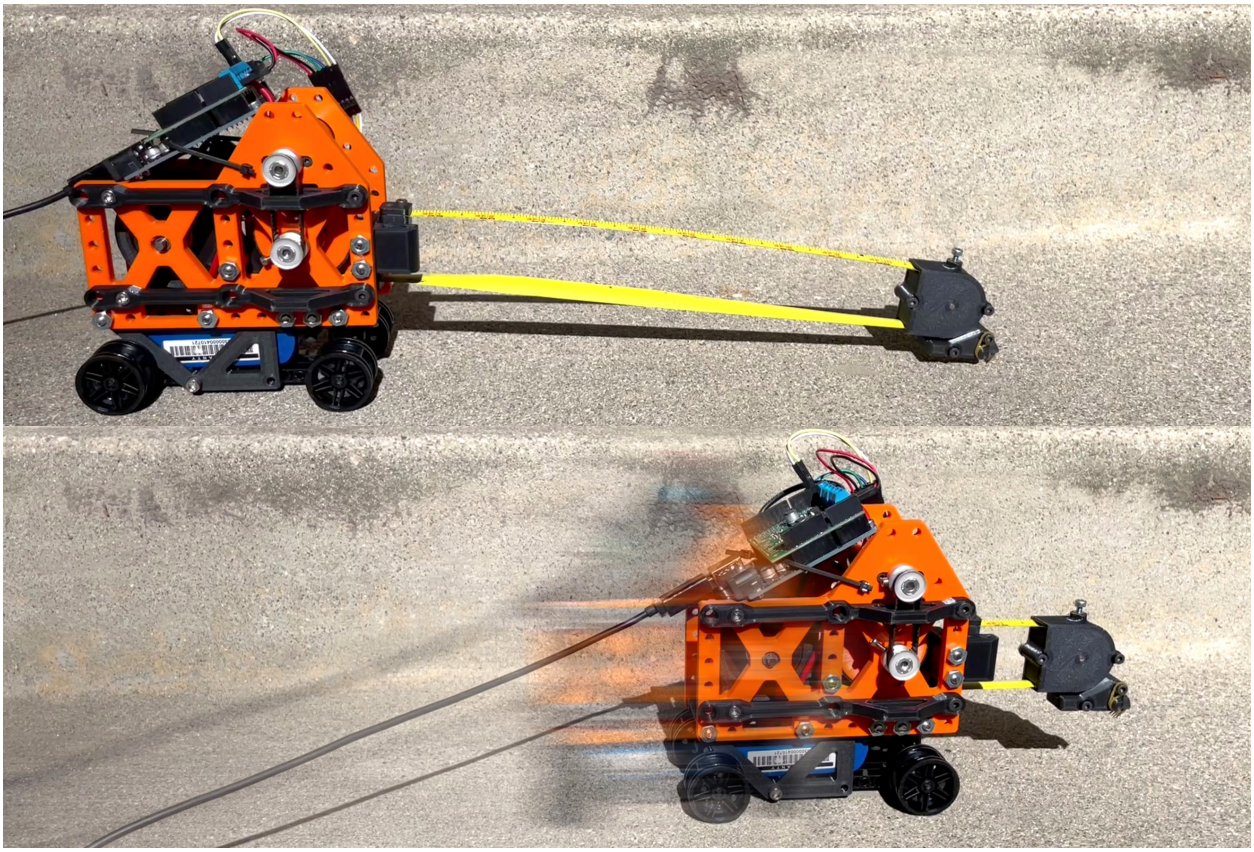

Figure 3.13: Snapshots of EEMMMa crawling demonstration, equipped with passive wheels.

These tests demonstrate the end effector's effectiveness at allowing the limb to handle compressive loads. Because the tape is a single continuous U-shape, loads can be transferred evenly between the two opposing segments. The end effector housing effectively confines the U-shaped tape fold without it splitting or propagating, which would result in a greatly reduced ability to handle loads as a leg or manipulator.

3.2.5 Crawling

As an additional test for mobility, EEMMMa was equipped with passive wheels on the underside of the main body to demonstrate 1-DOF crawling along the floor, depicted in Fig. 3.13. The end effector was equipped with the microspine attachment and the limb was extended. When outstretched, gravity causes the limb to sag slightly, allowing the

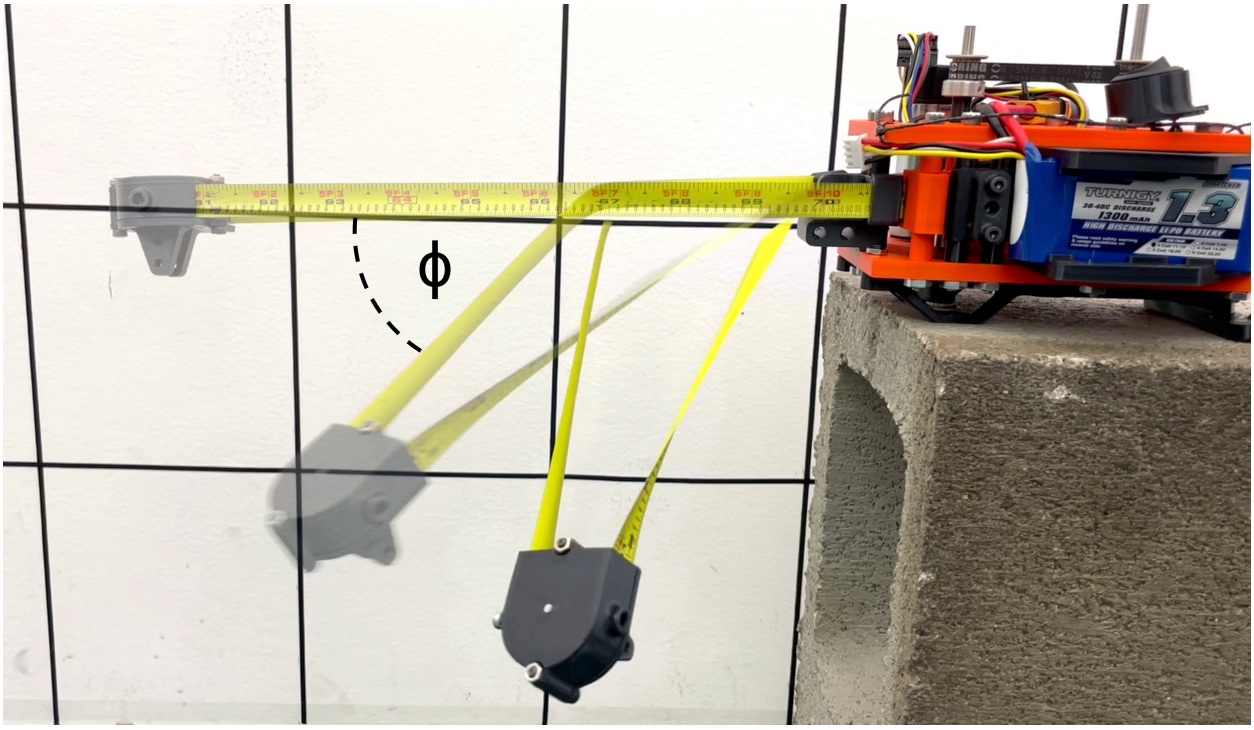

Figure 3.14: Demonstration of out-of-plane bending, where the applied bending moment is perpendicular to the moment from the end effector's weight.

end effector microspines to contact the floor. The tape was retracted slowly to engage the microspines, then a fast retraction pulled the body forward. The main body would then coast linearly on the floor, carried by momentum. As the body approaches the end effector, the microspines would naturally disengage due to the changing angle of engagement. This demonstrates EEMMMa's ability to be used with other mobility schemes, and operate with them in combinations for various effects. For example, this could be useful if a rover lost power to its wheels, but could still operate using its EEMMMa manipulator arm for mobility.

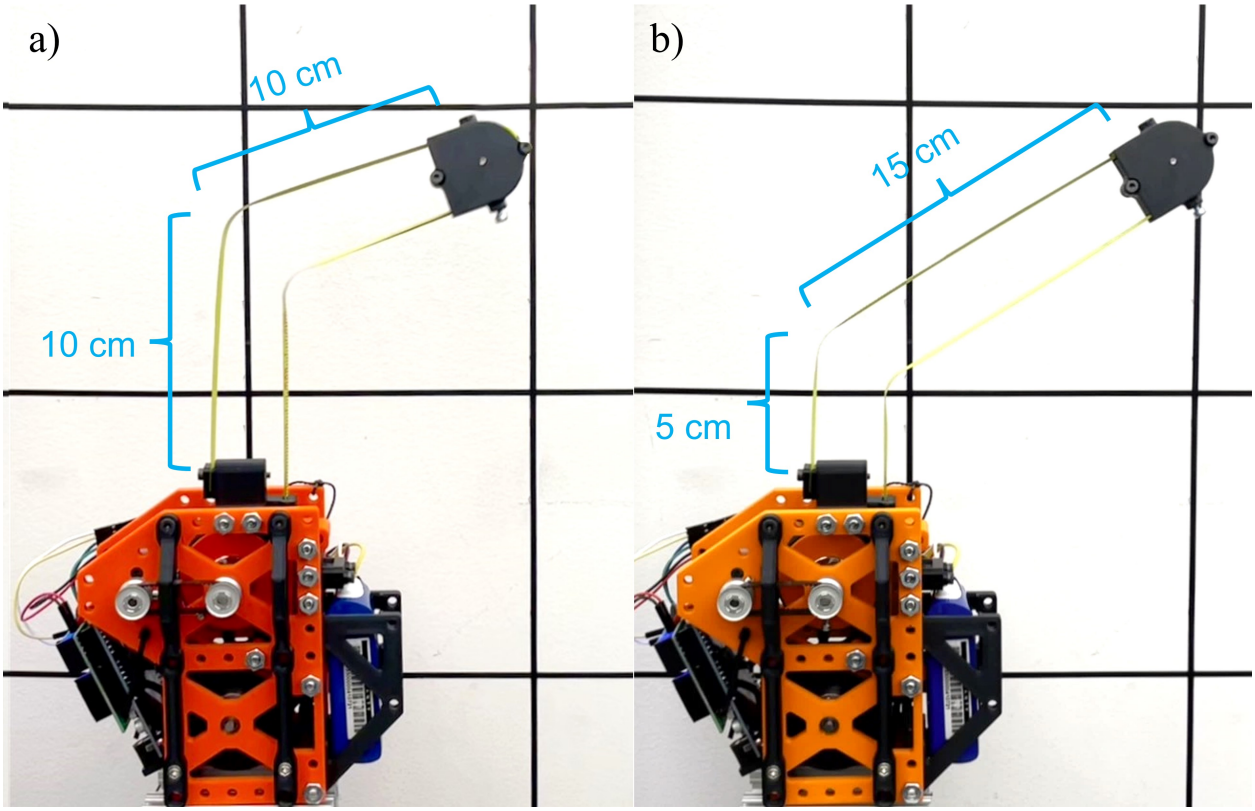

Figure 3.15: Example of the fold location changing from dynamic input. a) Base case where slowly actuating causes the fold to occur at the tape midpoints. b) Dynamic case where actuating in dynamic bursts causes the fold to occur at a different location.

3.2.6 Other Preliminary Investigations

3D Bending

In the bending demonstrations outlined above, all end effector movement occurs in the 2D X-Y plane only. This is because the tape is deployed vertically. Actuating the spool in this configuration applies a bending torque about the Z-axis, and the weight of the end effector generates a torque that is also about the Z-axis. Thus, all rotations and forces cause movement in X-Y only and the system remains in a single plane.

However, when the tape is deployed horizontally as depicted in Fig. 3.14, inducing a fold can cause the limb to bend out-of-plane, resulting in a 3D fold. This is because actuating the

spool applies a torque about the Y-axis, but the moment arm from the weight of the end effector causes a rotation about the Z-axis. In this case, the fold will exhibit both bending and twisting in θ and ϕ. Since ϕ is a function of the Z-axis moment arm, it can be controlled by simply extending the tape. This method allows effective control of the end effector's out-of-plane displacement until the peak moment is reached and the limb collapses. Future versions of EEMMMa can potentially use this phenomenon to grant the limb 3-DOF without another actuator, taking advantage of gravity to achieve out-of-plane movement.

Controlling Fold Location With Dynamic Inputs

Additional tests show that the limb can be manipulated in even more ways if dynamic inputs are used. In preliminary tests, the tape was retracted in short bursts, resulting in oscillations at the end effector. If the tape was retracted again before the oscillations settled, the fold location could be altered depending on the state of the end effector, depicted in Fig. 3.15. The timing of these actuation bursts can also potentially be used to minimize oscillations at the end effector by cancelling out vibrations with well-timed retractions. This phenomenon has been observed in previous tape spring studies where the fold travels due to impulse-momentum interactions [39] where the tape is modeled as a traveling hinge with hinge position and rotation angle as two independent degrees of freedom.

3.3 EEMMMa Experiments and Analysis

This section details preliminary, mostly qualitative and geometric studies of the limb's overall bending behavior to highlight certain phenomena while extending and bending. These observations will be used to form lay down the basis and assumptions for a simplified kinematic model of the system. Fully characterizing the tape's complex nonlinear behavior while

bending is highly challenging and was outside the scope of this initial investigation.

3.3.1 Bending Behavior

Snapshots from the bending trials are shown in Fig. 3.16 which displays three stages of behavior that the limb exhibits as it bends from 0° to 90°. Under normal 1-DOF operation, the tape operates as a single continuous piece of material, moving the end effector as the idler pulley rolls along the tape's length. Activating the brake at the end effector functionally separates the tape into two segments, S_1 and S_2. The actuated segment S_1 on the right is attached to the spool, and has a variable length that can be changed by actuating the motor. The segment S_2 on the left now has a fixed length due to its end attachment to the main body. By retracting the tape, S_1's length is reduced, and the end effector begins to rotate due to the disparity in lengths. As the bending angle increases, the limb goes through three stages of distinct bending behavior:

Stage 1: S_1 and S_2 are both unfolded and behave like beams.

Stage 2: S_2 has a fold, S_1 is unfolded but bends and twists.

Stage 3: S_1 and S_2 both have folds which each behave like a revolute joint.

In Stage 1, depicted in Fig. 3.16a, both tape segments experience a small horizontal displacement. S_2 is subjected to opposite-sense bending, and it can be treated as a single flexible beam until buckling occurs. However, due to the tape's very thin cross-section, this can be considered a large deflection, which exhibits geometric and material nonlinearities that will be studied in the future.

In Stage 2 (Fig. 3.16b), the fixed segment S_2 has folded while the actuated segment S_1 has not, but continues to experience combined bending and twisting. When folded, the curve flattens and the cross section becomes rectangular. Folds will generally occur at the midpoint

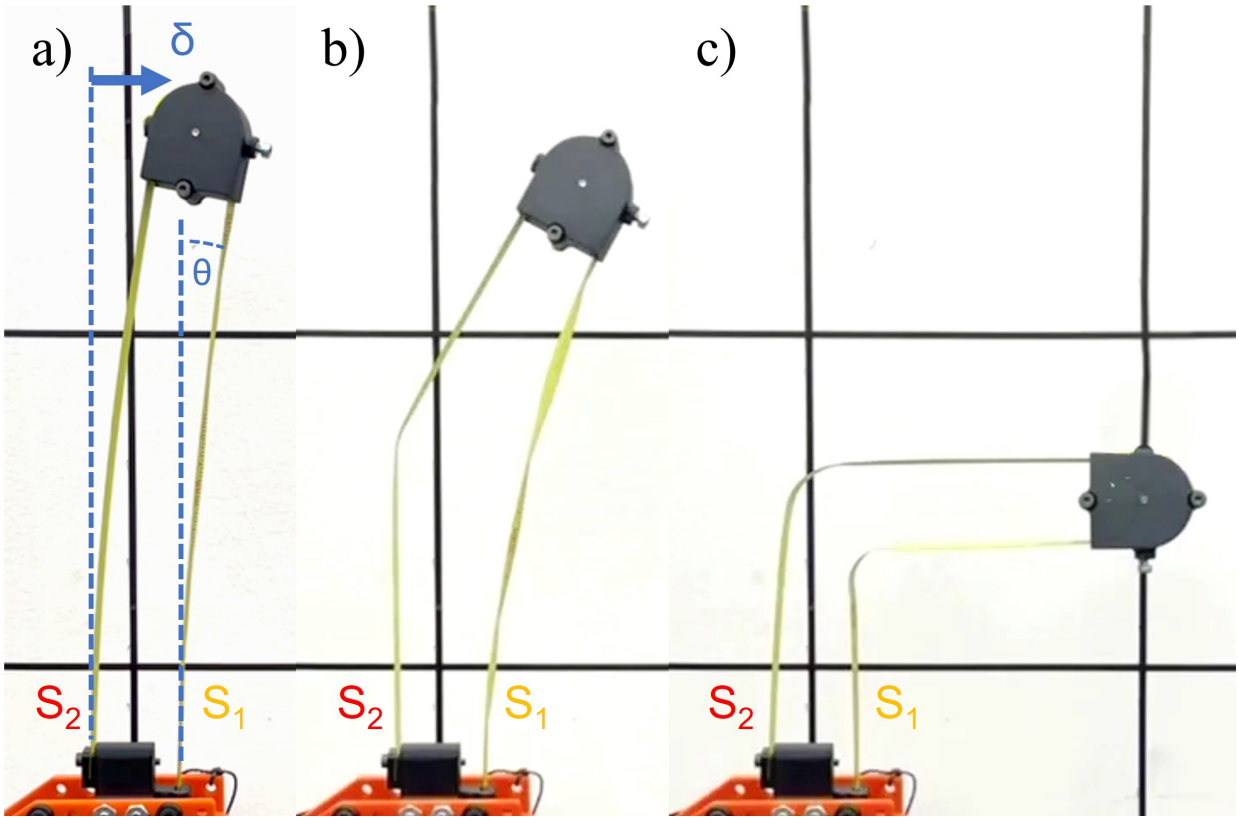

Figure 3.16: Three stages of behavior for bending. a) For small angles ($0° < \theta < 10°$), both segments are unfolded, and displace some distance δ. b) For medium angles ($10° < \theta < 40°$), S_2 has a fold while S_1 is unfolded, but experiences combined twisting and bending. c) For large angles ($40° < \theta < 90°$), both segments are folded, creating two revolute joints.

of segments, since the loads at the ends are equal and opposite. Due to this symmetry, the fold should not propagate or travel along the tape's length, assuming minimal effects from external forces.

In this stage, S_2 behaves as two rigid segments connected by a virtual "revolute joint", which approximates the rotation between the two segments as a point hinge, despite the fact that the fold is actually a finite length of tape with zero curvature. An analytical planar rod model outlined in Seffen's work [39] characterizes the folded configuration in this way, with two rigid bars and a non-linear rotational spring that accounts for the bending stiffness of the fold. Meanwhile, S_1 experiences combined flexural-torsional deformation that can potentially be characterized using Mansfield's equations [52] in future analyses.

In Stage 3 (Fig. 3.16c), both segments have folded at their centers, essentially creating a combined virtual revolute joint for the limb to form the L-shape. The limb can easily be returned to the straight prismatic configuration by equalizing the lengths. This is partially assisted by the tape itself, which will attempt to straighten in order to relieve the accumulated strain energy from bending [39].

3.3.2 Two-Dimensional Bending Kinematics

From these observations, a simplified model of the limb's bending kinematics was constructed to investigate the limb's potential workspace and behavior when deployed at different scales. Figure 3.17 shows the parameters that define the 2D kinematics for this vertically deployed limb at large bending angles.

The forward kinematics of the end effector at point C can be defined in terms of virtual link length L and bending angle θ:

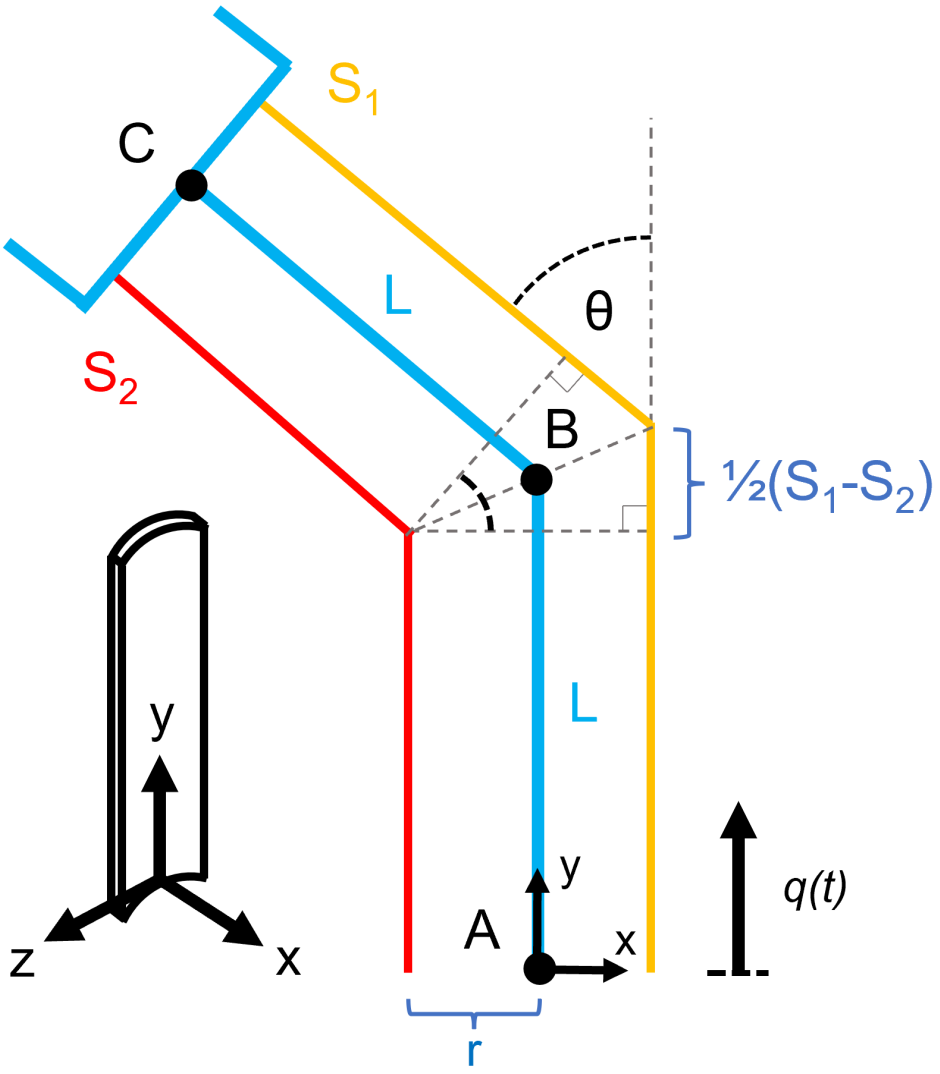

Figure 3.17: Limb bending kinematics. The state of the two opposing segments of tape S_1 and S_2 determine the state of the virtual links L at the center that approximate the overall limb.

$$x = -Lsin(\theta) \tag{3.1}$$

$$y = L + Lcos(\theta) \tag{3.2}$$

The limb consists of two virtual links: the first link goes from the midpoint of the base A to the center point between the two tape folds B, and the second goes from point B to the center of the pulley C. Since end loads of the two tape segments are symmetric about point B, both of their bends will occur at the midpoint of the segments. Thus, both links AB and BC have equal length L, which is dependent on the lengths of the right actuated segment S_1 and left fixed segment S_2. The bending angle theta is defined as the angle between the two virtual links, which is dependent on the difference between S_1 and S_2. The two tapes are parallel and offset by a distance r from the centerline, which is the radius of the end effector idler pulley (and also characteristic bending radius of the tape). Since L is located at the center between the two tapes, we can use triangle similarity rules to draw two conclusions:

$$L = \tfrac{1}{4}(S_1 + S_2) \tag{3.3}$$

$$tan(\frac{\theta}{2}) = \frac{\frac{1}{2}(S_1 - S_2)}{2r} \tag{3.4}$$

Both of these values are dependent on S_1 and S_2, which are determined by our single control variable $q(t)$, which is the length of tape extended/retracted from the base. However, the braking function gives us two modes for formulating S_1 and S_2. In "free" mode, the braking function is off, a change of $\dot{q}(t)$ will result in S_1 and S_2 changing lengths equally. In this case, lengths $S_1(t)$ and $S_2(t)$ are given by:

$$\begin{bmatrix} S_1 \\ \\ S_2 \end{bmatrix} = \begin{bmatrix} \frac{1}{2} \\ \\ \frac{1}{2} \end{bmatrix} q(t) + \begin{bmatrix} S_1(0) \\ \\ S_2(0) \end{bmatrix} \tag{3.5}$$

where $S_1(0)$ and $S_2(0)$ are the lengths of the tape segments at time $t = 0$. However, when in "brake" mode, only S_1 changes length while S_2 remains fixed at its initial length.

$$\begin{bmatrix} S_1 \\ \\ S_2 \end{bmatrix} = \begin{bmatrix} 1 \\ \\ 0 \end{bmatrix} q(t) + \begin{bmatrix} S_1(0) \\ \\ S_2(0) \end{bmatrix} \tag{3.6}$$

It can be observed that the two kinematic modes determine how theta is formulated. In the "free" mode, computing the $S_1 - S_2$ term results in $q(t)$ canceling out. This means that the theta is not dependent on $q(t)$ and will be unaffected by extending/retracting the tape. However, in "brake" mode, the $q(t)$ term reappears in theta and can now be controlled by inputs. Substituting either of these Equations into Equation 1 yields the system:

$$\begin{bmatrix} x \\ \\ y \end{bmatrix} = \frac{1}{4} \begin{bmatrix} -sin(\theta) \\ \\ 1 + cos(\theta) \end{bmatrix} q(t) + \frac{1}{4} \begin{bmatrix} -sin(\theta) \\ \\ 1 + cos(\theta) \end{bmatrix} [S_1(0) + S_2(0)]$$

3.3.3 Bending Experimental Validation

To analyze the accuracy of the formulated bending kinematic equations, a series of tests were conducted to compare the actual end effector position with calculated theoretical values during bending. This was also done to identify what factors might contribute most to deviations from the simplified model.

To collect position data, the end effector was outfitted with a colored marker that was tracked real-time via webcam. The collected position data was then mapped from pixel space to actual X-Y position in meters. For each experiment, the tape spring limb was extended to a set initial length ($S_1(0)$ and $S_2(0)$ set to some value). Bending mode was initiated, and the spool was commanded to slowly retract a set distance ($q(t) < 0$) until the limb reached $-90°$, with the end effector moving along a curved path through the first quadrant of the X-Y plane.

Figure 3.18 shows a selection of data points from multiple bending trials at two different initial lengths. Predicted values are overlaid as solid lines, which were calculated using the kinematics equations outlined in the previous section. For the first trial, the limb was extended to 27 cm before bending. This distance is half the total extension length and is a good representation of the limb's average behavior. In the second trial, the limb was extended to 14 cm before bending to show behavior at smaller extensions. Additionally, the limb was tested at greater extensions (above 40 cm) but the limb would frequently collapse after bending more than $-45°$ due to the greater sensitivity at long extensions. Slight vibrations would cause uncontrolled fold migration and limb collapse, leading to inconsistent results, so they are omitted for this study.

For these randomly selected data points, there is a small amount of variance in the measured positions between trials. This is likely due to a combination of minor factors, including slight disturbances from vibrations, tracking errors from the camera, and slightly different starting conditions caused by backlash and friction in the spool.

Figure 3.18 also shows 4th order polynomial trendlines for the collected data compared to the predicted values. These graphs show that the model tracks well from $0° < \theta < -70°$. For a given angle, the model deviates from the actual X-Y position by no more than 3% for both trials. Bending beyond this region causes the actual data to deviate significantly from the model's prediction.

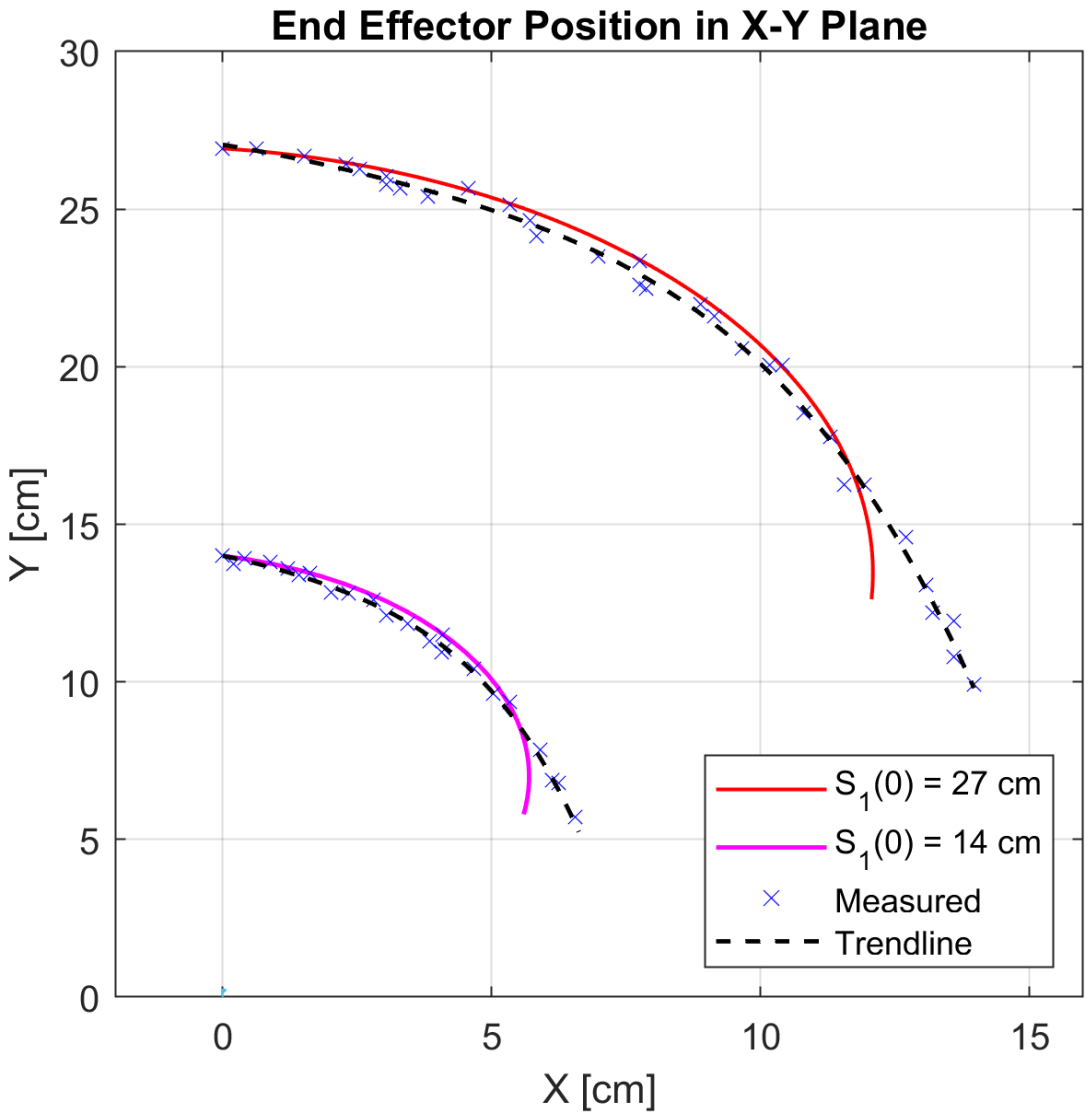

Figure 3.18: Comparison of predicted end effector positions vs actual measurements over multiple trials for bending from $0° < \theta < -90°$. Two sets of data are shown for an initial extended length of $S_1(0) = 27$ cm and $S_1(0) = 14$ cm. Predicted values from the simplified kinematic model are represented by the continuous lines. A random selection of measured position data points is shown as x-marks over multiple trials, with the average trendline shown as the dashed line

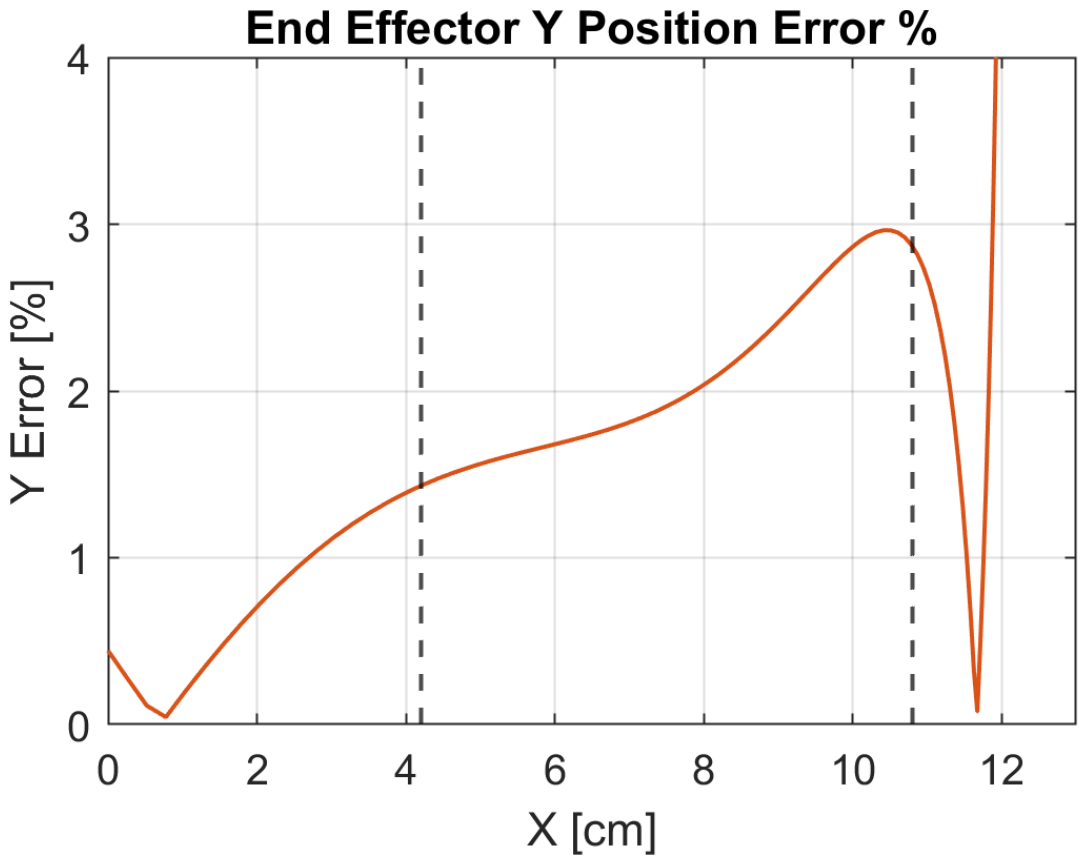

Figure 3.19: Y Position error between the predicted path and the measured value trendline for the 27 cm trials. The vertical dashed lines at X = 4.2 and 10.8 cm depict the transition points between the three stages of bending previously shown in Fig. 3.16.

These deviations can possibly be explained by the effects of gravity and the rotational spring forces from folding.While the model accounts for the fold's geometric properties by simplifying it as a point hinge, it does not account for moments at the hinge or the effect of external torques that can increase the applied bending moment and affect the rotation angle. The weight of the end effector generates an additional torque on the tape, causing the end effector to sag slightly in -Y just below the position predicted by the simple kinematic model. The model also does not account for the rotational spring force in the fold which partially counteracts this weight.

The fold location also appears to migrate slightly away from the midpoint when bending at angles beyond $-70°$. Since the kinematic equations were formulated with the assumption that the fold is always at the tape segments' midpoints, the end effector's actual position begins to deviate significantly from the model. It should be noted from Fig. 3.18 that the fold migration appears to be predictable, since the end effector traveled along the same approximate path between separate trials. This fold migration may be caused during the physical transition from Stage 2 to Stage 3. The sudden formation of the fold causes a significant disturbance to the system as the tape snaps through to its new configuration.

To better observe these effects, Fig. 3.19 shows the error in Y position between the predicted path and the trendline for the measured data for the 27 cm trials. As the end effector moves further in the +X direction, we can see the effects of the three stages of bending previously shown in Fig. 3.16. The vertical dashed lines at X = 4.2 cm and X = 10.8 cm separate the graph into the three bending stages as observed from captured test footage.

In Stage 1 ($0 < X < 4.2$), neither tape segment has a coherent fold. The end effector's weight is still supported by the mostly vertical tape segments, so it does not cause much sagging and the error remains relatively low. It is interesting to note that although the kinematic model does not account for the nonlinearities associated with the tape segments' large displacements, error is low in this region.

In Stage 2 ($4.2 < X < 10.8$), one of the tapes has folded.The newly generated fold causes the folded segment to have reduced rotational stiffness. The weight from the end effector contributes a growing amount of external torque since its moment arm increases as it moves further in +X, which causes the error to increase.

In Stage 3 ($X > 10.8$), both segments have formed folds, but the fold migration appears to take effect. The fold migration changes the kinematics of the system and causes the Y position to drop much faster than expected. After intersecting with the predicted path, the error increases rapidly as the end effector follows a new path. Additionally, the sagging effect from the end effector weight is much more pronounced due to its large +X distance, as well as from the decreased rotational stiffness of both tape segments.

With this model verified, we are now able to predict where the end effector will travel in the X-Y plane if a bend is initiated at different extension lengths. While outside the scope of this study, these tests reveal that a purely geometric study is limited and that future models should better capture the fold's moment characteristics. This includes more complex behaviors like fold formation and migration experienced between Stage 2 and Stage 3. The moment analysis should also take into account external torques from both the motor and the weight of the end effector, and possibly the weight of the tape itself at longer extensions.

Chapter 4

EEWOC: Extended-reach Enhanced Wheeled Orb for Climbing

4.1 Mechanical Design Overview

With the proven success of EEMMMa as a lightweight 2-DOF arm with extending and bending capabilities, EEWOC was developed with the goal of fully utilizing the optimized EEMMMa limb for climbing on 3D structures. EEWOC has additional actuated degrees of freedom to help aim its limb towards target surfaces. It also has wheels to assist with climbing over features, as well as drive efficiently on horizontal surfaces when climbing is not necessary. EEWOC improves upon EEMMMa's minimalist end effector with a fully actuated wrist and gripper, a significant upgrade from the previous purely passive hook grippers.

EEWOC's gripper uses a novel permanent magnetic mechanism with high adhesion force that allows it to attach and detach from ferromagnetic surfaces. This grants it full access to steel environments, making it useful for inspection or surveillance tasks on structures such as buildings, power transmission lines, ships, and factories.

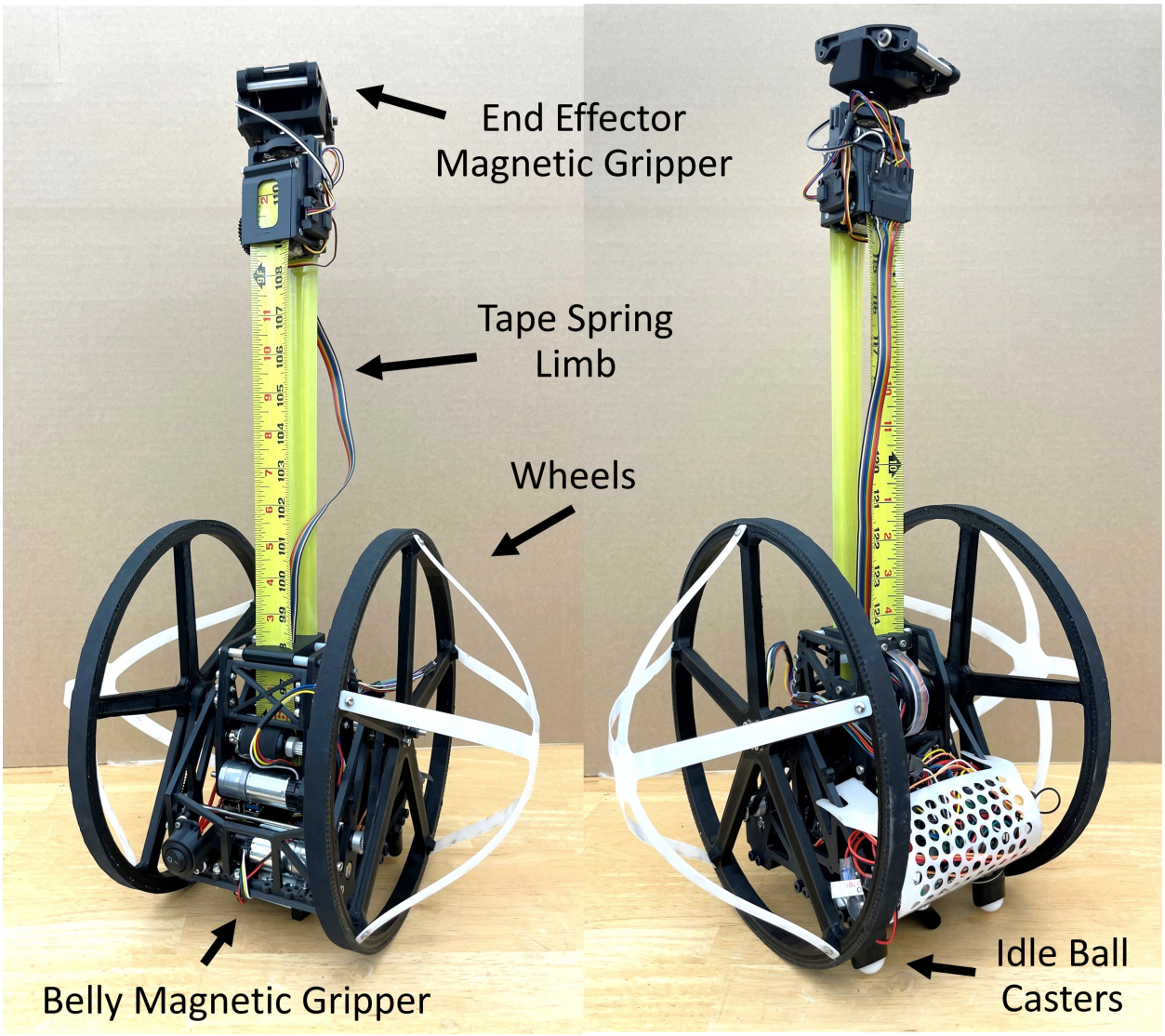

Figure 4.1: Front and back view of EEWOC prototype, with labeled major components.

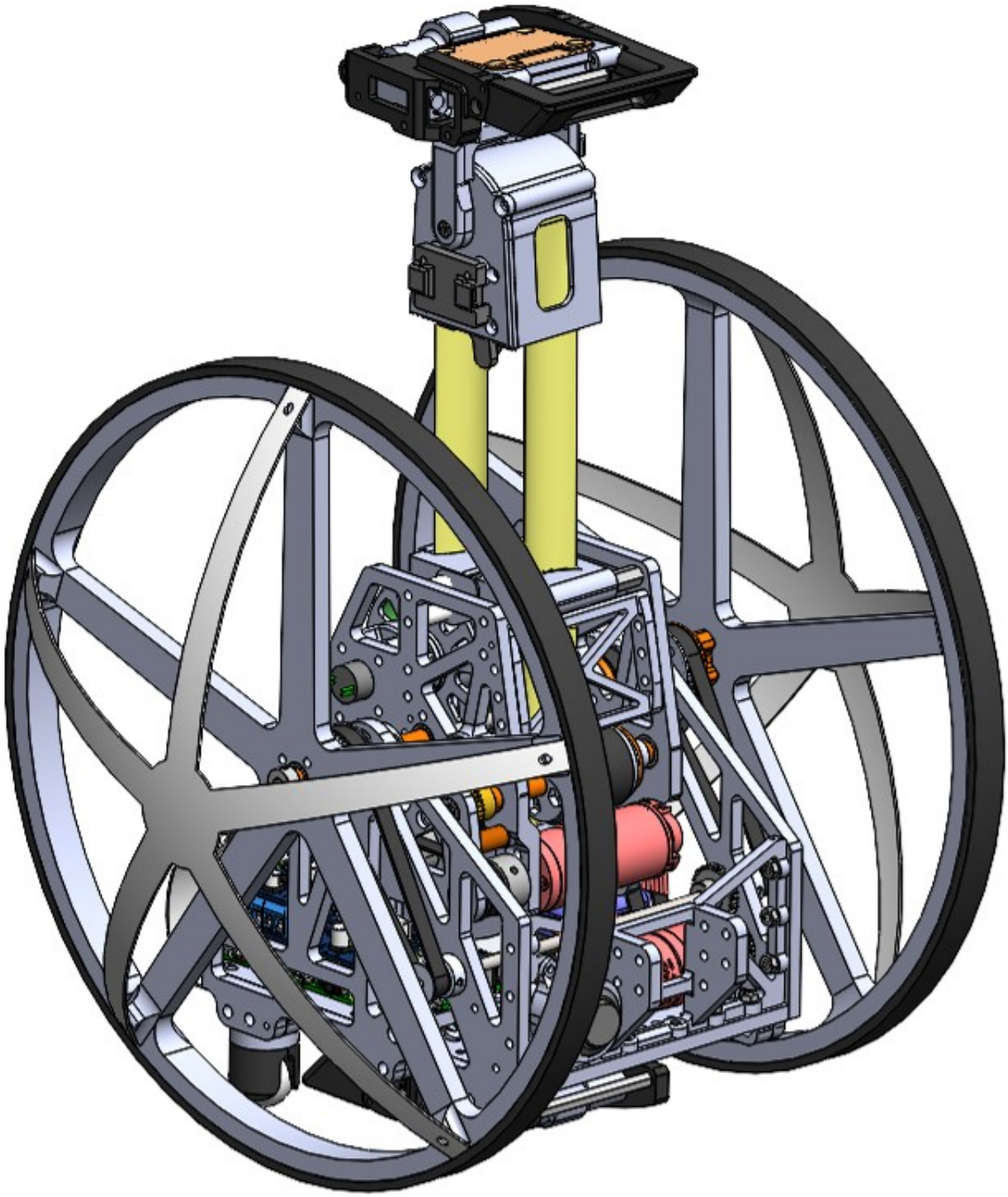

Figure 4.2: Full view of EEWOC CAD model.

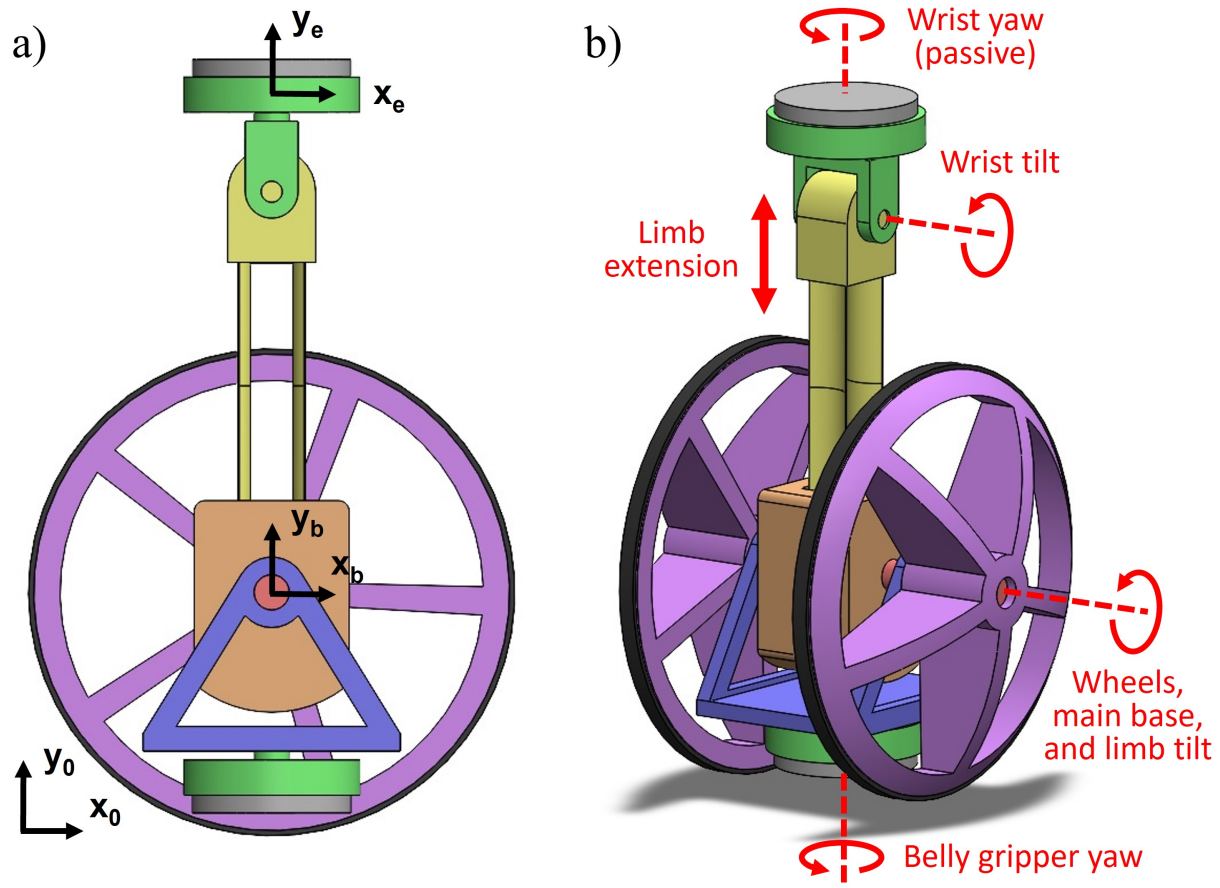

Figure 4.3: a) Simplified diagram of EEWOC's major components in its default configuration. This includes the EEMMMa limb module (orange), tape and end effector (yellow), two grippers (green), main base (blue), and wheels (purple). The limb module, main base, and wheels rotate around a single primary shaft (red). The global coordinate system is defined by X_0-Y_0, main body's axes are defined by X_b-Y_b, and the end effector's axes are defined by X_e-Y_e. b) Angled view showing EEWOC's primary degrees of freedom.

EEWOC's design will be broken down into five main parts: 1) overall morphology, 2) an overview of operations, 3) the upgraded EEMMMa limb module and end effector, 4) the magnetic gripper, and 5) the main base structure which houses the electronics, wheels, and belly gripper. A front and back view is shown in Fig. 4.1. The entire system is 26x30x30 cm and weighs 2.1 kg. A simplified model of the assembly with major highlighted parts and axes can be seen in Fig. 4.3.

4.1.1 Overall Morphology and DOF

Basic DOFs

To reduce system complexity, a minimal set of DOFs for the system was selected as seen in Fig. 4.3. Since the simplest limbed robot design is the single limb inchworm type as described in Section 1.2, EEWOC was designed with this overall morphology as a base, consisting of a single limb with an upper gripper and a lower gripper for adhesion. Magnetic adhesion was chosen due to its simplicity and its ability to naturally assist with pull-in towards the surface, making engagement easier. Based on this, EEWOC's DOFs and subsystems were designed with the assumption that it would be navigating through man-made steel-based environments, with mostly flat surfaces and straight edges.

For versatile climbing in a 3D environment, the system needs to be able to place its end effector on surfaces at arbitrary positions and orientations for anchoring. Since EEWOC is based on EEMMMa's tape spring limb, we began by designing around the system's one controllable DOF in prismatic extension (that can also be swapped to rotational bending). From this, EEWOC's design adds two actuated DOFS that allow the limb extension to be aimed by rotating in pitch about Z_b and yaw about Y_b. This makes it similar to a basic RRP robot like the Stanford arm, allowing it to reach to arbitrary positions within direct view.

Wrist DOFs

Conventional manipulator arms use actuated spherical 3-DOF wrists for orienting their end effectors. However, EEWOC eliminates the need for actuators on two of these DOFs by utilizing compliance and taking advantage of existing forces. First, wrist yaw in Y_e was added as a passive DOF. When climbing a vertical wall, EEWOC can use gravity as a free form of actuation since the robot's center of mass will always rotate the robot's main body

to move directly below the gripper. This passively realigns the body with the direction of gravity after each step. A second passive DOF comes from the tape spring's natural compliance. When deployed at full length, the limb is very rigid in the Y_e direction, but has good compliance in the X_e direction and some limited compliance in the Z_e direction. By simply pushing the limb towards the surface with the existing motors, the end effector can passively comply in the necessary directions until the magnets are close enough to pull in to the surface.

The wrist's third rotational DOF about Z_e is actuated, using a lightweight servo motor. This allows the wrist to compensate for the large rotations experienced when the limb is in bending mode. With this DOF, the limb can bend to place the gripper on top of a ledge, and the wrist can tilt downward to face the gripper towards the surface. This was the only extra DOF needed at the wrist, since bending only causes significant rotation in one axis.

Main Body and Wheel DOFs

With the limb's general morphology decided, the main body was then designed. Since the tape is directionally compliant and a heavy end effector is more likely to cause uncontrolled folding, the end effector weight should be minimized for best performance. Thus, the main body was designed to consolidate as much mass as possible from the other subsystems to avoid putting any extra mass at the end effector. Components on the main body were packaged into a thin space below the limb module. This is beneficial while climbing, since the COM can be rotated to be as close to the wall as possible using the limb pitch motor, minimizing the pitch-back moment.

Working with the assumption that EEWOC would be used on mostly flat steel surfaces, wheels were added. To save weight, these wheels are mounted concentrically with the limb pitch DOF, allowing only a single 4 mm steel shaft to be used for both rotations. Additionally,

only a single motor was used to power both wheels, allowing it to drive only forwards or backwards. For steering, the belly gripper was designed to lift the wheels slightly off the ground, allowing it to rotate using the yaw motor, which will be shown in more detail.

Although technically a redundant DOF on the system, the wheels offer several important benefits for robust movement. First, the wheels allow EEWOC to swap between two modes of locomotion for fast and efficient horizontal movement on the ground. Flat, level surfaces are very common in man-made environments, and the climbing mode of locomotion is unnecessarily complex for these easily traversable surfaces.

Second, the wheels provide a consistent point of contact for between the surface and the main body, and also protect the main base and belly gripper from grinding or colliding against the surface while climbing. They also allow the belly gripper to freely rotate to any angle without colliding with the surface. This is especially important when transitioning around sharp corners and over ledges. When the wheels have sufficient traction against a surface, they can also provide assistive torques to the belly gripper to allow it to aim more easily.

A set of passive ball casters are mounted slightly behind the wheels to provide the system with static stability and eliminate the need for two-wheel balancing control. Importantly, the ball casters provide support against the wall while climbing to reduce the unwanted pitch-back moment that can cause the system to fall by peeling away from the wall. This is similar to the support tails or lower limbs of multi-limbed climbing robots.

In total, there are four brushed DC motors that control the main motions, along with 2 micro servos and 2 mini worm-drive DC motors for the grippers.

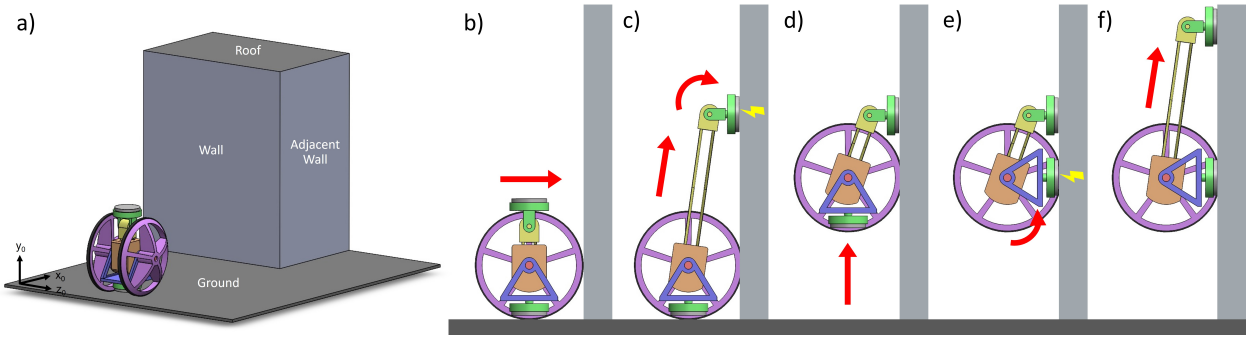

Figure 4.4: Overview of EEWOC's basic operations. a) Isometric view of the initial setup. b) EEWOC drives into the wall. c) The limb extends upward and rotates wrist to put gripper in contact with the wall, then magnetizes to anchor. d) The limb tape retracts, pulling the body upwards. e) When fully ascended, the belly gripper is activated to anchor the body to its current position. f) The limb is aimed again and the sequence can be repeated to scale the whole structure.

4.1.2 Overview of Operations

EEWOC's movement scheme is highly versatile, since it can essentially move between any two points on an external metal surface or structure. For a simplified scenario, the basic case detailed here will involve EEWOC first approaching the wall of a metal building, then ascending the wall, and finally maneuvering onto a roof or around a corner. An overview of this process can be seen in Fig. 4.4.

EEWOC starts as a simple wheeled vehicle on the floor. In its standard configuration, depicted in Fig. 4.3, the limb and end effector gripper are pointing upwards vertically, with the main base and belly gripper pointing downwards towards the floor. A single primary shaft supports the limb module, main base structure, and wheels, and all three components can rotate concentrically with respect to each other.

EEWOC begins by driving forward until both wheels are in contact with the wall, seen in Fig. 4.4b. EEWOC then extends its limb vertically. When a desired height is reached, it rotates its wrist to place the end gripper in contact with the wall and activates the magnets, depicted in Fig. 4.4c. This firmly anchors the end effector to the wall. If more stability is

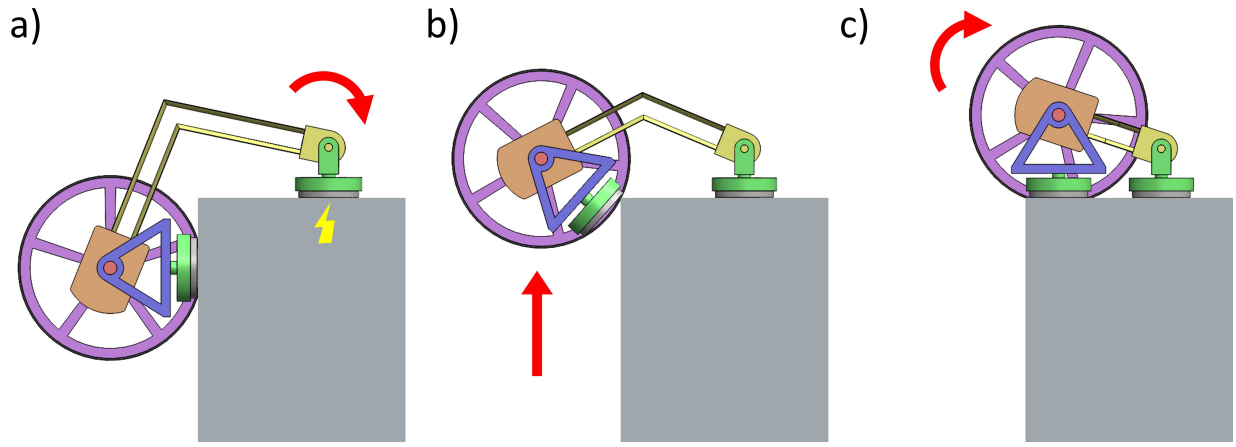

Figure 4.5: Overview of EEWOC ledge climbing sequence. a) The limb is extended and bends to place the gripper on the top of the ledge, and magnetizes to anchor. b) The limb is retracted, pulling the main body onto the ledge, assisted by the wheels. c) Ledge transition is complete.

needed at this ground stage, like if driving on a sloped surface, the belly gripper can be used to affix the main body to the ground to prevent the system from tilting backwards when extending the limb.

Next, the tape spring limb is retracted, pulling the main body upwards, seen in Fig. 4.4d. As it ascends, the wheels also rotate simultaneously to prevent unwanted skidding or grinding against the surface. Once it has fully ascended, it angles the main base upward to point the belly gripper towards the wall. It then magnetizes to anchor the main base to its current position, depicted in Fig. 4.4e. With its main body firmly attached, the end effector magnets are disengaged, and the limb is ready to be extended again. These steps can be repeated consecutively to scale large vertical distances.

To transition onto a roof or ledge, EEWOC first extends its limb, then bends it to place its gripper in contact with the top surface as depicted in Fig. 4.5. The limb can then be retracted to pull the main body up and over the edge of the roof, with the wheels providing additional assistance.

To transition around a corner, EEWOC rotates the belly gripper while attached to the wall.

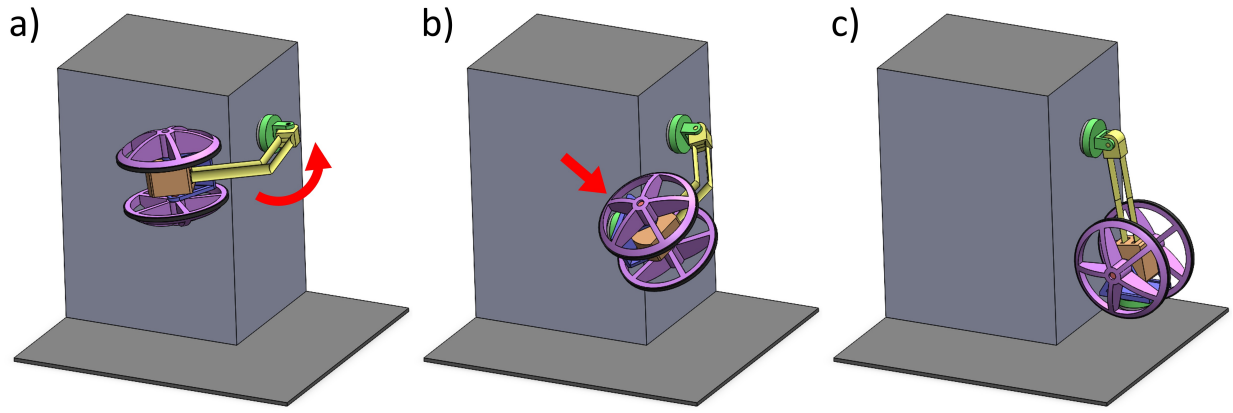

Figure 4.6: Overview of EEWOC corner traversing. a) The limb is angled and extended beyond the corner, then bends to anchor onto the adjacent wall. b) The belly gripper is released, allowing the main body to "swing" onto the next wall. c) Corner transition is complete.

The limb then extends past the corner, as depicted in Fig. 4.6. The limb then bends to place its gripper on the next wall, and the magnets are engaged. Now, by releasing the belly gripper, the main body "swings" onto the next wall. The additional passive degree of freedom on the wrist yaw allows the main body to realign itself vertically with gravity from any arbitrary angle.

4.1.3 Upgraded Limb Module Design

Upgraded Tape Spring Limb

EEWOC utilizes the latest version of the EEMMMa extending and bending robotic limb. Three CAD views of the limb module assembly can be seen in Fig. 4.7. This limb greatly extends the range of available anchor points for EEWOC to grapple and move between. The tape is now a 1" (2.54 cm) wide STANLEY PowerLock tape, offering enhanced rigidity, and can now extend to up to 1.2 m (4 ft). The limb's better rigidity allows it to remain in a straightened configuration without folding at further extensions, and allows there to be additional mass at the end effector.

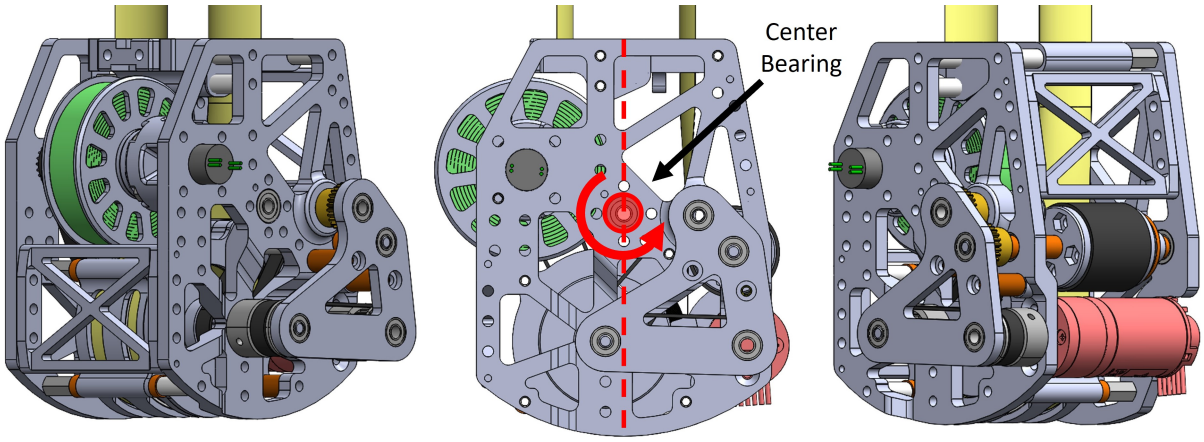

Figure 4.7: CAD views of full limb module assembly.

The entire assembly rotates about two deep groove ball bearings in the center as shown in Fig. 4.7, and masses are balanced as much as possible to have the COM be aligned with the center. The new wider tape has a characteristic bending radius of 18 mm, so the output and the fixed end of the U-shaped tape are located 18 mm from the centerline to make sure the limb deploys symmetrically as shown in Fig. 4.8a. This way, the limb's extension will behave the same regardless of the direction that it's pointing.

As shown in Fig. 4.8b, the main tape spool is actuated with a Pololu 25D HP 75:1 DC motor with encoder, which allows it to lift its weight with a factor of safety of 2. The tape spool shaft then transmits torque to the output roller and wire spool. All timing belts and pulleys have also been upgraded from MXL to GT2 for better torque handling.

Tension Management

The tension management system is upgraded from the EEMMMa version, with reduced size and weight. The tape spool is still surrounded by a PTFE lining to keep it confined like in the previous version. The output roller diameter has been reduced from 40 mm to 27.4 mm while geared to still feed the tape at a 1:1 rate with rolling contact. A small pair of spur gears reverse the direction of rotation to feed the tape in the correct direction. As seen in

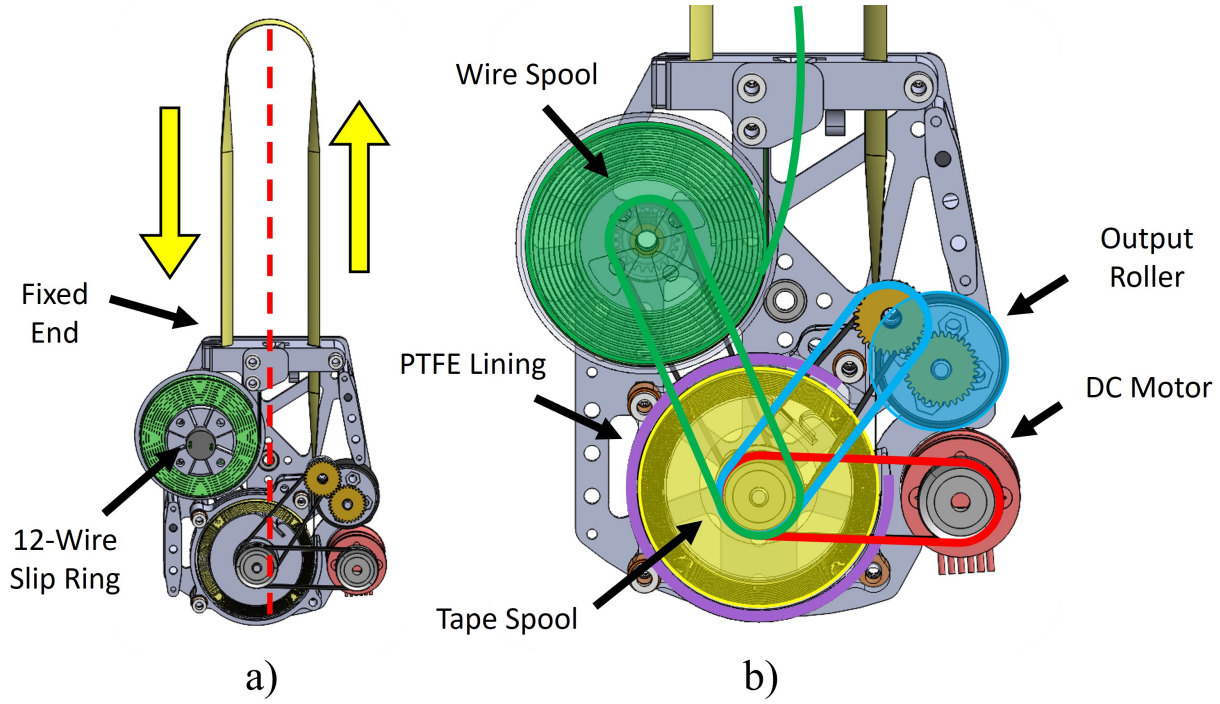

Figure 4.8: CAD of inside the limb module. a) Overall view showing the U-shaped tape, with one end fixed and the other fed to the spool. b) Closer view showing the belts that transmit power from the motor to the tape spool, then the output roller and the wire spool.

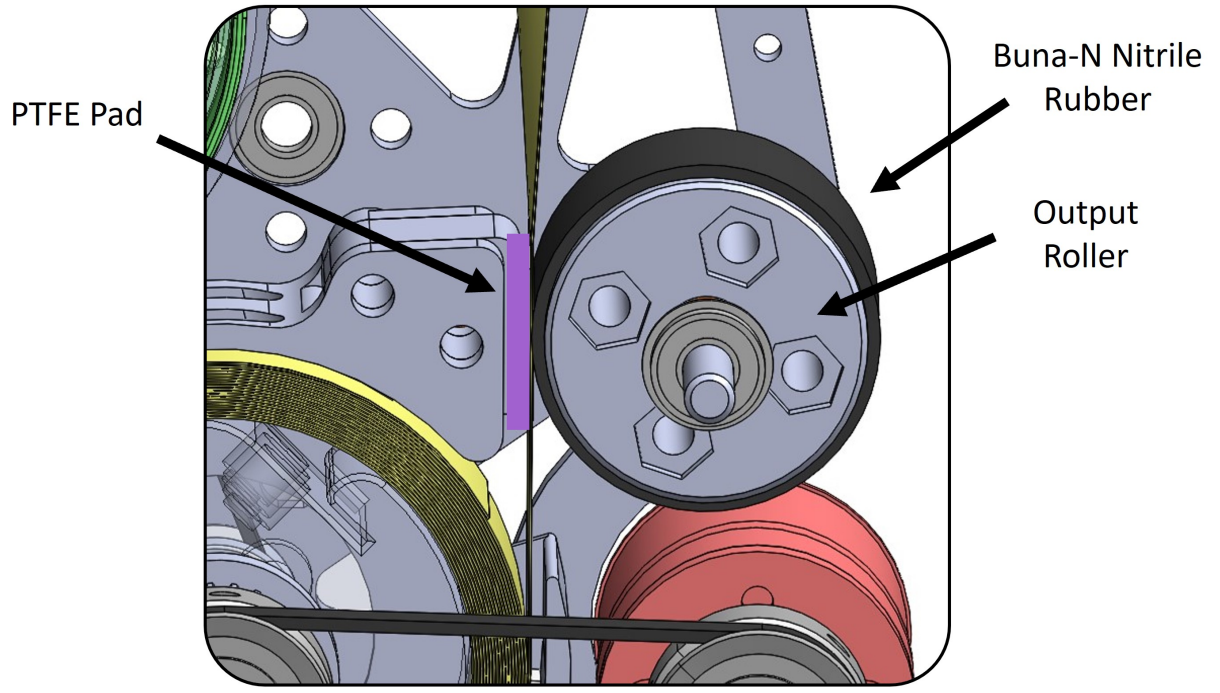

Figure 4.9: CAD of the tension management output roller and opposing PTFE lined surface.

Fig. 4.9, a small PTFE film contact on the tape spool frame now presses opposite the roller, instead of the large backing channel present in EEMMMa, reducing the structure by almost 90 percent.

Wire Management

To feed power and communications to the end effector components, an additional wire spool was added to the limb module, connected with timing belts to the tape spool. A 12 mm wide ribbon cable of ten 26AWG wires is wrapped around the spool that feeds out of a hole at the center of the limb module, between the tapes. The hole has heavily filleted edges to allow it to keep the ribbon cable's minimum bend radius even during an accident. Since the wire spool must rotate continuously, the ribbon cable feeds into an Adafruit miniature slip ring, with 12 wires and a 12 mm diameter. The output of the slip ring then connects to the electronics on the main body.

When the limb is extended, the wire spool rotation timing belt ratio supplies the ribbon cable at a slightly faster rate than the tape. This ensures the cable is always slack and is never in tension, since this can affect the end effector's movement. The wire spool is also protected by a small clear strip of laser-cut PETG that is bent around the spool's maximum radius. This loosely prevents the wires from losing too much tension, which could cause them to sag below the spool sides and jam the mechanism.

4.1.4 End Effector Design

The original EEMMMa end effector has been significantly upgraded with additional features. The new end effector weighs 250 g and has a new gripper, additional DOFs, and an automated braking system to switch to bending mode. The casings are made of PLA, with heat-set

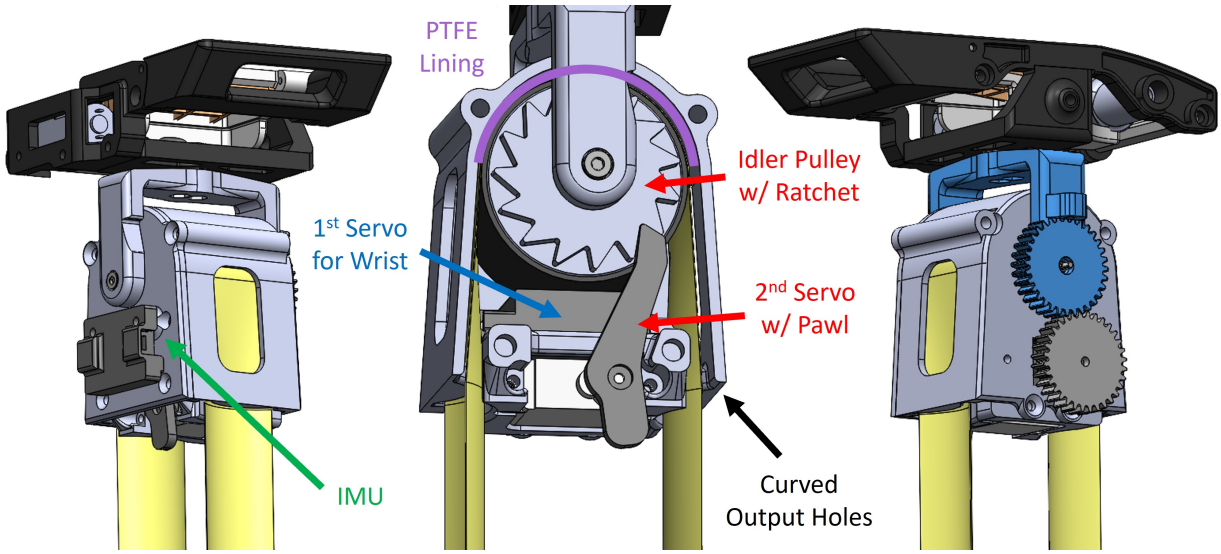

Figure 4.10: CAD of the end effector. a) Full view, with the IMU and manual brake release lever visible. b) Detailed view of the inside, with the idler pulley, PTFE lining, ratchet and brake, two servos, and curved output holes. c) Opposite view of the end effector, with the wrist bracket highlighted in blue.

inserts and a small number of steel fasteners. Both the idler pulley and wrist bracket are mounted on a single 3 mm shaft to save weight. The idler pulley now has a diameter of 36 mm to match the characteristic bending radius of the new tape. Additionally, the housing has been lengthened to accommodate the two micro servos for the brake and wrist, as well as accommodate for the longer transition region length of the tape between the folded and unfolded regions. The end effector casing is lined with PTFE film like before, but with a higher area of contact to ensure loads on the gripper are transferred properly into the casing.

The end effector now features a 6-DOF IMU (Adafruit ISM330DHCX) that can be used to collect data on the end effector's rotation and acceleration. This data can be used to predict the end effector's position and orientation when it is extended away from the main body. This information is especially valuable when verifying whether an anchoring attempt was successful. Before transitioning between points, EEWOC can retract the tape spool gently to tug on the end effector. From this, the IMU data can show whether the magnetic anchor has firmly attached, or if it has slipped or otherwise failed.

Brake

The end effector can now switch to bending mode autonomously using a small 4.8 g Hi-Tec HS-40 nanoservo motor to actuate the braking function. The idler pulley has a ratchet feature that can lock its rotation when the servo-actuated pawl is engaged. A detailed view of the mechanism can be seen in Fig. 4.10b. The ratchet can prevent rotation in both directions, but the pawl and teeth are positioned such that it is easier to disengage when the tape is extended. This is based on the assumption that more torque is needed when retracting to initiate the bend, rather than the reverse. To allow the brake to be manually disengaged by hand, the pawl has a small lever that protrudes outside of the end effector, allowing for easy access.

Wrist

A Hi-Tec HS-70 MG microservo motor controls the wrist pitch, which allows it to orient the gripper towards a desired surface while bending around obstacles. This 12.5 g servo allows the wrist to rotate up to 194 degrees, which is sufficient to orient the gripper towards a surface without colliding into the housing or tape at its limits.

The servo transmits torque to a U-shaped wrist bracket with a set of 3D printed gears that attach to the servo horn, as shown in Fig. 4.10c. The gear ratio is 1:1 for packaging reasons and simplicity, since a large gear may extend beyond the casing and interfere with the bracket moment. Additionally, the wrist bracket cannot rotate beyond 194 degrees anyway, eliminating the need for a gear ratio. The wrist bracket is connected to the magnetic gripper with a 12 mm ID sleeve bearing that grants the gripper its passive yaw DOF. The gripper can freely rotate up to $\pm 200^{\circ}$. A small piece of elastic allows the wrist to return to a zero position after a rotation in order to prevent the wires from tangling.

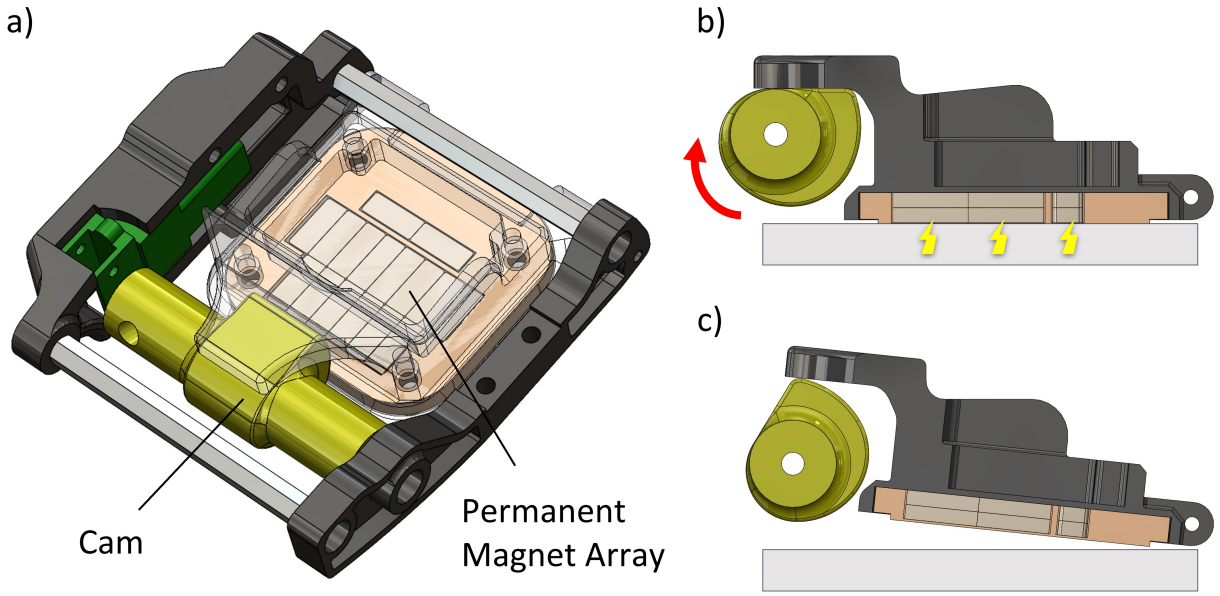

Figure 4.11: a) CAD view of EEWOC's magnetic gripper. b) The gripper in its active state. c) The gripper in its inactive state, where the cam has rotated to peel the magnetic lever from the surface.

As mentioned before, the wrist does not include a passive degrees of freedom in roll to assist with aligning the gripper to the target surface. This is because the tape itself provides sufficient compliance to allow the magnetic gripper to easily align itself, which is further assisted by the magnetic attraction force.

4.1.5 Magnetic Gripper Design

EEWOC possesses two magnetic grippers: one on the end effector, and one on the underside of the main base structure. By attaching and detaching these consecutively to move between points, EEWOC can quickly climb metal structures. A detailed view of the gripper's mechanics is depicted in Fig. 4.11.

The magnetic gripper at the end effector allows EEWOC to utilize its long reach to grasp distant points. The other magnetic gripper (or "belly" gripper) is mounted on the underside of the main base. This gripper faces away from the center of the robot, pointing downwards

towards the floor or outwards towards target surfaces. The belly gripper allows the main body to affix itself to its current location. Each gripper weighs 106 g, with a minimal mass design focus to reduce the amount of weight at the end effector.

EEWOC's magnetic grippers utilize an array of small neodymium permanent magnets that produce a large magnetic force. Each magnet is 10x4x2 mm and 32 magnets are placed inside a hinged lever arm that rests against a small cam, which is covered with a slippery PTFE film. When the gripper needs to disengage, the cam rotates, causing the magnet-filled lever to peel away from the wall until the cam reaches its maximum radius. The magnets are inset at the far end of the lever arm, away from the fulcrum to maximize their distance from the surface while disengaged. The magnets are inset into a small removable 3D printed housing, with the bottom layer being 0.3 mm thick to protect the magnets while minimizing the distance between the magnets and the surface. The removable housing also makes it easy to change the number of magnets and their orientations.

A small N20 12 V DC motor with a 1:118 worm gear drive allows the assembly to self-lock so that EEWOC can continuously remain in the desired active or inactive state. The cam also allows the magnetic force to be modulated by adjusting the clearance between the ground and the magnetic pad.To help with adhesion, the magnet array's outer edge is equipped with small strips of rubber as seen in Fig. 4.12a. This increases friction between the gripper and the target surface, which improves its ability to handle shear forces and prevent sliding. Additionally, a small extension on the frame d_{ex} provides a contact point with a larger moment arm to help resist peeling moments from the tape when it is loaded.

One of the gripper's major advantages is that the magnetic force assists with anchoring, since the gripper will automatically align itself to the surface. This eliminates the need for additional passive degrees of freedom at the wrist to orient the gripper. When the gripper approaches a target surface, the tape spring limb's natural compliance causes it to simply deform until the magnetic gripper makes contact.

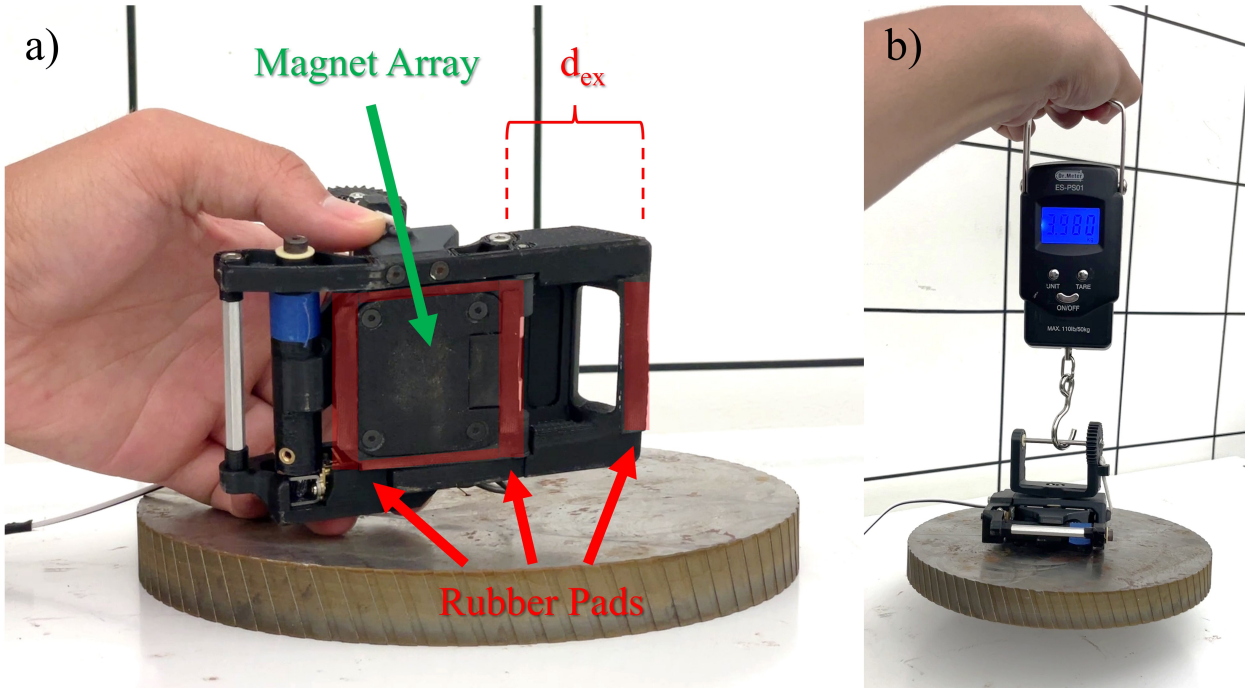

Figure 4.12: a) EEWOC gripper prototype, with magnet array in the center and rubber pads highlighted in red. b) EEWOC lifting a 4 kg steel block.

As seen in Fig. 4.12b, this system is capable of lifting a 4 kg steel block, twice the weight of the total system. The gripper's upper performance limits have not been tested, and normal and shear forces will be examined in future studies. The gripper can switch between on and off states in 0.7 s, which requires the cam to rotate 90 degrees.

4.1.6 Main Body and Wheel Design

The main body frame is composed of four PLA 3D printed planar structures, including the bottom base, front, and two sides as seen in Fig. 4.13. The frame contains the microcontroller, base DOF motors, and all the electronics for power and communications, as well as a second IMU. It also supports the primary shaft that the wheels and limb module rotate around. EEWOC has redundant degrees of freedom at this shaft that allow it to aim its major components relative to one another. By actuating both the arm pitch motor and the wheel motor at the same time, the main base can rotate to position the belly gripper towards

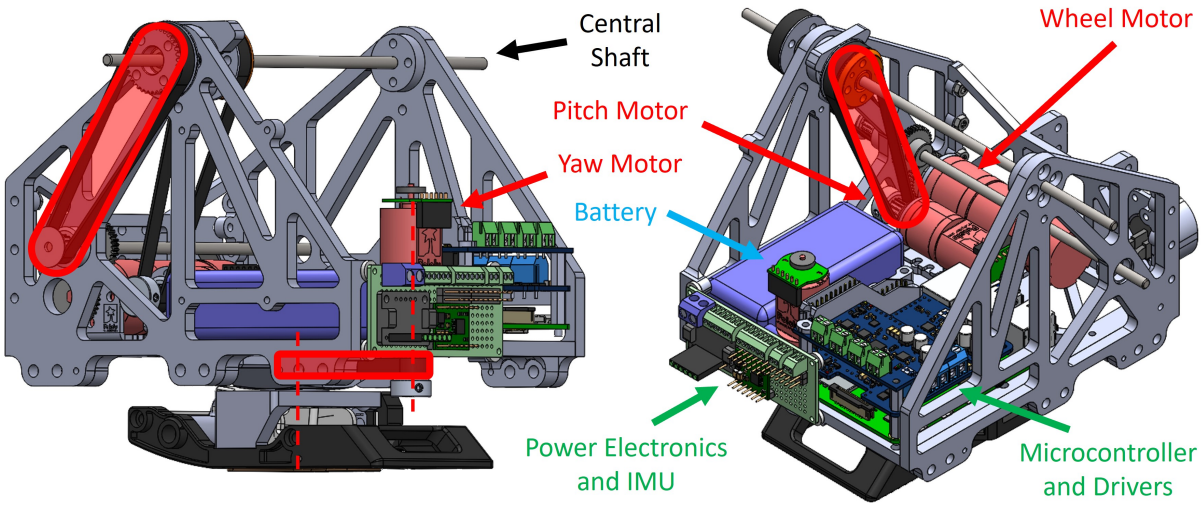

Figure 4.13: CAD of the main base. Motors and attached timing belts are marked with red, electronics with green and blue, and battery with purple. a) Side view showing the timing belt that connects to the wheels. b) Isometric view showing the timing belt that connects to the limb module.

a wall. By rotating the main base towards the wall, the system's center of mass moves closer to the surface, which is advantageous while climbing. This minimizes the pitch-back moment that could cause the robot to fall.

The limb module contains two more actuated DOFs that use Pololu 20D 12V 195:1 brushed DC motors with encoders. The first is connected to a brushed DC motor that allows its pitch to be controlled, aiming the limb up or down. It has a range of motion of 200°, which grants it enough range to be aimed towards surfaces that the wheels are in contact with. The belly gripper is connected to another brushed DC motor that allows the entire body to control its yaw angle when it is latched onto a surface. This combined with the pitch angle allows it to aim its limb towards any point in 3D space.

Wheels

The wheels are connected to another DC motor that allows them to drive either forward or backward. The motor is a Pololu 25D HP 47:1 DC motor with encoder, chosen for its good speed with enough torque to both drive with the system's weight and provide sufficient assistive torques during transition movements.

To allow the main base to rotate itself freely in pitch, the wheels have a diameter of 260 mm, which is large enough to fully conceal the belly gripper when stowed as seen in Fig. 4.14a. Keeping the gripper fully within the wheel profile prevents the gripper assembly from skidding or grinding with the external surfaces. The wheel is wrapped with a 3 mm thick neoprene rubber strip to increase friction for driving and climbing. This also assists with impact mitigation when attempting to swing around corners, or when dropping to the ground. To further protect the system during impacts, the outer face of the wheel is equipped with a curved piece of laser-cut 0.8 mm thick delrin sheet that acts like a spring to absorb side impacts.

Belly Gripper

The belly gripper operates much like the gripper at the end effector, but has slightly different attributes. With the wheels on the ground, the gripper is mounted such that there is 1 mm of clearance with the ground, as shown in 4.15. When the gripper is activated, the magnetic pad and rotating cam are allowed to extend beyond the wheel's diameter, allowing it to contact the ground or climbing surface and lifting the wheels above the surface. This now allows it to rotate in yaw and steer and with the belly yaw motor without interference from the wheels. The gripper connects to the main body with two thin 20 mm deep groove ball bearings. The gripper housing has a GT2 timing pulley fused to it that connects to the belly yaw motor below the main base plate as seen in Fig. 4.14b.

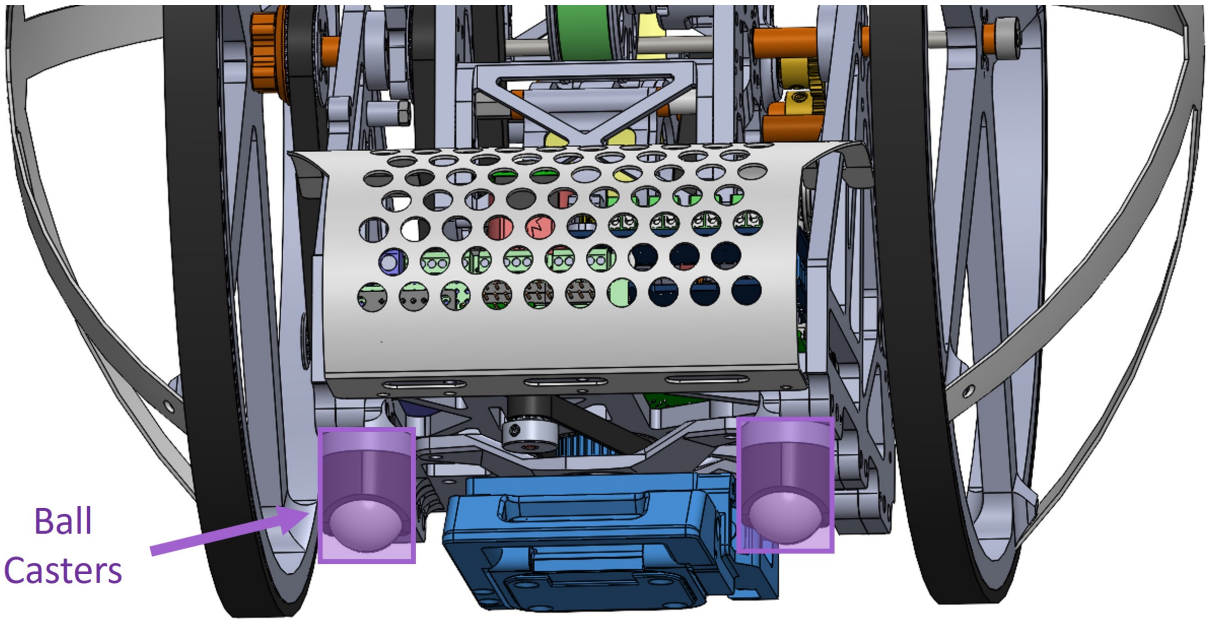

Figure 4.14: Bottom view of the wheels and belly gripper CAD, showing the belly gripper highlighted in blue. The bottom timing belt that connects to the belly gripper housing can be seen.

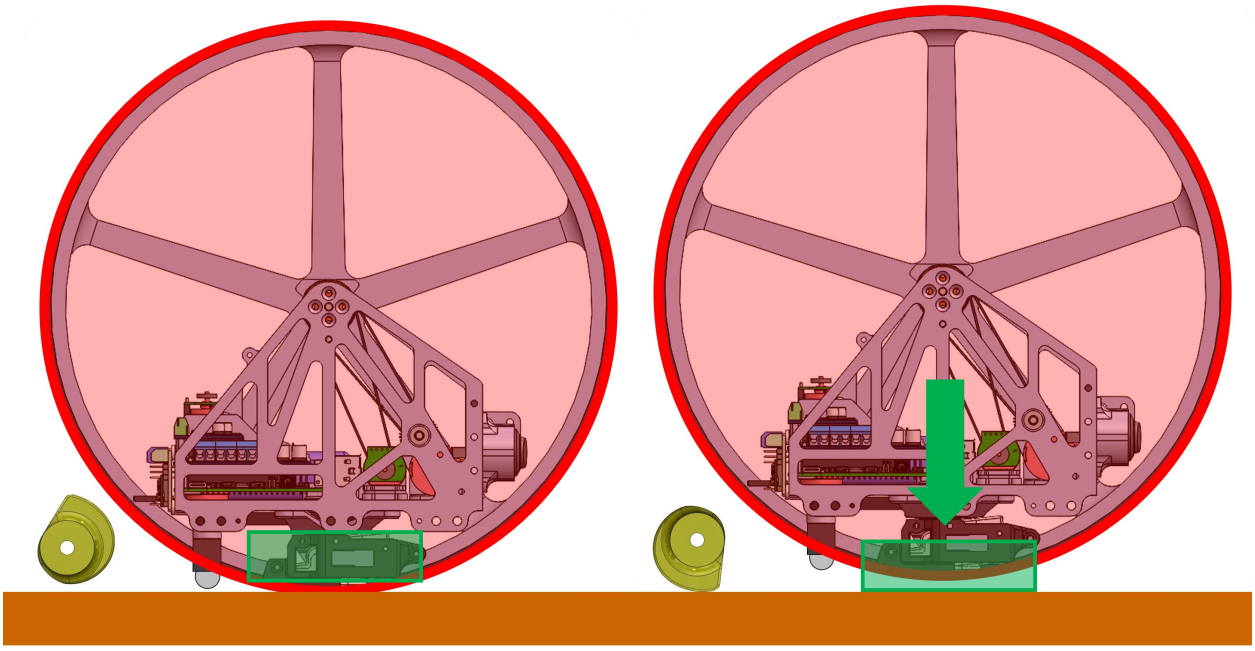

Figure 4.15: Side view of the wheels and belly gripper CAD. a) Initial view showing belly gripper's mounting position for full wheel coverage. The cam position is shown on the left (not to scale). b) When the cam is rotated, the belly gripper lifts the wheels above the surface, allowing EEWOC to rotate in yaw and steer without interference.

Electronics and Computer

EEWOC is controlled by a Raspberry Pi 4 B, which was chosen for its potential to be used in future efforts to integrate vision processing and autonomous path planning. Software is programmed in python and sent to the system via wireless keyboard. Button commands are structured similarly to EEMMMa's, with simple PWM control for basic functions and pre-programmed sequences of complex motions.

EEWOC has three motor drivers to run its six DC motors. The largest 25D motors for the tape spool and wheels are connected to a Motoron M2H18v18 Dual High-Power Motor Controller, chosen for its ability to handle the 5 A stall current of each motor (up to 18 A per channel). The smaller 20D motors for the base DOFs and N20 motors for the grippers are run by a combination of a Motoron M3H256 Triple Motor Controller and DRV8876 Single Brushed DC Motor Driver Carrier. These drivers were chosen for their small size and light weight. I2C control was used to interface with the motor drivers and IMUs.

Power is supplied by the same battery as EEMMMa, a Turnigy 1300 mAh 3S 30C Lipo pack weighing 107 g. An on/off rocker switch is located on the front frame. Power is split from the battery into a 12 V line that supplies power to the four larger DC motors, and 5 V line that supplies power to the Raspberry Pi, microservos, drivers, and sensors including motor encoders and IMUs. Two Adafruit UBEC DC/DC 5 V step-down voltage converters step down the voltage from the 12 V line. Each voltage converter can handle 3A max, with one regulator connected to the Raspberry Pi (which can draw a max of 3 A), and the other connected to all the other 5 V components.

To protect the electronics, a laser-cut sheet of delrin is bolted to the bottom frame and bent over the wires and boards to protect them. The delrin sheet has clip features that deform to connect back to the frame to hold it in place. These can easily be undone by hand for easy access when needed.

4.2 EEWOC Demonstrations

In the following demonstrations, EEWOC shows its versatility as a mobile robot. With the ability to drive, climb, and bend around obstacles, EEWOC possesses a wide variety of 3D movement options in complex real-world environments. Tests were conducted on a variety of steel structures commonly found on commercial buildings and industrial spaces including walls, struts, pipes, machines, and ducting. Most tests were carried out on a roof at UCLA, which possesses a large variety of HVAC equipment with naturally worn surfaces from exposure to the elements. All demonstrations were performed with simple open-loop control and manual input. Videos of these demonstrations can be found in the Appendix.

4.2.1 In-lab Tests

EEWOC was first subjected to a series of basic tests in a controlled lab environment. As seen in Fig. 4.16, a small test setup was made to simulate a ledge, with a steel block taped to the top for the gripper to adhere to. EEWOC was commanded to rotate its wrist to face the steel block, then extend above the ledge. The end effector brake was then activated and the tape was retracted to bend the limb and place the gripper in contact with the steel block. In this scenario, bending occurs in a single plane, with X_r, Y_r, X_e, and Y_e all lying in the same plane (refer to Fig. 4.3 for axes). Gravity provides a force in the Y_0-direction that draws the gripper closer to the surface, making engagement easier. The rubber pads on the gripper assisted in dampening its impact on the surface, preventing it from bouncing off the surface.

With a firm anchor established, the brake was disengaged and the tape was retracted to make the main body ascend. While ascending, the main body was angled towards the wall to minimize the pitch-back moment. In many trials, retracting the tape beyond some critical

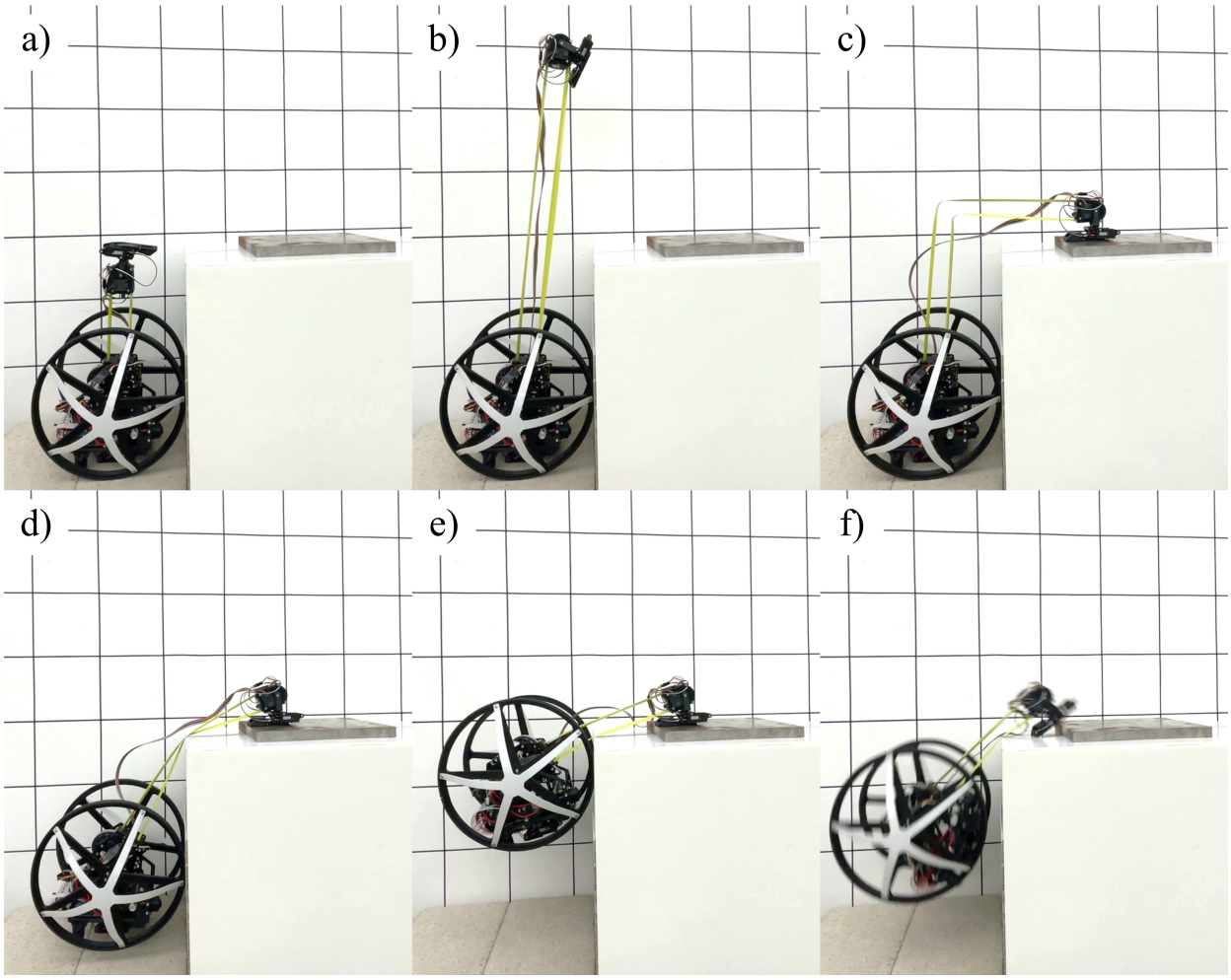

Figure 4.16: Screenshots from EEWOC lab demonstrations for climbing a small simulated ledge with a steel block. a) EEWOC in its initial position. b) The wrist is angled and the limb is extended. c) The limb bends to place the gripper on the steel block. d) The brake is released and the tape is retracted. e) The main body ascends, angling the main body towards the wall to reduce pitch-back moment. f) In some cases, the body would fall.

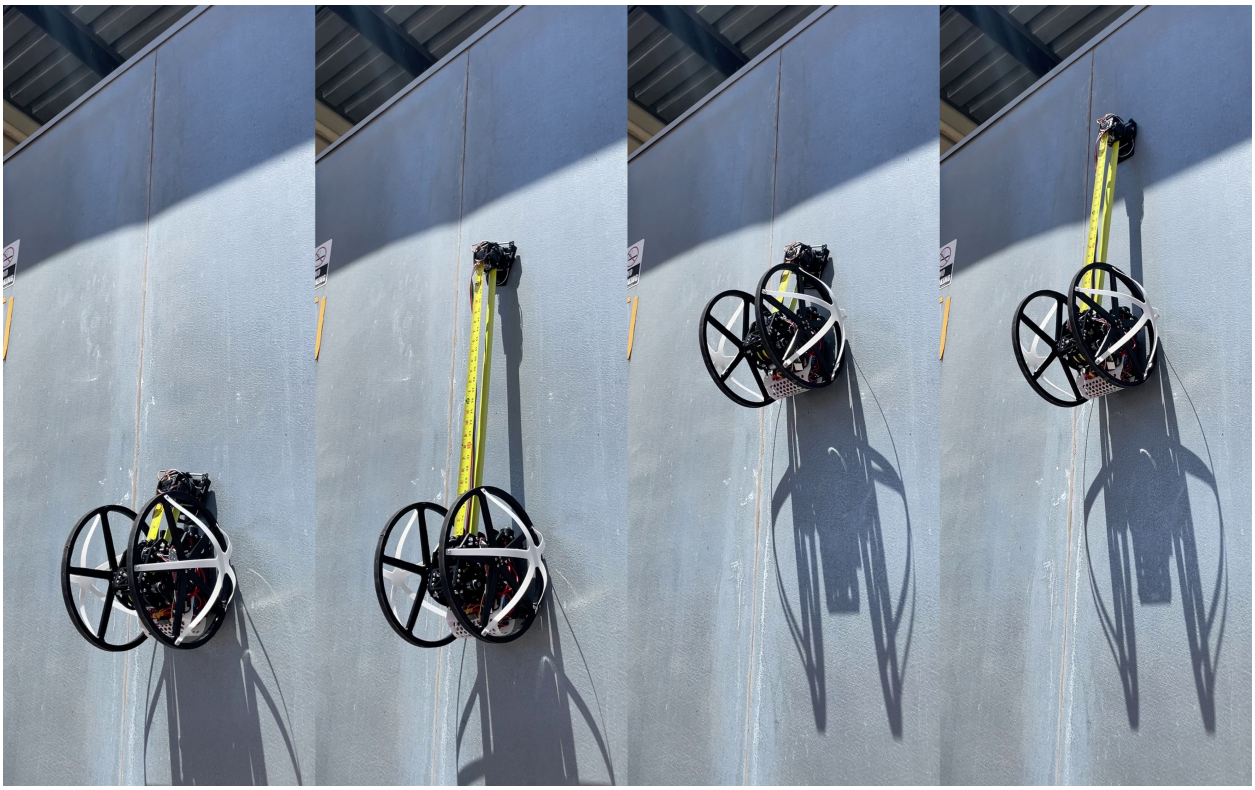

Figure 4.17: Screenshots from EEWOC vertical climbing demonstrations.

point caused the gripper to fail and the main body to fall as depicted in Fig. 4.16f. This is due to forces experienced at the main body, where the reaction moment arm between the wheel contacts and the line of tension in the tape constantly shrinks as the line of tension gets closer to horizontal. This causes the pitch-back moment to become too large relative to the opposing moments from the wheel contacts and gripper friction force, so the gripper fails. Additional trials with the steel block raised 5 cm and 10 cm showed a much greater success rate since the wheel contact moment arms remain large enough to adequately compensate for the pitch-back moment.

4.2.2 Climbing

To test its ability to scale vertical structures in a real-world environment, EEWOC was taken to the roof of UCLA and subjected to a series of climbing trials on structures there.

Figure 4.18: EEWOC straight sideways deployment demonstration. This can be useful for traversing gaps or moving between distant features.

The first demonstration tested basic linear movement on a flat steel wall by sequentially extending and anchoring between points, as seen in Fig. 4.17. For each step, a safety test was performed before releasing the belly gripper. Successful anchoring was determined by gently retracting the tape and verifying that the IMU data showed no change. During trials, the gripper's magnets naturally pulled the end effector towards the wall, assisting the wrist pitch servo and eliminating the need to rotate the limb towards the wall for engagement. After this initial test, controlled descending was demonstrated by performing the climbing sequence in reverse to gently lower the main body to ground level.

To determine EEWOC's climbing speed, the steel wall was measured (8 ft or 2.44 m) and video footage was reviewed. The calculated max climbing speed was 0.24 m/s. With EEWOC's body length of 0.26 m (the diameter of the wheels), this comes out to 0.92 bodylengths per second, placing it among the fastest climbing robots for its scale.

EEWOC was also able to reach high above to attach to overhangs that would be inaccessible

Figure 4.19: EEWOC reaching at maximum length to attach to an overhang.

to other conventional limbed robots, as shown in Fig. 4.19. It can perch below steel ceilings for extended periods of time and could remain rigidly attached even when hit, since the energy is mostly absorbed by the tape's compliance and the body's ability to swing. The ability to stably perch in this manner shows EEWOC'S potential for long-term surveillance, since it would be resistant to wind or other forces if deployed at high elevation environments like trees or skyscrapers.

As a final test, the belly gripper was rotated to deploy the limb sideways. This maneuver could be useful for passing windows or crossing gaps between buildings. In this orientation, the tape maintains its rigidity quite well while extended, thanks to its thickest dimension being in the direction of gravity. The gap distance that could be traversed using this method was limited however, since swinging too far a distance could cause the gripper to peel off from the wall. This is due to the main body's wheels no longer being in contact with the wall during the swing phase, and its weight causes the pitch-back moment to peel the gripper

away from the wall.

Maximum payload was determined by attaching a force meter to EEWOC's lower gripper and retracting the tape to measure the lifting force. The result was 3.4 kg or 33.4 N. With its weight of 2.1 kg, the calculated payload-to-weight ratio is 1.62, which is quite strong for its weight. To verify this value, EEWOC was subjected to the same steel wall climbing trial with additional weights attached. Weight was progressively added until EEWOC was unable to ascend, which confirmed the previous measurement.

4.2.3 Bending to Climb Onto Ledge

To test basic maneuvers that involve bending, ledge climbing tests were conducted on 45° and 90° angled surfaces, as depicted in Fig. 4.20. The limb was extended beyond the top edge of the ledge, and bending was initiated to place the gripper on the top surface. With the magnetic gripper engaged, the limb was commanded to retract to let the main body ascend, with the wheels providing assistance at the corners. EEWOC successfully demonstrated the ability to climb on top of these ledges. However, the 90° ledge had a lower rate of success due to the shrinking wheel moment arm issues mentioned in the previous section.

We also observed that with the limb bent, its much lower rigidity and heavy load from the main body causes it to press against the corner of the ledge during the transition, causing undesirable stress in the tape at that point. Possible solutions for this will be discussed in the future work section.

4.2.4 Bending to Transition to Adjacent Walls

While the previous demonstration only involved bending in a single plane, bending around corners is much more complex due to the development of a 3D fold. While folded, the tape

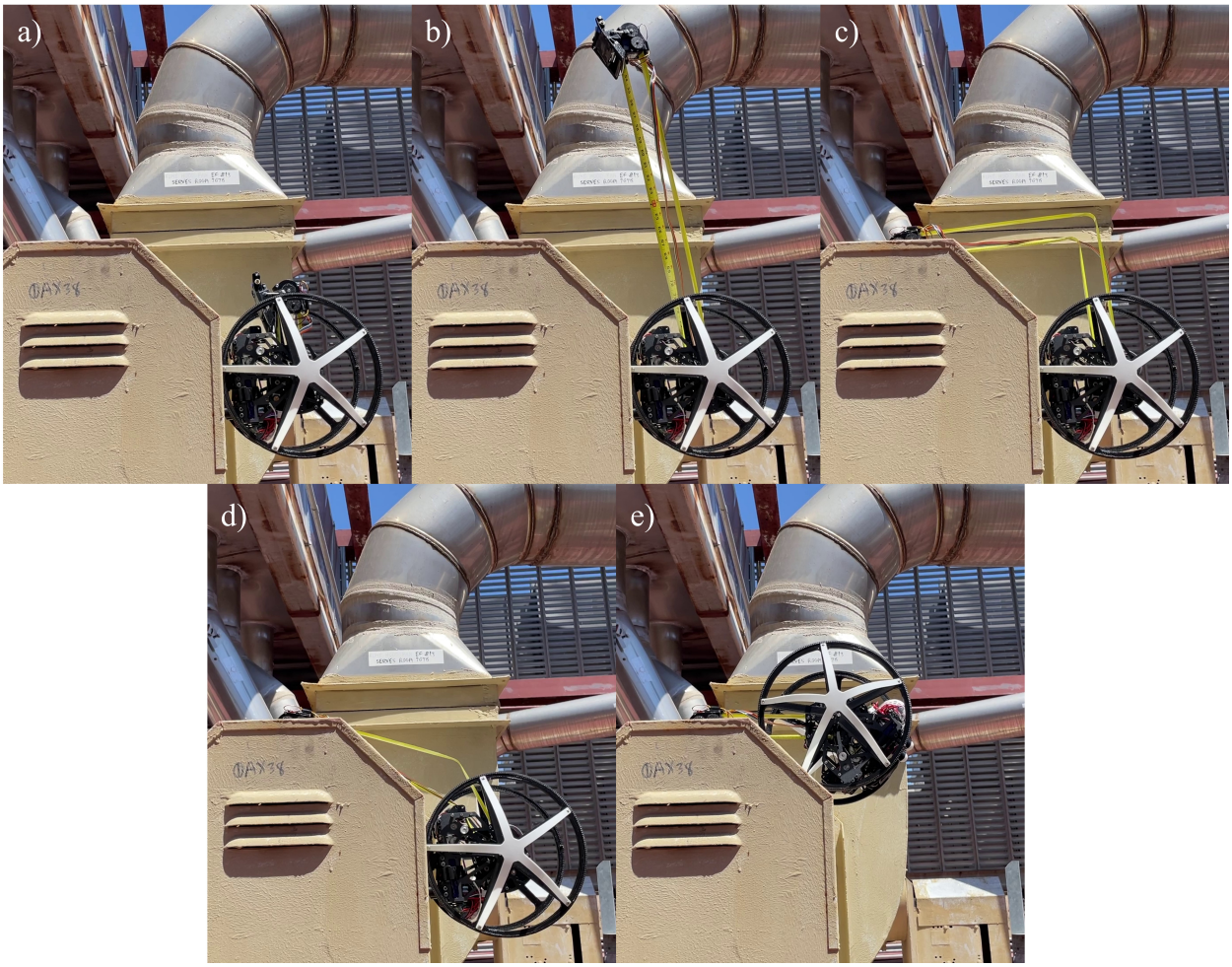

Figure 4.20: Screenshots from EEWOC bending demonstrations. EEWOC bends its limb to place the magnetic gripper on a top surface, allowing it to transition from the wall to the top of a ledge.

Figure 4.21: EEWOC bending its limb to place its gripper on top of a 90° ledge.

Figure 4.22: Screenshot from EEWOC corner transitioning attempt.

spring limb possesses different stiffness properties that makes it more susceptible to out-of-plane displacement. While reaching around a corner, the gravitational force in Y_0 is no longer coplanar with the other frames, causing the end effector to displace slightly in Y_0. The resulting 3D fold is difficult to control and account for, but will explored more in-depth in future work.

Similar to the ledge climbing scenario, the limb was first extended sideways beyond the edge of the corner. Then limb was then bent to place the gripper on the adjacent wall and the end effector gripper was activated. The belly gripper was released, resulting in the robot "swinging" towards the new wall as the main body falls.

While EEWOC could successfully bend and place the gripper on an adjacent wall, it was unable to perform a successsful transition. The swinging maneuver requires significant air time, during which the main body is supported only by the end effector gripper. Without the wheels contacting any surface, the main body's weight applies a torque on the gripper that causes it to peel back away from the wall and the system to fall. In ongoing work, we are developing improved maneuvers to transition around corners with continuous wheel contact. This can potentially be done with the previously mentioned partially activated magnetic gripper method. A gripper housing redesign may also help distribute loads enough to counteract the pitch-back torque and allow the gripper to maintain hold.

4.2.5 Driving

EEWOC also performed some simple driving and steering tests shown in Fig. 4.23. To measure its ground speed, EEWOC was driven at maximum speed next to a tape measure and video footage was reviewed. Its top speed was found to be 0.65 m/s, but it should be noted that the motor chosen was for torque and not speed, and should theoretically be able to drive up to three times faster if a different motor is used. With a ground speed of

Figure 4.23: Screenshots from EEWOC driving and turning demonstrations.

2.5 bodylengths/s, it has good horizontal mobility on par or exceeding other ground based rovers.

Steering abilities were also tested on the ground. When the belly gripper is activated on the ground, the cam pushes the wheels slightly off the ground. This allows the belly yaw motor to rotate the entire body on the spot. EEWOC could easily reposition itself and angle its body to approach different surfaces.

We also observed some issues with the design relating to driving on uneven surfaces. EEWOC would occasionally experience small jolts or stops while driving over bumpy surfaces or be unable to steer properly when over divots or pits. This is because the belly gripper is mounted very close to the surface, and the wheel outer diameter barely extends beyond the gripper. Thus, large bumps on the ground could cause the belly gripper to hit the surface while driving, resulting in a jolt. This also explains the steering issue, since a divot directly below the belly gripper will cause it to not properly contact the ground below and the wheels will not be lifted off the ground. This means that the wheels cannot be used to drive on top of heavily curved surfaces like pipes, where it would have to use its slower climbing mode of locomotion instead.

4.3 Climbing Behavior Observations

4.3.1 Effects of Surface Conditions on Reliability

Since EEWOC's magnetic grippers rely on friction to support shear forces while climbing, we identified a variety of surface factors that affect adhesion effectiveness and can increase EEWOC's potential to slip during maneuvers. Many factors have to do with the proximity, quality, and thickness of the ferromagnetic material that the structure is made of.

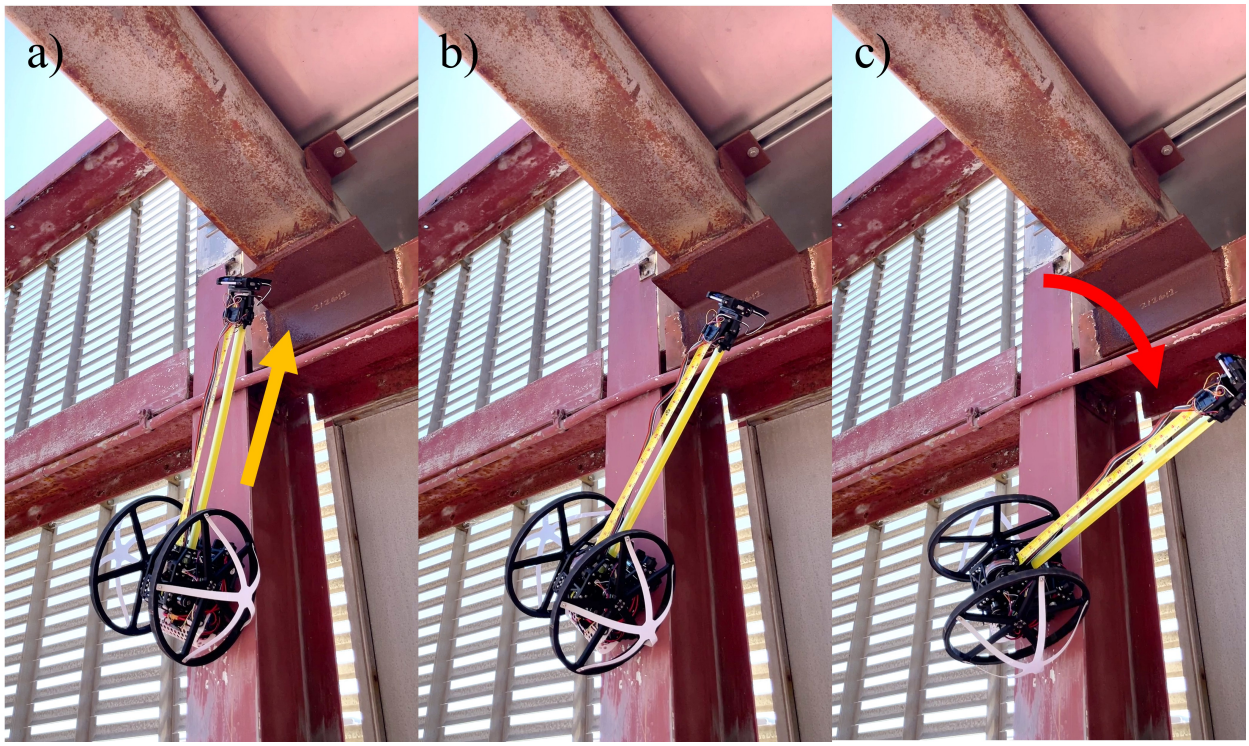

Figure 4.24: Example of belly gripper failure due to poor surface conditions. The surface is dusty and has peeling paint, reducing friction. As the limb is extended, a large moment at the belly gripper causes it to slip and twist, and the limb falls uncontrollably (although the body remains attached).

One important factor that can reduce adhesion is the presence of surface coatings. Many steel surfaces have protective coatings such as zinc that are not magnetic. In most cases, a thin layer of non-magnetic metal or paint has a minimal effect on adhesion, since the coating only adds a small amount of distance between the gripper's magnets and the steel beneath. In other cases however, the layer is thick enough to make the gripper unusable.

Another important factor is the actual amount of ferromagnetic material present in the structure being climbed. This is most obvious when considering the thickness of the structure. Many steel plates used for casings or housings are thin. Compared to a thicker structure, these thin plates have a lower number of iron atoms in close proximity to the gripper magnets, and thus have less attractive force. Attaching EEWOC to steel plates less than 2mm thick resulted in a noticeable reduction in payload capacity. Additionally, some structures are made of iron alloys that are less magnetic. The presence of other non-magnetic metals in the alloy reduces the number of iron atoms in close proximity to the magnets, resulting in reduced adhesion.

Many conditions associated with wear and weathering also reduced the gripper's effectiveness. Steel surfaces with thick patches of rust result in reduced magnetic adhesion force and thus less friction since iron oxide is not magnetic. Surfaces with slick or loose top-level layers also resulted in occasional slipping, with dusty, dirty, or slimy surfaces being less safe to attach to. An example of this is shown in Fig. 4.24, where EEWOC was attached to a dusty surface with peeling paint. The belly gripper experienced a large twisting moment from the end effector weight as the limb was extended at an angle. When extended beyond some critical point, the moment became large enough to twist the belly gripper from the surface, causing the limb to fall uncontrollably (although the main body remained attached to the wall).

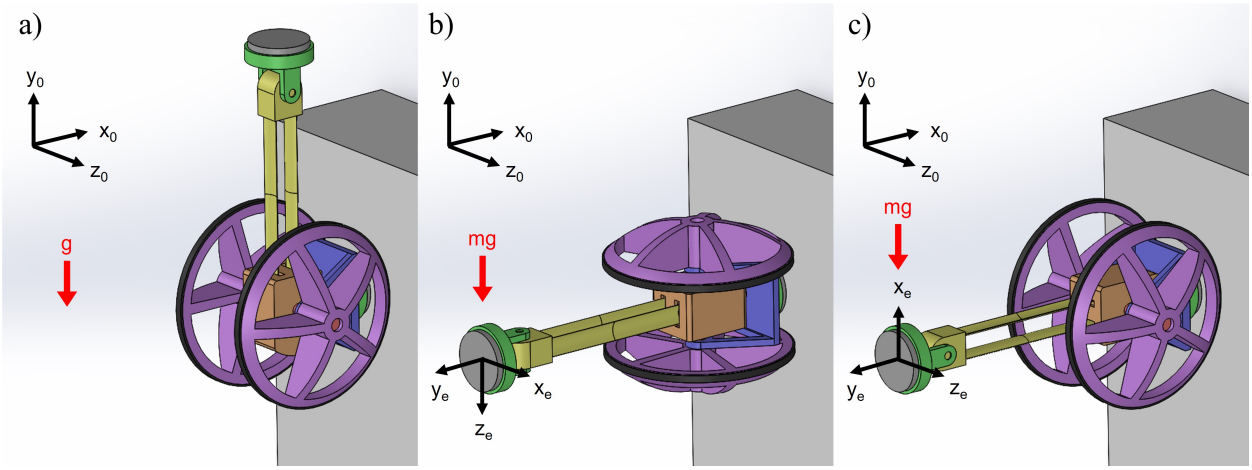

Figure 4.25: EEWOC limb deployment orientations. a) Standard configuration, with the limb deployed in the same direction as gravity. b) Sideways configuration, with the limb's Z_e axis

4.3.2 Effects of Deployment Orientation on Limb Rigidity

The tape spring limb's asymmetric stiffness properties causes it to have some important considerations when identifying preferred anchor points. The limb is most rigid and best at supporting weight when the tape is loaded in its strongest directions. Thus, it is important to consider the limb's deployment direction with respect to gravity to ensure maximum limb stiffness. To illustrate this, Fig. 4.25 shows the three basic ways the limb can be oriented with respect to gravity.

In Fig. 4.25a, the limb is in its standard vertical deployment direction. In this case, the limb's axis Y_e is aligned with global axis Y_0. The limb is very rigid when deployed in this direction, since the weight of the end effector and the limb itself is being supported by the tape's strongest and thickest dimension. When deployed straight sideways with the Z_e axis aligned with gravity as shown in Fig. 4.25b, it can still support its full 1.2m length since the weight is supported by the tape's wide dimension. But when deployed with the X_e axis aligned with gravity in Fig. 4.25c, it is much weaker and susceptible to collapsing under its own weight since the tape is most compliant in X_e.

This will be important for path planning in the future, since large environments will present multiple potential surfaces with anchor points in many directions. An intelligent path should prioritize anchor points that load the limb in its preferred directions to maximize limb controllability and safety.

4.4 Swinging Experiments and Analysis

Like other legged climbing robots, EEWOC's movement options are limited to grasping points within the length of its 1.2 m extendable limb. This issue is exacerbated by the steel tape's directional stiffness as previously mentioned, which makes it stronger or weaker when loaded in different axes. In some orientations, it is unable to extend straight horizontally without collapsing under its own weight.

To address these potential limitations, we explored the development of a dynamic swinging maneuver to allow EEWOC to traverse gaps larger than its limb could normally reach. In these experiments, EEWOC places its gripper on an overhanging arch to act as a pivot, and swing across a gap to a surface. If swinging from a horizontal surface, this motion can be assisted by the wheels to provide an initial velocity.

4.4.1 Swinging Model

Planning a swinging maneuver is tricky, since EEWOC needs to have accurate positioning to reach zero velocity on the other side; too much velocity and it will bounce off, too little and it won't reach the target. Thus, we set out to develop a model that could help calculate exactly where to place the anchor for a successful swing.

The swinging maneuver can be modeled as a pendulum system, shown in Fig. 4.26. We

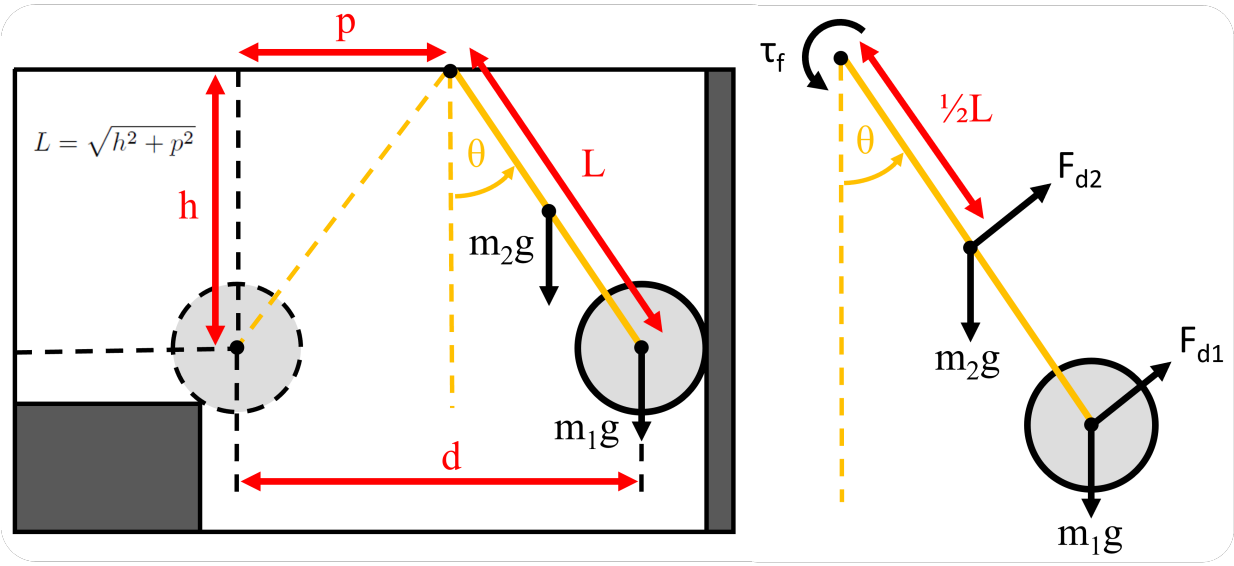

Figure 4.26: Overview of parameters for formulating the swinging model.

assume the end effector is rigidly attached to the ceiling, and we ignore the mass from the end effector and gripper. The length is not massless, since the limb itself is around 8% of the system's total weight when fully outstretched, so it is split into main body mass $m_1 = 1.85$ kg and limb mass m_2 which changes according to $m_2 = L * 0.06369$ kg which accounts for the deployed length deployed length L. The pendulum length L is dependent on the pivot point distance p and ceiling height h which is set by the environment. These will determine the gap distance d that the system can traverse.

$$L = \sqrt{h^2 + p^2} \tag{4.1}$$

The pivot point would ideally be at the midpoint of the gap distance, but we have to consider damping effects, which are detailed in Fig. 4.26. The first damping effect is from the friction torque τ_f at the pivot caused by the weights as they oscillate, which changes direction depending on the velocity, as indicated by the signum function.

$$\tau_f = -\mu R F_n sgn(\dot{\theta}) \tag{4.2}$$

where μ is the coefficient of friction (assumed to be 0.4), R is the radius of the pivot bearing (assumed to be 1.5 mm), and F_n is the normal force at the pivot from the weights,

$$F_n = (m_1 + m_2)gcos(\theta) \tag{4.3}$$

We also approximate air drag from the main body F_{d1} and the limb F_{d2} with a combined shape of cylinders and rectangles using the general drag equation:

$$F_d = \frac{1}{2}\rho v^2 C_d A sgn(\dot{\theta}) \tag{4.4}$$

For the drag equation, the main body is approximated as a rectangular prism with $C_{d,m} = 1.05$ and frontal area $A_m = 1.66 * 10^{-2}$ m^2, the wheels are approximated as cylinders with $C_{d,w} = 0.3$ and frontal area $A_w = 3.51 * 10^{-3}$ m^2, and the limb as a thin rectangle with $C_{d,l} = 1.9$ and frontal area $A_l = L * 2.29 * 10^{-2}$ m^2. From these parameters we can construct the equations for the drag forces:

$$F_{d1} = -\frac{1}{2}\rho(L\dot{\theta})^2(C_{d,m}A_m + 2C_{d,w}A_w)sgn(\dot{\theta}) \tag{4.5}$$

$$F_{d2} = -\frac{1}{2}\rho(\frac{1}{2}L\dot{\theta})^2(C_{d,l}A_l)sgn(\dot{\theta}) \tag{4.6}$$

Using the torque method to derive the equation of motion, we can sum the torques about pivot point p to get:

$$\sum \tau_p = \tau_f + LF_{d1} + \frac{1}{2}LF_{d2} \tag{4.7}$$

We can then combine this with the second definition of torque using the time derivative of angular momentum $\mathcal{L}$: $\tau = \frac{d}{dt}\mathcal{L}$. Calculating this, we get:

$$\frac{d}{dt}\mathcal{L} = (m_1 + \frac{1}{4}m_2)L^2\ddot{\theta} \tag{4.8}$$

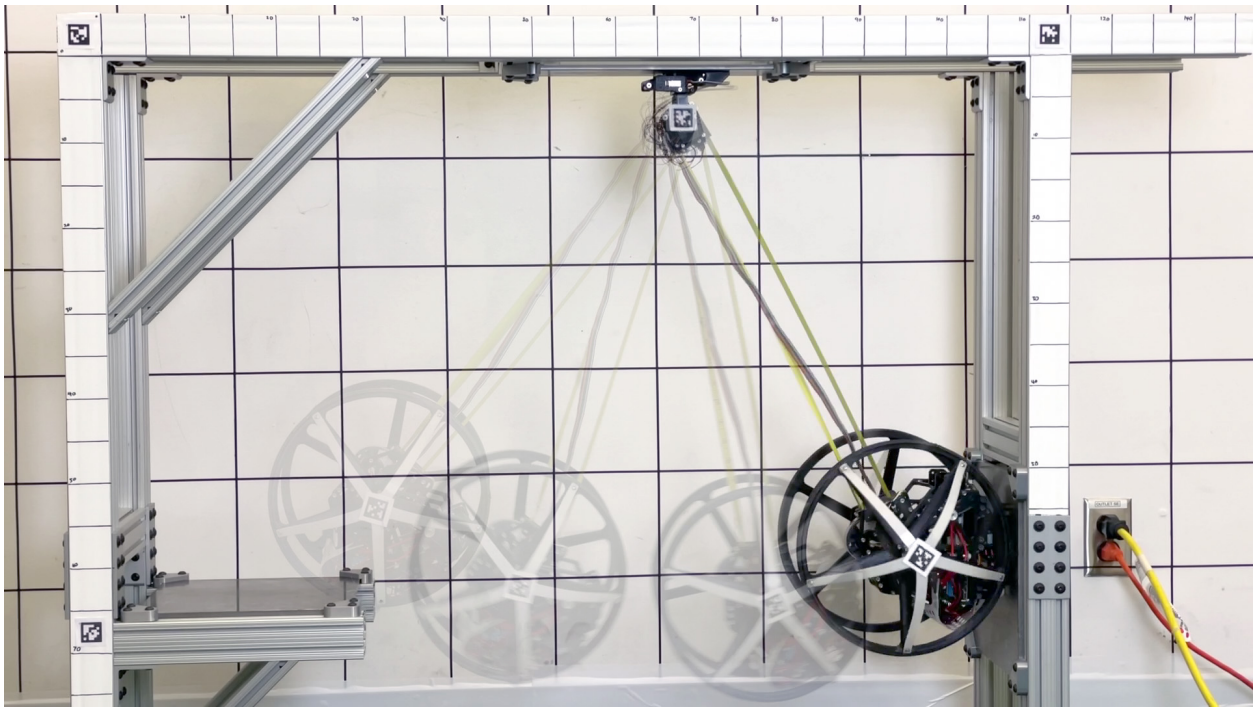

Figure 4.27: View of lab test bed with overlaid screenshots during swinging maneuver.

which we can combine with the sum of torques to get our equation of motion:

$$(m_1 + \frac{1}{4}m_2)\ddot{\theta} = -\frac{1}{L^2}\mu Rg(m_1 + m_2)cos(\theta)sgn(\dot{\theta}) \\ - \rho L\dot{\theta}^2(\frac{1}{2}C_{d,m}A_m + C_{d,w}A_w + \frac{1}{16}C_{d,l}A_l)sgn(\dot{\theta}) \quad (4.9)$$

The resulting equation of motion is nonlinear, but we cannot simplify further by using the commonly used small angle approximation or drag linearization since we're moving at large angles and velocities. Thus, we solve it numerically using the Dormand–Prince method (via ode45 in Matlab) to calculate its trajectory while swinging from one surface to the other, with initial conditions $\theta(0) = tan^{-1}(p/h)$ and $\dot{\theta}(0) = 0$.

With this model, if we can measure the ceiling height h and gap distance d using a camera or IR distance sensor, we can calculate the correct pivot distance p to place our anchor that will let us reach the other side at zero velocity.

4.4.2 Swinging Experimental Validation

To verify the model, a test bed was constructed as shown in Fig. 4.27. The test bed features three steel plates: one plate placed horizontally that serves as the starting surface that EEWOC is placed on, a second on the ceiling facing downward for the pivot attachment, and a third placed at the opposite end of the gap that functions as a vertical wall. The locations of the ceiling and opposite end plates could be adjusted to test various swing distances. To track the pivot location and main body while swinging, AprilTags with a high speed camera were used for visual tracking. Small marks were also added on the test bed frame to allow for easier manual positioning of the pivot and gap distance.

To begin each test, EEWOC's belly gripper was activated and magnetically attached to the starting plate for stability while reaching. The opposite end plate position was adjusted to a desired gap distance, and the end effector gripper was attached at the corresponding pivot distance. EEWOC was then driven up to the edge of the starting plate.

Before swinging, the belly gripper was rotated upwards to face the opposite end plate. This is to avoid adjusting the orientation of the belly gripper mid-swing, which is risky since it changes the location of the center of mass. The swing time is also very short, only 1-2 seconds. The tape was then retracted slightly, allowing the wheels to lift off of the surface by 1-2 mm. The body would then swing to the opposite surface and attach to the opposite end plate for a successful swing.

We found that swings were more stable when initiated by retracting the tape rather than driving off the edge with the wheels. This is because driving forward without changing the length of the limb will cause the limb to experience compression, creating unwanted reaction forces in the body just before swinging. We also determined that the shortening of the limb by 1-2 mm did not have a significant effect on the swinging dynamics, and still resulted in successful swings. This "lost" distance can potentially be gained by extending the limb

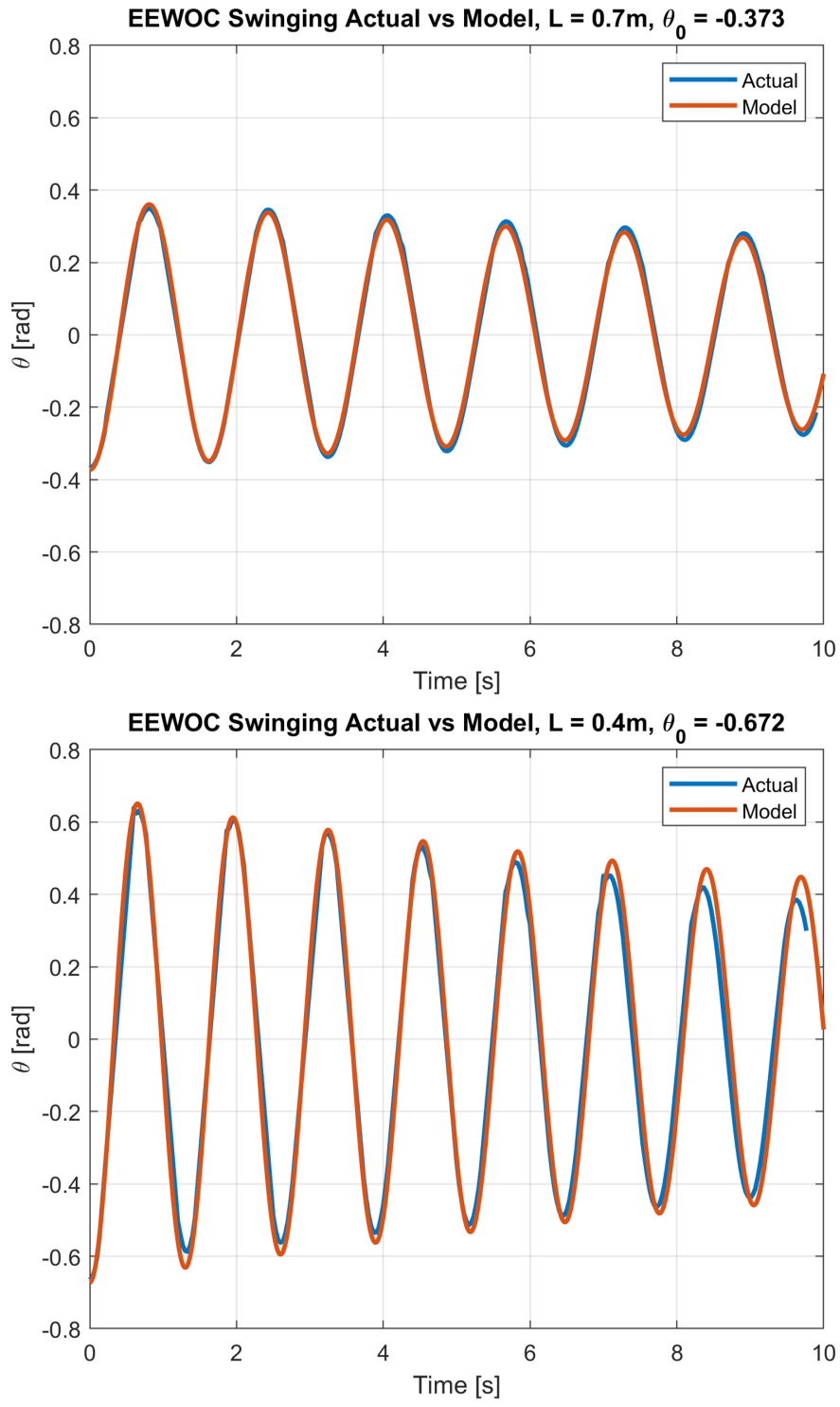

Figure 4.28: Actual vs calculated swinging trajectories.

Figure 4.29: Overlaid screenshots of EEWOC swinging between two surfaces on HVAC equipment.

mid-swing as well, though the system will lose some angular acceleration.

We also found that success was sensitive to the initial orientation of the main body and wheels. If the body was angled on the starting plate before swinging, this could cause the wheels to not leave the surface at the same time. This would result in the body twisting in yaw, which would cause the belly gripper to be misaligned with the opposite end plate before contact. In this case, the wheels would hit the plate first and the system would bounce off instead of attaching.

To test the accuracy of the selected damping parameters, data was also collected for free swinging at different pendulum lengths over multiple periods.

Figure 4.28 shows example trajectories of EEWOC swinging with different values for L and $\theta(0)$, where the model appears to track well with the measured data. With a smaller pendulum length and higher frequency, the model begins to track less well after a few cycles,

but is sufficient for this maneuver since swinging occurs over only half a period.

To demonstrate swinging in a real-world environment, EEWOC was subjected to swinging tests on the roof of UCLA. Two HVAC housings made of steel plates were selected to swing between based on their spacing (44 in or 1.1 m). EEWOC performed successful swings in this environment as well.

While the method to perform a swing remained the same for these tests, we noticed some additional phenomena in this new environment. In some cases, EEWOC would bounce off the surface at first approach, but could still attach successfully after waiting a period to swing back a second time or even third time. This may be caused by the pivot point being incorrectly positioned, causing EEWOC to swing with too large an amplitude and too much kinetic energy when reaching the surface the first time, resulting in it bouncing off. After the amplitude decays slightly during the second swing, attachment can be successful. This could also be caused by initial body misalignment, with the gripper at a slightly incorrect angle at first approach. After waiting a period to twist and settle, the gripper can potentially adjust to the correct orientation to attach successfully.

4.5 Performance Comparison and Analysis

To better understand the impact of EEWOC's different design strategies, we performed an in-depth comparison of EEWOC's performance metrics with data compiled from a wide range of existing robots.

4.5.1 EEWOC Climbing Performance

For the sake of comparison, EEWOC's climbing experiments used test conditions similar to existing robot studies, climbing a flat vertical wall with no obstacles.

Climbing speed was calculated by reviewing video footage of EEWOC climbing a flat steel wall at top speed across several trials. To achieve top speed, EEWOC's arm was extended to its full 1.2 m per step to minimize the number of attach/detach cycles. From this, EEWOC's top climbing speed was found to be 0.76 m/s or 4.4 m/min on average. To take a single step of 1.2 m, EEWOC took 15.8 s total, including the 2.8 s taken for each attach/detach cycle.

To test maximum climbing payload, EEWOC's end effector gripper was attached to the wall and weights were added to its belly gripper. If EEWOC could ascend successfully, more weights were added until EEWOC could no longer ascend due to motor stall or from the top gripper slipping. EEWOC could lift up to 3.4 kg of extra mass before reaching motor stall, over 160% of its own weight. This value was subsequently verified using a digital force gauge.

4.5.2 Existing Robot Performance Compilation

We then compiled climbing performance data for a wide variety of existing robots, with data from 14 of the top performing ones seen in Table 4.1. We omitted obvious outliers that had limited usefulness for real-world applications, such as robots with excessive tethering for offboard power or clamp-type robots that could only move in 1-DOF along a wire or pipe. Tethers can greatly limit the accessible locations, motions, and operational range of the robot. Additionally, long tethers can cause force management problems with having to carry the cable weight while climbing, and can restrict movement paths (to prevent it getting wrapped on itself, caught on things, etc.). Clamp-type climbing robots are greatly

Robot	Locomotion Type	Weight	Body Length	Step Length	Climbing Velocity	Normalized Velocity	Climbing Payload	Normalized Payload	End Effector	Environment
EEWOC by RoMeLa	Hybrid	2.1 kg	0.26 m	**1.2 m***	4.4 m/min	17 BL/min	3.4 kg	1.62	Magnetic	Steel surface + overhang
LEMUR 3 by JPL [20]	Legged (4)	35 kg	0.40 m	0.10 m	0.0027 m/min	0.0067 BL/min	N/A	N/A	Radial spine array	Rough surface + overhang
MARVEL by KAIST [24]	Legged (4)	8 kg	0.33 m	0.1 m	42 m/min	127.2 BL/min	2 kg	0.25	Magentic switchable	Steel surface + ceiling
SCALER by RoMeLa [25]	Legged (4)	6.3 kg	0.35 m	0.075 m	0.35 m/min	1 BL/min	3.4 kg	0.54	Spine array (2-finger)	Rough surface + ceiling
RiSE V3 by GRASP [10]	Legged (4)	5.4 kg	0.70 m	0.175 m	12.6 m/min	18 BL/min	1.5 kg	0.28	Spine array	Wood telephone pole
BOBCAT by FSU [21]	Legged (4)	5.0 kg	0.46 m	0.17 m	10.5 m/min	22.8 BL/min	N/A	N/A	Spine array	Singe wire mesh
HubRobo by Tohoku U [22]	Legged (4)	3.0 kg	0.35 m	0.15 m	4.2 m/min	12 BL/min	0.5 kg	0.17	Gecko adhesive	Rough surface
DynoClimber by GRASP [23]	Legged (2)	2.6 kg	0.40 m	0.13 m	40.2 m/min	100.5 BL/min	N/A	N/A	Spine array	Single carpeted surface
W-Climbot by BIRL [4]	Inchworm	16.1 kg	1.26 m	0.75 m	2.2 m/min	1.75 BL/min	1.5 kg	0.093	Suction cups	Smooth, flat surface + ceiling
Treebot by SIAIT [11]	Inchworm	0.6 kg	0.325 m	0.34 m	0.224 m/min	0.69 BL/min	1.75 kg	**2.92***	Spine array (4-finger)	Tree trucks + branches
OmniClimber by ISR [14]	Hybrid	1.1 kg	0.264 m	N/A, 90°	**8.4 m/min***	**31.8 BL/min***	1.2 kg	1.09	Magnetic switchable	Steel surface + ceiling
Magnebike by ETH Zurich [15]	Wheel	3.5 kg	0.22 m	N/A	2.7 m/min	12.3 BL/min	**3.57 kg***	1.02	Magnetic	Steel surface
MINOAS by DFKI [3]	Wheel	0.67 kg	0.38 m	N/A	30 m/min	78.9 BL/min	N/A	N/A	Magnetic	Steel, flat surface
DROP by JPL [8]	Wheel	0.3 kg	0.15 m	N/A	15 m/min	100 BL/min	0.1 kg	0.33	Spine array	Rough, flat surface
Waalbot by CMU [16]	Wheel	0.1 kg	0.13 m	N/A	3.6 m/min	27.7 BL/min	N/A	N/A	Gecko adhesive	Smooth, flat surface

Table 4.1: Table of performance metrics, sorted by locomotion type, then by system weight.

limited due to their simple 1D motion and they are typically not able to change between surfaces/cables/structures without human assistance.

In Table 4.1, *body length* is considered to be the length of the body in normal configuration, excluding the length of long tails used only for balance. *Step length* is the maximum distance the robot can reach with its limbs. This basically estimates the robot's reachable workspace with no dexterous orientation, since each robot has different needs for end effector orientation while climbing. Wheeled robots have a step length of essentially 0 since they generally require continuous rolling contact and can only reach anchor points directly next to their current position. However, some with discontinuous adhesion, such as DROP [8] can potentially overcome small gaps or cracks based on the spacing of their microspines or adhesion arrays. Notably, several robots did not publish climbing payload stats. These robots focused solely on achieving a high climbing speed, had a stated purpose of only visual inspection, or used highly dynamic movements that would have been adversely affected by added weight.

Among the many climbing robots summarized in Table 4.1, we chose a select few for direct comparison to EEWOC shown in Fig. 4.30. We chose 2 of each type: legged, inchworm, and hybrid wheeled, which exhibit some of the best climbing speeds, strengths, and step lengths.

SCALER from RoMeLa [25] is a quadrupedal free-climbing robot that uses microspines for rough surfaces, and is very strong with excellent payload capacity. The quadrupedal HubRobo from Tohoku U [22] also uses microspines and is very fast for a free-climbing robot, even beating some wheeled robots. W-Climbot from BIRL [4] is a large scale inchworm robot based on a conventional robotic arm that has a long steplength of 0.76 m. Treebot from SIAIT [11] is a unique inchworm robot with a compliant lightweight body structure and very lightweight microspine grippers, with excellent strength-to-weight ratio. Omniclimber from ISR [14] uses magnetic wheels and a small arm to transition between surfaces and is very compact. Finally, the very strong Magnebike from ETH Zurich [15] can lift 3.6 kg thanks to its powerful magnetic wheels.

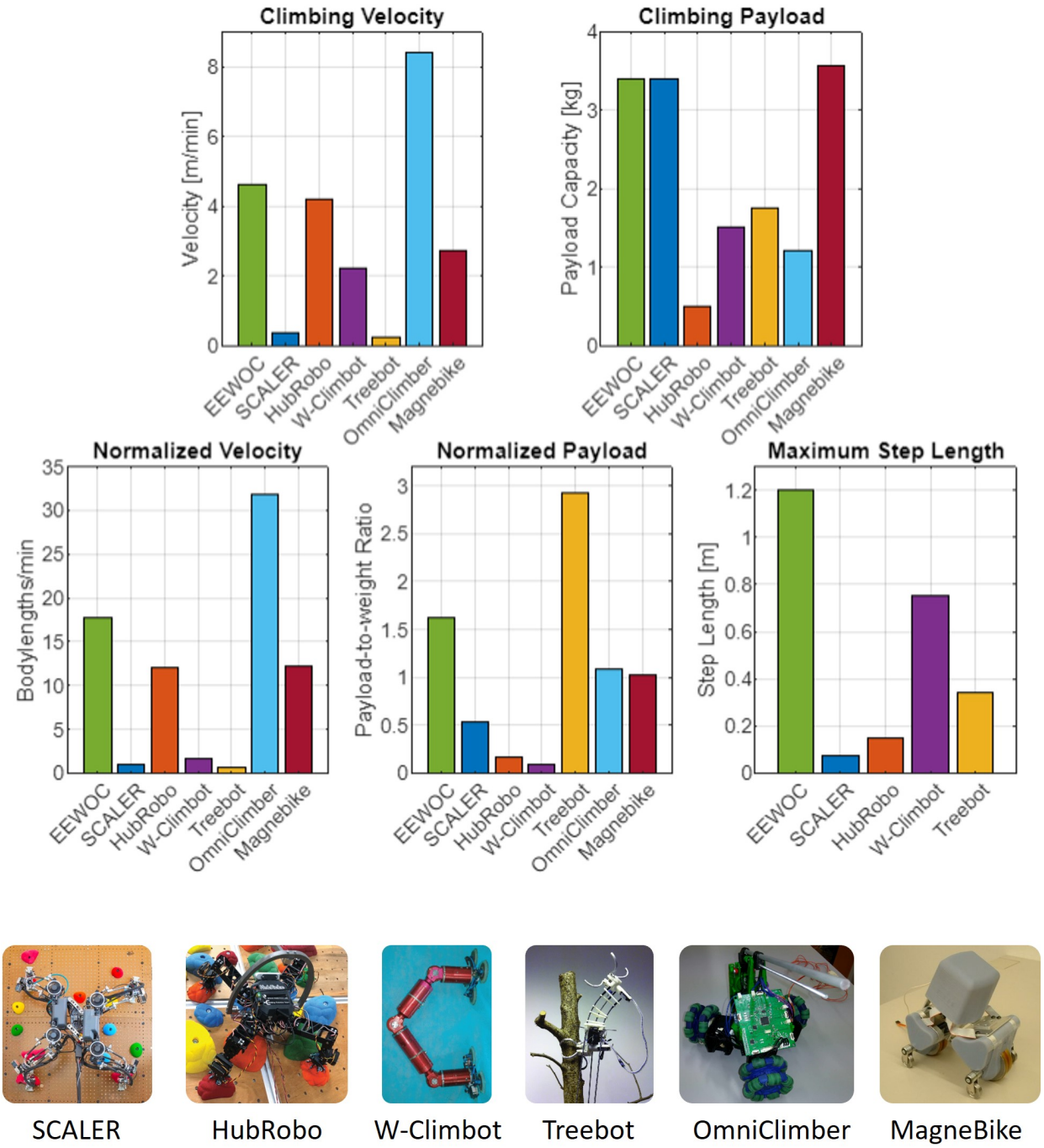

Figure 4.30: Graphs comparing performance metrics between EEWOC and the six other chosen climbing robots: SCALER [25], HubRobo [22], W-Climbot [4], Treebot [11], OmniClimber [14], and MagneBike [15]. These exhibit some of the best climbing speeds, strengths, and step lengths for their locomotion types.

These six robots were selected due to their clearly demonstrated ability to freely climb more complex 3D surfaces. This includes being able to overcome small gaps and protruding features, and more importantly the ability to transition between different angled surfaces, such as a vertical wall and horizontal ground. This condition eliminates almost all robots designed for single, flat surfaces. These robots tend to perform well in a controlled lab setting, but are impractical for deployment in real-world environments since they would require a human operator to manually place and relocate the robot onto different surfaces.

We also only considered robots with published payload-to-weight ratios. This is because many robots that focus purely on fast climbing speed are not designed to carry additional task-specific equipment, which limits their ability to perform useful tasks. Other robots that focus on high speed have issues with dynamics and poor adhesion reliability, since quickly shifting masses and contact conditions can cause unpredictable forces that result in attachment failure.

4.5.3 Comparison with EEWOC

As seen in Fig. 4.30, EEWOC's climbing abilities are either first or second best in all categories. EEWOC's raw and normalized vertical climbing speed are top ranked among all the legged and inchworm-type robots. Only the hybrid wheeled OmniClimber exceeds EEWOC's speed, but has only 1/3 EEWOC's payload capacity and minimal surface adaptability.

For raw payload capacity, EEWOC has nearly equal performance with the top ranked MagneBike and its strong magnetic wheel system. However, MagneBike climbs at half of EEWOC's speed despite being the same size. For payload-to-weight ratio, the inchworm Treebot has impressive normalized payload capacity thanks to its novel lightweight design, but can only carry half the weight that EEWOC can and climbs nearly 20 times slower, despite being twice EEWOC's size.

Looking at all of the compiled data reveals a few interesting trends. Multi-legged robots intended for free-climbing, like SCALER and HubRobo, have generally slower climbing speeds than other legged robots because they accounted for path planning and identifying anchor points during their climbing trials. Many other quadrupedal robots did not account for this time when measuring their top speed. For example, MARVEL has one of the fastest top climbing speeds at 42 m/min while climbing a flat vertical surface. However, video footage of MARVEL shows that its speed is significantly lower when attempting to climb over a small obstacle on the wall. This demonstrates the fact that multiple limbs with small step size can slow down the system significantly since careful planning is needed for each step. Thus, it is important to note that the impressive top climbing speeds of certain robots are not fully representative of their abilities in real-world environments.

The data also shows that inchworm robots are not necessarily faster climbers even with their reduced limbs compared to multi-legged robots. However, the lightweight Treebot shows that a simplified morphology and minimized structures can grant the system excellent strength-to-weight ratio, as it can lift nearly three times its own weight, and the inchworm design gives it good reachability, able to extend 100% of its body length. Interestingly, the fastest robot among the six, the hybrid wheeled Omniclimber, went through a design process similar to EEWOC, where previous versions had a robotic arm that went through significant simplifying and structural reduction. In earlier prototypes, OmniClimber was equipped with a 4-DOF manipulator arm attached to the wheeled base, where it granted the capabilities of a wheeled and inchworm robot. However, the latest version instead uses a much more simplified 2-DOF mechanism, which guides its magnetic anchor in a mostly linear path using a long thin rod to reach adjacent walls. This greatly reduces the weight and complexity of control compared to the 4-DOF version, and is a great example of gaining adaptability while minimizing the amount of extra structures and actuators needed.

It is also important to note how much the adhesion mechanism can affect the performance of

the system. Two of the top ranked climbers, MARVEL and MagneBike, have great speed and strength despite their relatively bulky designs, thanks to their innovative magnetic adhesion mechanisms. These seek to maximize magnetic force while diminishing the airgap between the wall and the gripper's rubberized surfaces as much as possible for maximum adhesion. This could be useful for future versions of EEWOC's magnetic gripper.

As a final note, while EEWOC clearly leads all others in terms of maximum step length with its 1.2 m reach, this value was not normalized since the size of obstacles to traverse depends entirely on the specific environment that the robot is in. However, it could be useful to analyze a normalized step length or "*reachability ratio*" by dividing the robot's step length by its body length. Performing this calculation for all the robots shows EEWOC's impressive reachability ratio of 4.62, able to stretch over 400% of its body length. Unsurprisingly, the second and third place robots are both inchworm robots, with Treebot having a value of 1.05 and W-Climbot having a ratio of 0.6. The other legged robots all have values around 0.2-0.4, showing their relatively small step lengths for their size.

While there seems to be a general trend of designing for either high climbing speed or payload capacity, EEWOC's unique design allows it to be among the best in both fields, while also being able to overcome much larger obstacles with its long-reach limb, and being low-cost thanks to its reduced number of actuators and simple morphology.

Chapter 5

Conclusion and Future Work

5.1 Conclusion

In this work, we set out to develop a novel climbing robot that addresses the current limitations of the existing systems. Existing climbing robots have relied on conventional designs that are not well suited for climbing, which has prevented their practical use for inspection or maintenance tasks. Wheeled climbers suffer from the inability to overcome even small obstacles due to their very small reachable workspace, and legged climbers have relied on ground-based designs with overly complex morphologies that are heavy, slow, and expensive.

To achieve this, we performed a detailed re-examination of the requirements of climbing as they relate to robotic platforms. Taking inspiration from biomechanical studies of climbing animals, a more detailed model of the forces was developed, including lifting force and restrictions on friction and substrate conditions that were previously ignored in studies. A clear set of preferred high level design attributes was established, which can be used to qualitatively compare the many different climbing robot designs.

From these findings, an innovative robotic limb EEMMMa was developed that uses a tape spring as a lightweight, spoolable structure. The tape offers a greatly enhanced reachable workspace and can handle very high loads in tension while climbing. Its unique U-shape also allows it to handle loads in compression, and it can easily support the weight of its end effector while ascending even with its minimized structure. EEMMMa's bending mechanism takes advantage of the U-shaped structure by granting the limb a second degree of freedom with only a single primary motor. The usefulness of EEMMMa as a robotic limb was proven through successful climbing of shelves and ladders, as well as bending to reach the top of stairs and move the end effector to desired points. A simplified model was developed for the tape's bending behavior to allow the end effector to be controlled effectively.

Next, the EEWOC mobile robot combined the EEMMMa limb with additional features and degrees of freedom to allow it to travel freely along ferromagnetic 3D surfaces. EEWOC's morphology is highly simplified relative to other limbed robots, resulting in a system that is much lighter and faster thanks to its reduced structures and number of actuators. EEWOC demonstrated versatile movement options in unstructured environments, using the extending and bending capabilities of the tape spring limb combined with wheels. EEWOC was shown to be capable of climbing up vertical metal structures, hoisting itself onto roofs, and swinging across gaps. To better understand the impact of EEWOC's unique design, we collected performance data from a wide variety of existing climbing robots and performed a detailed comparison to determine how well each robot meets the high level design requirements detailed in our study.

The success of EEWOC's design philosophy serves as a reminder that designs can be improved by re-considering the core requirements of a system, and that seeking solutions outside of the conventional design space can be highly valuable.

5.2 Future Goals and Improvements

5.2.1 Limb Model

The next stage of research for this project will be forming a more complete model of the limb's tape spring segments and accurately predicting the end effector's movement while straightened or bent. Given the highly nonlinear nature of the tape spring, this may involve combining several existing models, techniques, and approximations to properly characterize the limb's behavior. Considering the straightened limb mostly behaves like a beam, and the bent limb behaves like two beams with a revolute joint, it would be best to use principles that can approximate its behavior as an underactuated semi-rigid link manipulator, rather than hyper-redundant continuum or soft robot.

Existing works can help analytically or numerically characterize the tape's initial large deflection in Stage 1 using large-deflection curved beam theories, especially for thin-walled structures [53, 54, 55]. For future real-time control schemes, analytical methods would be preferred for lighter computational load.

Additionally, the folded bending stiffness and rotation behavior should be characterized for deflection in Stage 3. The planar rod model developed by Seffen [39] that assumes a point hinge with two rigid bars is limited in that it does not account for the creation or migration of folds. A semi-analytical method used by Brougeois and Guinot [40, 56] builds upon this by accounting for the changes in the tape's cross-sectional shape. This method can be used to model the creation, splitting, and migration of folds, and should be able to identify where the fold will be generated given its end loading conditions. It should be noted that many of these existing theories deal primarily with opposite-sense bending, with S_1's combined equal-sense bending and twisting in Stage 2 proving difficult to model.

When bending at larger extensions, it may be necessary to consider the tape's own weight

as a distributed load since this will cause the tape to curve and invalidate the planar rod model's assumption that the unfolded segments are rigid. In this case, it might be necessary to adjust each segment's geometry and end conditions to account for the curvature of the member depending on the amount of extension, allowing for increased accuracy without an entirely new model.

The 2D bending case will be the primary focus, since most of these existing models are intended only for the 2D planar case. There is currently very little literature on 3D multi-axis bending for these thin materials. Equations can possibly be formulated in a general way to address 3D bends, as Walker [57] details an analytical model that can be used to determine the hinge moment for 3D bending in a skewed tape spring system. However, this model is slightly limited in that it is only valid for a hinge located at the midpoint of the tape segment.

It will likely be necessary to characterize the Stage 2's more complex combined bending and testing, due to its known difficulty to model. This could involve starting with existing literature on fold formation and initial buckling behavior with generalized beam theory for thin-walled structures [58, 59], and subsequently find some method to intelligently interpolate the behavior between this starting point and the post-buckling bending stiffness and rotation models for folded tape springs [39, 60]. While not a true analysis, this could offer a simple way to deal with the discontinuous behavior of the system.

5.2.2 Climbing Model

Another goal will be creating a modified model for climbing, including transitioning over ledges and corners. This combines the basic model of limb deployment with additional layers of complexity from the gripper forces, surface contact with the EEWOC body and wheels, and contact between the tape and the corner of the surface during transitions.

To verify and properly use the models detailed above, it will be necessary to experimentally characterize EEWOC's specific tape spring properties including snap-through peak moment and directional spring stiffness properties while straightened or folded. Previous works lay out a dedicated procedure to measure and identify these and attempt to relate the tape's geometric and material properties to these constants. It should be noted that the model constructed will be for this specific tape and limb only, and not be a general case for tapes of all materials and geometries. Once the full model is constructed, it can be experimentally verified with extending and bending tests deploying the limb to reach target points in different orientations with respect to gravity.

5.2.3 Autonomous Climbing and Path Planning

With proper models formed for the limb bending and climbing maneuvers, a proper closed-loop control system should be developed to improve positioning reliability. This could also involve sensor fusion from the IMUs and encoders, as well as with additional sensors such as cameras for vision or IR distance sensors to use with the swinging model.

With the addition of cameras at the end effector, we could develop autonomous path planning for EEWOC, developing a vision processing system for localization and identification of suitable anchor points. With path planning, EEWOC could safely move between anchor points and around obstacles. The planner should also consider the limb's preferred deployment directions when prioritizing potential anchor points. This will also be helpful for comparing EEWOC with existing robots that already have autonomous path planning, since we have yet to properly study the effects of a very large step length on overall path planning time.

5.2.4 Additional Climbing Demonstrations

There are several additional test maneuvers planned to explore the EEWOC's movement and manipulation capabilities. First, the corner traversing maneuver should be reattempted to gain additional insights on preventing the gripper failure after the belly gripper contact is lost. Another maneuver to test is attempting to use a partially activated belly gripper to maintain continuous contact with the surface while transitioning around the corner. Since the gripper operates with a cam system, it can be partially rotated to modulate the amount of magnetic force being applied. By adding a small amount of adhesion to gain traction for the wheels, it may be possible to transition around corners with more control without fully swinging to the next surface. This same tactic may also be useful for reducing the stress on the tape as it bends on sharp corners while climbing ledges.

5.2.5 Manipulation Demonstrations

Another area of interest is testing the tape spring limb's capabilities as a manipulator arm. With a model constructed, it should be able to serve as the base for planning manipulation tasks. A simple task that can be demonstrated is sample retrieval, which will involve moving the end effector to a desired location and retrieving a small steel block. This will also be useful for observing changes in behavior when the limb has extra mass at the end effector, or when it attempts to climb, drive, or transition between surfaces with a significant payload.

5.2.6 Additional Tail Mechanism

One beneficial subsystem to add would be a small 1-DOF actuated tail that can deploy from the back of EEWOC's main body. This tail could serve several purposes, namely increasing stability and reliability while climbing. A tail would allow EEWOC to apply a second point

of contact much further than the idle ball casters to better compensate for the pitchback moment. It could also assist with transitioning above ledges, with the tail maintaining a point of contact lower on the vertical wall while climbing over the ledge corner. This would provide the additional benefit of offloading some of the forces that the tape experiences as it digs into the corner of the ledge during transition.

Another exciting application of the tail would be to actuate it during swinging maneuvers to change EEWOC's trajectory while mid-swing. While this is technically possible on the existing system by actuating the main body, an additional tail would provide a much greater effect since its shifting weight would be at a much longer moment arm than the main body's. This could allow for larger and faster changes to its swinging trajectory, and could even be used to allow EEWOC to work up to a swing from a rest, static hanging position, similar to the motion used by gymnasts.

5.2.7 Additional Microspine Gripper

Another useful development for EEWOC would be the creation of additional end effectors to grant new ways for EEWOC to interact with environments. A prototype radial microspine gripper is already in development that will allow EEWOC to adhere to rough surfaces, shown in Fig. 5.1. This utilizes a radial array of compliant linkages made from laser-cut delrin sheets for simple and lightweight construction. The linkages are actuated by an N20 motor that will close the gripper using a similar two-state cam system as the original gripper. The microspine gripper should be much lighter than the magnetic gripper due to it containing less metal, which should reduce the load on the tape spring limb for more controlled extending and bending.

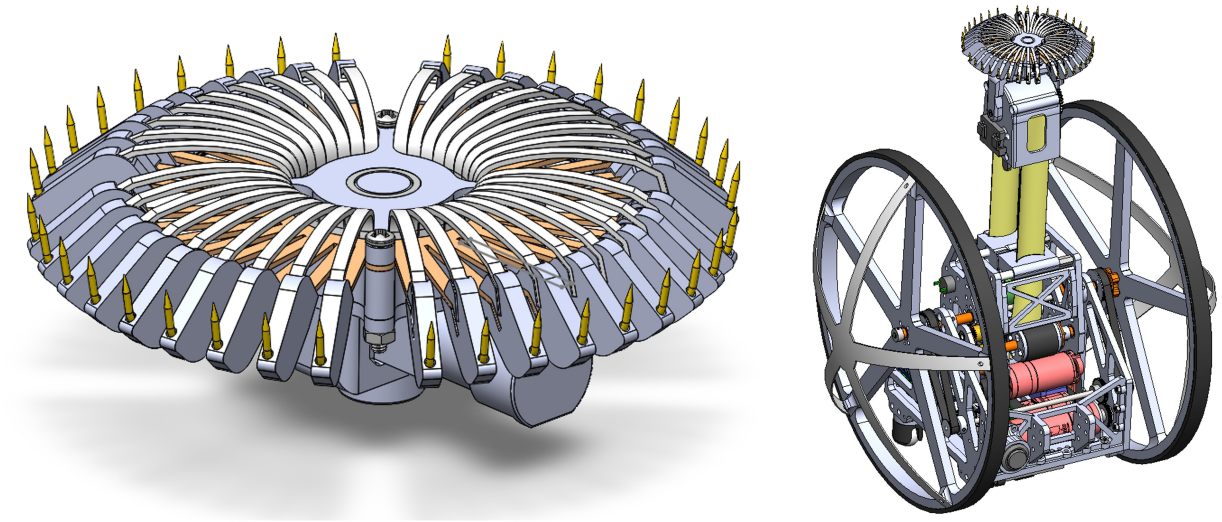

Figure 5.1: CAD of the proposed microspine gripper. a) Close up view of the gripper. Two sheets of laser-cut delrin form the top and bottom links (in white and orange). b) Full view of the gripper mounted on EEWOC.

5.2.8 Additional Performance Studies

There are several additional studies that would be useful to test EEWOC's performance as a mobile robot. An energy efficiency study of the system while driving or climbing would be very useful for determining EEWOC's maximum deployment duration and how task complexity affects its battery life. This can involve calculating the energetic cost of transport and comparing them to existing animals or other robots designed for efficiency.

Reliability studies will also be useful, especially for grippers and magnetic attachment. This will involve identifying surface parameters and measuring metrics to figure out what exact factors are beneficial or harmful for successful attachment. A reliability study of swinging and other dynamic or risky maneuvers would be beneficial as well.

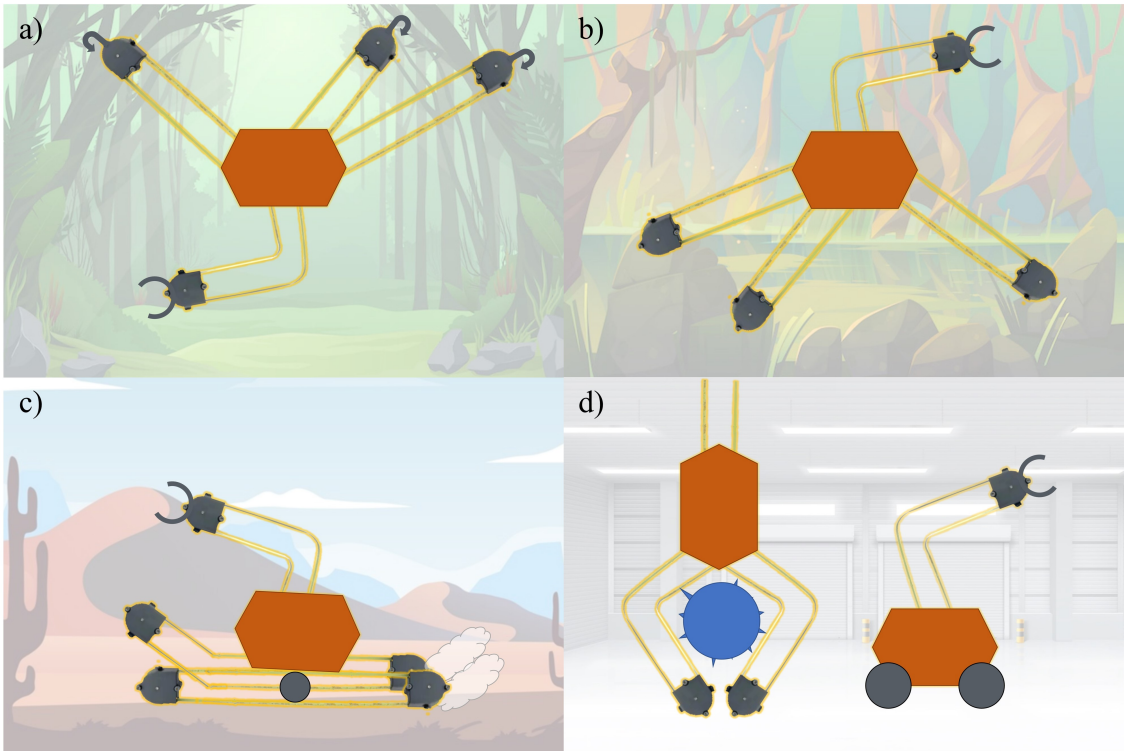

Figure 5.2: Concept art of potential EEMMMa configurations. Many concepts have redundant limbs that can be repurposed for inspection or manipulation tasks. a) Suspended robot that deploys anchors to trees. b) Quadruped with telescopic point feet. c) Tread morphing closed-loop tape tank robot. d) Manipulation focused robots.

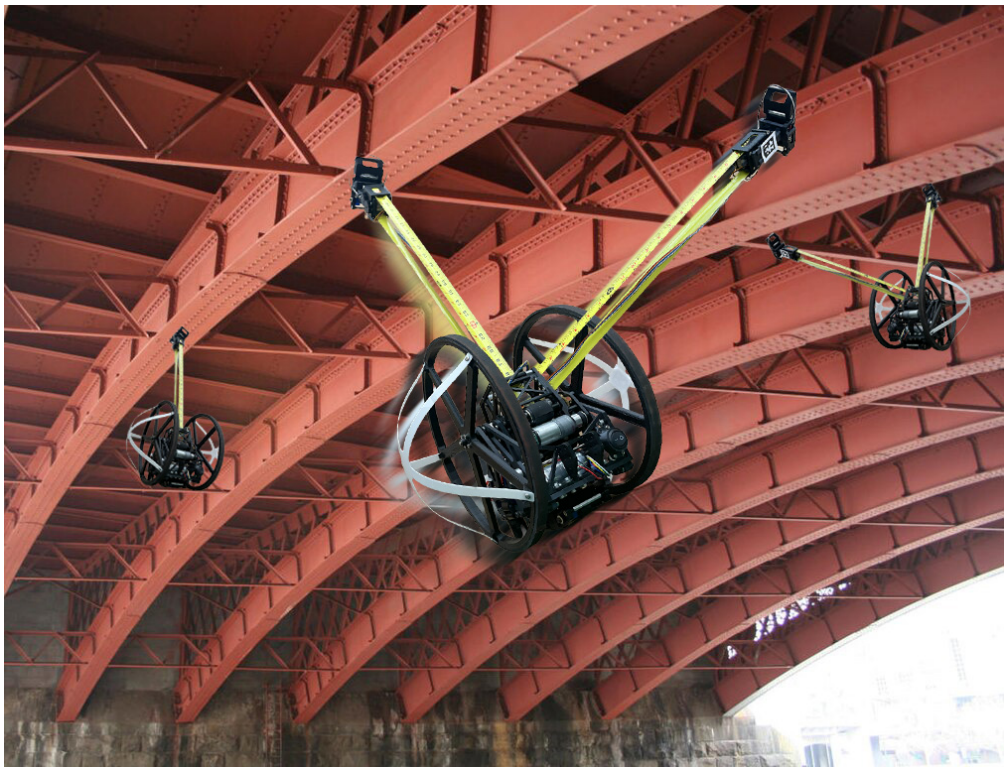

Figure 5.3: Concept art of future EEWOC units below a bridge, swinging with multiple limbs to move quickly between points of interest.

Figure 5.4: Concept art of future EEWOC units in a cave, suspending with microspine grippers to traverse over water and rocky terrain.

Figure 5.5: Concept art of future EEWOC units in a forest, swinging and suspending with multiple limbs to collect samples from the forest floor.

5.3 Future Vision

This research will be the first step in a variety of dynamic movement options for mobile robots utilizing EEMMMa and EEWOC's novel tape spring limbs. The ultimate future goal envisioned for this project is a versatile mobile robot with multiple tape spring limbs that can suspend itself in midair and swing between distant points, as shown in Fig. 5.2a. Since this mobility scheme only requires three anchor points for safe motion, this system would be excellent for navigating through caves or dense forests where terrain is highly unstructured and there are large vertical structures for anchoring and climbing. For a three-limbed system, since only two limbs are needed to suspend the body, the third limb could be used to deploy a camera or retrieve a sample from below. For a four-limbed system, the multimodal nature of each limb grants the system built-in redundancy for both mobility and manipulation tasks. Even if a limb is damaged, the system can continue functioning by simply repurposing the remaining limbs.

Beyond climbing robots, there are many other mobility schemes that can be explored. Legged

locomotion could use EEMMMa-based extendable legs for a quadrupedal system, depicted in Fig.5.2b. This could be highly advantageous for stepping over obstacles rather than traveling around them. In environments that feature wide-spanning hazards like water and mud, such as swamps, this would make path planning much easier and safer. For manipulation tasks, the quadruped could establish three stable points of contact with the floor and use the fourth limb as a bendable arm for tasks such as reaching submerged objects.

The principles explored with these tape spring limbs could also be applied to other robotic systems. EEMMMa's morphability could be used for a closed-loop continuous tape as a tank tread for movement, utilizing the pulley-brake mechanism to morph the shape of the treads to move over obstacles, as seen in Fig. 5.2c. Smaller scale EEMMMa limbs could serve as fingers for a compliant gripper that morphs its shape to conform around objects, shown in Fig. 5.2d. The tape's steel construction could be favorable for conforming to shapes with sharp corners that could damage other soft robotic shape-morphing manipulators.

In the future, we envision a versatile, strong, fast, efficient, and safe mobile robot that can swing through cities, caves, or forest canopies like a spider monkey, performing inspection, surveillance, or retrieval tasks in remote locations that are difficult to reach with conventional robots. Figures 5.3, 5.4, and 5.5 show concept art illustrating this possible future. The principles learned through the development of EEWOC could be revolutionary for creating even more advanced climbing robots in the future.

Appendix A

Summary Videos

EEMMMa 2-minute summary: https://www.youtube.com/watch?v=DUqitknbvWo

EEMMMa full presentation: https://www.youtube.com/watch?v=kpfhz2M1VF4

EEWOC 2-minute summary: https://www.youtube.com/watch?v=usxON_JnEmw

Appendix B

General Notes on Adhesion

Before analyzing the different adhesion methods in detail, it is important to remember the major preferred attributes of adhesion, namely strong adhesion force, minimized time to attach/detach, and reliability or probability of success, as described in the main text.

B.1 Gripper and Wrist Mechanisms

Since the adhesion force is applied normal to the surface, and since 3D surfaces can have widely varying topologies, most climbing robots also feature a wrist or gripper mechanism to ensure the adhesion force is applied to the surface properly. This usually takes the form of additional DOF to align hooks or suction cups in the correct orientation for attachment. These additional DOF can either be actively controlled with extra motors, or added passively using compliant mechanisms.

Gripper mechanisms can also involve "fingers" or other structures to generate adhesive force in multiple directions, which improves the robustness of the attachment point. The gripper complexity is highly dependent on the robot's intended climbing environment. For example,

many cable climbing robots only need a single additional hinge to clamp down on a standard diameter cable. Other robots such as JPL's LEMUR require a full 3-DOF wrist and a radial gripper with many microspine fingers at all angles to ensure proper engagement as it climbs cave walls with random orientations [20].

In general, a gripper mechanism should be as lightweight as possible, since it is generally located at the end effector and distal mass is undesirable. Since higher adhesion force is always desirable, a high adhesion strength-to-weight ratio is also desired. Additionally, the gripper assembly should be preferably thin to minimize the moment arm between the attachment point and the force on the gripper from the robot's center of mass. Finally, the gripper should ideally spread the adhesion force over a large area to improve its robustness. Spreading out the adhesion forces over multiple points decreases the overall effect of any local surface defects like cracks or weak substrate that could cause attachment to fail.

B.2 Magnetic Attachment

The first and most simple form of adhesion is magnetic adhesion, used for climbing ferromagnetic environments. Robots equipped with magnetic grippers are commonly designed for climbing steel structures which are ubiquitous in urban environments. This includes pipes, poles, power lines, towers, ships, factories, and bridges, all vital pieces of infrastructure that require regular inspections and maintenance to ensure safety.

A major advantage of magnetic adhesion is its ability to apply a force before contact is made with the surface. When approaching the surface, the magnetic force assists with pulling the gripper towards the surface in the correct orientation until a firm grip is achieved. The adhesion force can either be actively applied using electromagnets [61], or entirely passive using permanent magnet's natural attraction to steel structures [3, 12, 15, 17, 62]. Other

methods use a combination of the two, with a permanent magnet that gets "turned off" with an electromagnet. There are also "switchable" permanent magnets and polymagnets that can alter their applied magnetic field when poles are rotated relative to each other, allowing a small motor to easily switch them "on" or "off" for fast attachment and detachment [14].

Robots that employ magnetic grippers tend to have heavier end effectors, since they're dependent on magnetized metals for their adhesive force. Electromagnets can easily be switched on and off, but permanent magnets need additional mechanisms to reduce or redirect the magnetic force while climbing. Permanent magnets are are still generally preferred over electromagnets, which have a weaker pull-in force and require constant power to remain active. Combination electro + permanent magnets and "switchable" permanent magnets both result in even heavier grippers, since the amount of magnetic material is essentially being doubled just to cancel out the existing field. Additionally, "switchable" permanent magnets have poor strength-to-weight ratios compared to their non-switchable counterparts. This is because they fundamentally apply their magnetic force using the sides of the magnets, where the magnetic flux is about 50% lower compared to at the poles.

B.3 Pneumatic Attachment

Another simple form of attachment uses pneumatic elements, utilizing air pressure differentials to push the robot toward the wall. This is commonly achieved by creating negative pressure with powered vacuums or passive suction cups that attach to the surface [4, 9, 63]. Robots can also use propellers to pushes the robot towards the surface with directed air flows.

Like magnetic adhesion, powered pneumatic adhesion with vacuums or propellers also benefits from non-contact force application, since air pressure can be used to push the gripper

towards the wall. These methods also have the additional advantage of being able to adhere to many types of surfaces, regardless of surface finish or material and is not limited to steel surfaces like magnets nor rough surfaces like microspines. However, passive suction cups are less flexible since they still require surface contact to activate, and can only be used on surfaces with smooth, flat faces that can form a tight seal.

Most robots that use pneumatic adhesion have a limited load capacity, since it's just air pressure keeping them attached to the surface. This means they are almost always unable to carry useful equipment beyond their own body weight, or require a tether which greatly limits their movement options. Additional issues arise from the mechanics of moving air, as vacuum suction can require air pumps which are heavy, bulky, and loud. Propeller-based climbers must constantly consume power to stay adhered to the surface, making them inefficient. Finally, the effectiveness of these systems can be heavily affected by changes in air temperature and humidity, and they cannot be used at all in environments with little or no air such as on other planets or the vacuum of space.

B.4 Microspine and Hook Attachment

Microspine attachment is a form of adhesion that uses small, sharp hooks to physically engage into microscale pores on rough surfaces. Microspines are usually dragged across a rough surface until the sharp tip locks into a micropore, allowing loads to be transfered. Microspines are lightweight and can be used in a wide variety of environments thanks to the high occurrence of rough surfaces in nature. They can be used to grip into rocks to climb up cave walls [22, 25] or softer materials like wood, tree bark, and branches [10, 11]. Rough surfaces are also present in manmade environments like bricks, pavement, and concrete [8, 50, 64, 65]. Microspines also have space-based applications, where they can be used for adhering to asteroids for drilling samples, or for exploring cave systems and lava tubes on

distant planets with low gravity [20]. Microspine grippers are relatively power efficient, since most use a locking mechanism such as a screw to allow the grip to be sustained passively without supplying power.

Since microspines are essentially small hooks, they require directional engagement. The microspine tips must approach the surface at a specific range of angles and must be loaded in specific directions to generate enough friction for a proper grip. Because each microspine is very small, they are generally mounted into large arrays that allow large loads to be shared between many individual spines. Microspine arrays come in a wide variety of shapes, with some using a single row of microspines, and others using two sets of arrays pointed in opposite directions in order to resist pitch-back torques better. There are also others that use a radial pattern of spines to guarantee successful engagement at any angle. Many microspine arrays also use passive compliant mechanisms that allow each spine to move in one or more directions to deform around small scale bumps and variations until they encounter a micropore.

Since they physically engage with a surface by locking on microscale geometries, microspines can carry very large forces when distributed across the array. However, the strength of the grip is highly stochastic and dependent on the density of suitable micropores on the surface. This makes them somewhat unreliable in environments with variable surface roughness. Their performance can also degrade over time, since the sharp tips wear down from scraping on surfaces. This reduces the probability of encountering suitable micropores in the rough surface, making the spines less reliable unless they are occasionally replaced. Microspine arrays also tend to have complex construction and assembly processes due to the need for compliance on each individual spine. The sharp tips can also cause damage to surfaces while climbing, especially in soft materials like wood.

B.5 Dry Adhesive Attachment

Dry adhesives refers to a class of adhesive materials that utilize the van der Waals forces between an array of microscopic features and the substrate for adhesion. These are also commonly referred to as "gecko adhesives", since they are based the properties of gecko footpads. Unlike wet adhesives like glue or tape, dry adhesives do not leave a residue.

Dry adhesives generally take the form of large patches of small directional compliant microscale stalks that push against the surface for very close contact, since the intermolecular forces decrease significantly from any distance caused by surface variations [16, 66, 67]. Many grippers equipped with dry adhesives utilize flexible base pads or fingers to handle millimeter or centimeter scale variations [6]. Dry adhesives are very easy to engage and disengage since they require no force to activate, only requiring contact. They also have an excellent strength-to-weight ratio, since they are primarily made of lightweight elastomers, and take up almost no space due to their thin nature.

However, dry adhesives have limited practical uses due to their very high sensitivity to surface conditions. Since the microstalks need extremely close contact with the surface, current dry adhesives can only be used to climb smooth surfaces such as glass, metal, or plastic. They perform well on highly polished surfaces, but perform poorly on slightly textured or porous surfaces. The need for microscale compliance also means that most examples are limited to climbing only flat, featureless surfaces.

Dry adhesives also have a limited payload capacity due to their dependence on intermolecular van der Waals forces. They scale well for handling small loads, but are impractical for handling large loads, despite their good strength-to-weight ratio. Their complex microscale structure also means they are expensive and difficult to manufacture, and are not cost effective for use on large projects.

B.6 Clamping Attachment

Clamp-type adhesion is the final form of adhesion, which entails clamping directly onto the climbing medium by physically compressing it. This type of adhesion is usually to climb thin structures with a regular outer shape, especially cylindrical ones such as wires, cables, pipes, and poles [7, 13, 19]. The outer shape can be fully surrounded by contacts from wheels or fingers, which are then compressed around the structure to generate enough friction to resist gravity. This simple form of adhesion allows wheeled cable climbing robots to climb at high speeds. Clamping adhesion is also very reliable since it is only ever used in very controlled environments with regular and consistent geometries.

However, clamping adhesion offers almost no adaptability, making it impractical for automating tasks in the real world. Climbing robots that use this method are generally confined to 1D motion in a straight path along the wire or pipe, and most need assistance from a human operator to relocate them onto different surfaces.

Bibliography

[1] G. Fang and J. Cheng, "Advances in climbing robots for vertical structures in the past decade: A review," *Biomimetics*, vol. 8, no. 1, p. 47, 2023.

[2] M. F. Silva and J. T. Machado, "A survey of technologies and applications for climbing robots locomotion and adhesion," *Climbing and walking robots*, pp. 1–22, 2010.

[3] M. Eich and T. Vögele, "Design and control of a lightweight magnetic climbing robot for vessel inspection," in *2011 19th Mediterranean Conference on Control & Automation (MED)*. IEEE, 2011, pp. 1200–1205.

[4] Y. Guan, H. Zhu, W. Wu, X. Zhou, L. Jiang, C. Cai, L. Zhang, and H. Zhang, "A modular biped wall-climbing robot with high mobility and manipulating function," *IEEE/ASME transactions on mechatronics*, vol. 18, no. 6, pp. 1787–1798, 2012.

[5] S. Wang, H. Jiang, and M. R. Cutkosky, "A palm for a rock climbing robot based on dense arrays of micro-spines," in *2016 IEEE/RSJ International Conference on Intelligent Robots and Systems (IROS)*. IEEE, 2016, pp. 52–59.

[6] S. Kim, M. Spenko, S. Trujillo, B. Heyneman, V. Mattoli, and M. R. Cutkosky, "Whole body adhesion: hierarchical, directional and distributed control of adhesive forces for a climbing robot," in *Proceedings 2007 IEEE International Conference on Robotics and Automation*. IEEE, 2007, pp. 1268–1273.

[7] A. Baghani, M. N. Ahmadabadi, and A. Harati, "Kinematics modeling of a wheel-based pole climbing robot (ut-pcr)," in *Proceedings of the 2005 IEEE international Conference on Robotics and Automation*. IEEE, 2005, pp. 2099–2104.

[8] A. Parness and C. McKenzie, "Drop: the durable reconnaissance and observation platform," *Industrial Robot: An International Journal*, vol. 40, no. 3, pp. 218–223, 2013.

[9] J. Xiao, B. Li, K. Ushiroda, and Q. Song, "Rise-rover: A wall-climbing robot with high reliability and load-carrying capacity," in *2015 IEEE International Conference on Robotics and Biomimetics (ROBIO)*. IEEE, 2015, pp. 2072–2077.

[10] G. C. Haynes, A. Khripin, G. Lynch, J. Amory, A. Saunders, A. A. Rizzi, and D. E. Koditschek, "Rapid pole climbing with a quadrupedal robot," in *2009 IEEE International Conference on Robotics and Automation*. IEEE, 2009, pp. 2767–2772.

[11] T. L. Lam and Y. Xu, "A flexible tree climbing robot: Treebot-design and implementation," in *2011 IEEE International Conference on Robotics and Automation*. IEEE, 2011, pp. 5849–5854.

[12] S. T. Nguyen, A. Q. Pham, C. Motley, and H. M. La, "A practical climbing robot for steel bridge inspection," in *2020 IEEE International Conference on Robotics and Automation (ICRA)*. IEEE, 2020, pp. 9322–9328.

[13] K. H. Cho, Y. H. Jin, H. M. Kim, H. Moon, J. C. Koo, and H. R. Choi, "Multifunctional robotic crawler for inspection of suspension bridge hanger cables: Mechanism design and performance validation," *IEEE/ASME Transactions on Mechatronics*, vol. 22, no. 1, pp. 236–246, 2016.

[14] M. Tavakoli, J. Lourenco, C. Viegas, P. Neto, and A. T. de Almeida, "The hybrid omniclimber robot: Wheel based climbing, arm based plane transition, and switchable magnet adhesion," *Mechatronics*, vol. 36, pp. 136–146, 2016.

[15] F. Tâche, W. Fischer, G. Caprari, R. Siegwart, R. Moser, and F. Mondada, "Magnebike: A magnetic wheeled robot with high mobility for inspecting complex-shaped structures," *Journal of Field Robotics*, vol. 26, no. 5, pp. 453–476, 2009.

[16] M. P. Murphy and M. Sitti, "Waalbot: An agile small-scale wall-climbing robot utilizing dry elastomer adhesives," *IEEE/ASME transactions on Mechatronics*, vol. 12, no. 3, pp. 330–338, 2007.

[17] H. Eto and H. H. Asada, "Development of a wheeled wall-climbing robot with a shape-adaptive magnetic adhesion mechanism," in *2020 IEEE International Conference on Robotics and Automation (ICRA)*. IEEE, 2020, pp. 9329–9335.

[18] J. Ye, Y. Guan, Z. Bi, G. Zhao, D. Luo, and T. Liu, "A novel miniature modular wire inspection robot with multiple locomotion modes," in *2013 IEEE International Conference on Mechatronics and Automation*. IEEE, 2013, pp. 1185–1190.

[19] Z. Zheng, W. Zhang, X. Fu, S. Hazken, X. Hu, H. Chen, J. Luo, and N. Ding, "Ccrobot-iv: An obstacle-free split-type quad-ducted propeller-driven bridge stay cable-climbing robot," *IEEE Robotics and Automation Letters*, vol. 7, no. 4, pp. 11 751–11 758, 2021.

[20] A. Parness, N. Abcouwer, C. Fuller, N. Wiltsie, J. Nash, and B. Kennedy, "Lemur 3: A limbed climbing robot for extreme terrain mobility in space," in *2017 IEEE international conference on robotics and automation (ICRA)*. IEEE, 2017, pp. 5467–5473.

[21] M. Austin, "Towards dynamic legged multimodal field robotics: Running and climbing," Ph.D. dissertation, The Florida State University, 2018.

[22] K. Uno, N. Takada, T. Okawara, K. Haji, A. Candalot, W. F. Ribeiro, K. Nagaoka, and K. Yoshida, "Hubrobo: A lightweight multi-limbed climbing robot for exploration in challenging terrain," in *2020 IEEE-RAS 20th International Conference on Humanoid Robots (Humanoids)*. IEEE, 2021, pp. 209–215.

[23] G. A. Lynch, J. E. Clark, P.-C. Lin, and D. E. Koditschek, "A bioinspired dynamical vertical climbing robot," *The International Journal of Robotics Research*, vol. 31, no. 8, pp. 974–996, 2012.

[24] S. Hong, Y. Um, J. Park, and H.-W. Park, "Agile and versatile climbing on ferromagnetic surfaces with a quadrupedal robot," *Science Robotics*, vol. 7, no. 73, p. eadd1017, 2022.

[25] Y. Tanaka, Y. Shirai, X. Lin, A. Schperberg, H. Kato, A. Swerdlow, N. Kumagai, and D. Hong, "Scaler: A tough versatile quadruped free-climber robot," in *2022 IEEE/RSJ International Conference on Intelligent Robots and Systems (IROS)*. IEEE, 2022, pp. 5632–5639.

[26] H. Preuschoft, "What does" arboreal locomotion" mean exactly and what are the relationships between" climbing", environment and morphology?" *Zeitschrift für Morphologie und Anthropologie*, pp. 171–188, 2002.

[27] C. Vehar, S. Kota, and R. Dennis, "Closed-loop tape springs as fully compliant mechanisms: preliminary investigations," in *International Design Engineering Technical Conferences and Computers and Information in Engineering Conference*, vol. 46954, 2004, pp. 1023–1032.

[28] B. H. Do, O. G. Osele, and A. M. Okamura, "A lightweight, high-extension, planar 3-degree-of-freedom manipulator using pinched bistable tapes," *arXiv preprint arXiv:2110.09751*, 2021.

[29] C. C. Kemp, A. Edsinger, H. M. Clever, and B. Matulevich, "The design of stretch: A compact, lightweight mobile manipulator for indoor human environments," *arXiv preprint arXiv:2109.10892*, 2021.

[30] S. Teshigawara and H. H. Asada, "A mobile extendable robot arm: Singularity analysis and design*," *2019 IEEE/RSJ International Conference on Intelligent Robots and Systems (IROS)*, pp. 5131–5138, 2019.

[31] A. Shikari and H. Asada, "Triple scissor extender robot arm: a solution to the last one foot problem of manipulation," *IEEE Robotics and Automation Letters*, vol. 3, no. 4, pp. 3975–3982, 2018.

[32] D. Rus and M. T. Tolley, "Design, fabrication and control of soft robots," *Nature*, vol. 521, no. 7553, pp. 467–475, 2015.

[33] N. K. Uppalapati and G. Krishnan, "Valens: Design of a novel variable length nested soft arm," *IEEE Robotics and Automation Letters*, vol. 5, no. 2, pp. 1135–1142, 2020.

[34] A. K. Mishra, E. Del Dottore, A. Sadeghi, A. Mondini, and B. Mazzolai, "Simba: Tendon-driven modular continuum arm with soft reconfigurable gripper," *Frontiers in Robotics and AI*, vol. 4, p. 4, 2017.

[35] M. Aliff, S. Dohta, and T. Akagi, "Control and analysis of robot arm using flexible pneumatic cylinder," *Mechanical Engineering Journal*, vol. 1, no. 5, pp. DR0051–DR0051, 2014.

[36] M. Taffetani, F. Box, A. Neveu, and D. Vella, "Limitations of curvature-induced rigidity: How a curved strip buckles under gravity," *EPL (Europhysics Letters)*, vol. 127, no. 1, p. 14001, 2019.

[37] V. Pini, J. Ruz, P. M. Kosaka, O. Malvar, M. Calleja, and J. Tamayo, "How two-dimensional bending can extraordinarily stiffen thin sheets," *Scientific reports*, vol. 6, no. 1, pp. 1–6, 2016.

[38] A. M. Watt and S. Pellegrino, "Tape-spring rolling hinges," in *Proceedings of the 36th Aerospace Mechanisms Symposium*. Citeseer, 2002, pp. 15–17.

[39] K. Seffen and S. Pellegrino, "Deployment dynamics of tape springs," *Proceedings of the Royal Society of London. Series A: Mathematical, Physical and Engineering Sciences*, vol. 455, no. 1983, pp. 1003–1048, 1999.

[40] F. Guinot, S. Bourgeois, B. Cochelin, and L. Blanchard, "A planar rod model with flexible thin-walled cross-sections. application to the folding of tape springs," *International Journal of Solids and Structures*, vol. 49, no. 1, pp. 73–86, 2012.

[41] S. Jeon and T. Murphey, "Design and analysis of a meter-class cubesat boom with a motor-less deployment by bi-stable tape springs," in *52nd AIAA/ASME/ASCE/AHS/ASC Structures, Structural Dynamics and Materials Conference 19th AIAA/ASME/AHS Adaptive Structures Conference 13t*, 2011, p. 1731.

[42] K. Seffen, Z. You, and S. Pellegrino, "Folding and deployment of curved tape springs," *International Journal of Mechanical Sciences*, vol. 42, no. 10, pp. 2055–2073, 2000.

[43] F. Dewalque, J.-P. Collette, and O. Brüls, "Mechanical behaviour of tape springs used in the deployment of reflectors around a solar panel," *Acta Astronautica*, vol. 123, pp. 271–282, 2016.

[44] W. Gan and S. Pellegrino, "Closed-loop deployable structures," in *44th AIAA/ASME/ASCE/AHS/ASC Structures, Structural Dynamics, and Materials Conference*, 2003, p. 1450.

[45] S. Schneider, A. Bylard, T. G. Chen, P. Wang, M. Cutkosky, and M. Pavone, "Reachbot: A small robot for large mobile manipulation tasks," *arXiv preprint arXiv:2110.10829*, 2021.

[46] K. Seffen and S. Pellegrino, "Deployment of a rigid panel by tape-springs," 1997.

[47] S. Pellegrino, C. Green, S. Guest, and A. Watt, *SAR advanced deployable structure*. University of Cambridge, Department of Engineering, 2000.

[48] S. Oberst, S. Tuttle, D. Griffin, A. Lambert, and R. Boyce, "Experimental validation of tape springs to be used as thin-walled space structures," *Journal of Sound and Vibration*, vol. 419, pp. 558–570, 2018.

[49] S. Pellegrino, "Folding and deployment of thin shell structures," in *Extremely deformable structures*. Springer, 2015, pp. 179–267.

[50] M. J. Spenko, G. C. Haynes, J. Saunders, M. R. Cutkosky, A. A. Rizzi, R. J. Full, and D. E. Koditschek, "Biologically inspired climbing with a hexapedal robot," *Journal of field robotics*, vol. 25, no. 4-5, pp. 223–242, 2008.

[51] A. Pedivellano and S. Pellegrino, "Stability analysis of coiled tape springs," in *AIAA Scitech 2019 Forum*, 2019, p. 1523.

[52] E. H. Mansfield, "Large-deflexion torsion and flexure of initially curved strips," *Proceedings of the Royal Society of London. A. Mathematical and Physical Sciences*, vol. 334, no. 1598, pp. 279–298, 1973.

[53] K.-J. Bathe and S. Bolourchi, "Large displacement analysis of three-dimensional beam structures," *International journal for numerical methods in engineering*, vol. 14, no. 7, pp. 961–986, 1979.

[54] H. Chen and G. E. Blandford, "Thin-walled space frames. i: Large-deformation analysis theory," *Journal of Structural Engineering*, vol. 117, no. 8, pp. 2499–2520, 1991.

[55] S. Ghuku and K. N. Saha, "A review on stress and deformation analysis of curved beams under large deflection," *International Journal of Engineering and Technologies*, vol. 11, pp. 13–39, 2017.

[56] S. Bourgeois, B. Cochelin, F. Guinot, and E. Picault, "Buckling analysis of tape springs using a rod model with flexible cross-sections," *European Journal of Computational Mechanics*, vol. 21, no. 3-6, pp. 184–194, 2012.

[57] S. J. Walker and G. S. Aglietti, "Modeling the hinge moment of skew-mounted tape spring folds," *Journal of Aerospace Engineering*, vol. 20, no. 2, pp. 102–115, 2007.

[58] P. B. Dinis, D. Camotim, and N. Silvestre, "Gbt formulation to analyse the buckling behaviour of thin-walled members with arbitrarily 'branched'open cross-sections," *Thin-Walled Structures*, vol. 44, no. 1, pp. 20–38, 2006.

[59] N. Silvestre, D. Camotim, and N. Silva, "Generalized beam theory revisited: from the kinematical assumptions to the deformation mode determination," *International Journal of Structural Stability and Dynamics*, vol. 11, no. 05, pp. 969–997, 2011.

[60] E. Picault, S. Bourgeois, B. Cochelin, and F. Guinot, "A rod model with thin-walled flexible cross-section: Extension to 3d motions and application to 3d foldings of tape springs," *International Journal of Solids and Structures*, vol. 84, pp. 64–81, 2016.

[61] Z. Bi, Y. Guan, S. Chen, H. Zhu, and H. Zhang, "A miniature biped wall-climbing robot for inspection of magnetic metal surfaces," in *2012 IEEE International Conference on Robotics and Biomimetics (ROBIO)*. IEEE, 2012, pp. 324–329.

[62] M. Eich, F. Bonnin-Pascual, E. Garcia-Fidalgo, A. Ortiz, G. Bruzzone, Y. Koveos, and F. Kirchner, "A robot application for marine vessel inspection," *Journal of Field Robotics*, vol. 31, no. 2, pp. 319–341, 2014.

[63] S. Kawasaki and K. Kikuchi, "Development of a small legged wall climbing robot with passive suction cups," in *The 3rd International Conference on Design Engineering and Science, ICDES*, vol. 2014, 2014, pp. 112–116.

[64] Y. Liu, S. Sun, X. Wu, and T. Mei, "A wheeled wall-climbing robot with bio-inspired spine mechanisms," *Journal of Bionic Engineering*, vol. 12, no. 1, pp. 17–28, 2015.

[65] A. T. Asbeck, S. Kim, A. McClung, A. Parness, and M. R. Cutkosky, "Climbing walls with microspines," in *IEEE ICRA*. Fla., 2006, pp. 4315–4317.

[66] M. Henrey, A. Ahmed, P. Boscariol, L. Shannon, and C. Menon, "Abigaille-iii: A versatile, bioinspired hexapod for scaling smooth vertical surfaces," *Journal of Bionic Engineering*, vol. 11, no. 1, pp. 1–17, 2014.

[67] S. Kalouche, N. Wiltsie, H.-J. Su, and A. Parness, "Inchworm style gecko adhesive climbing robot," in *2014 IEEE/RSJ International Conference on Intelligent Robots and Systems*. IEEE, 2014, pp. 2319–2324.